Titre: Title:	Substrate integrated waveguide e-plane coupling dual-mode cavity filter synthesized with arrays of metallic via slots
Auteur: Author:	Xiaoma Jiang
Date:	2005
Type:	Mémoire ou thèse / Dissertation or Thesis
Référence: Citation:	Jiang, X. (2005). Substrate integrated waveguide e-plane coupling dual-mode cavity filter synthesized with arrays of metallic via slots [Master's thesis, École Polytechnique de Montréal]. PolyPublie. https://publications.polymtl.ca/7632/

URL de PolyPublie: PolyPublie URL:	https://publications.polymtl.ca/7632/
Directeurs de recherche: Advisors:	Ke Wu
Programme: Program:	Unspecified

UNIVERSITÉ DE MONTRÉAL

SUBSTRATE INTEGRATED WAVEGUIDE E-PLANE COUPLING DUAL-MODE CAVITY FILTER SYNTHESIZED WITH ARRAYS OF METALLIC VIA SLOTS

XIAOMA JIANG

DÉPARTEMENT DE GÉNIE ÉLECTRIQUE
ÉCOLE POLYTECHNIQUE DE MONTRÉAL

MÉMOIRE PRÉSENTÉ EN VUE DE L'OBTENTION
DU DIPLÔME DE MAÎTRISE ÈS SCIENCES APPLIQUÉES
(GÉNIE ÉLECTRIQUE)
DECEMBER 2005

Your file Votre référence
ISBN: 978-0-494-16801-1
Our file Notre référence
ISBN: 978-0-494-16801-1

UNIVERSITÉ DE MONTRÉAL

ÉCOLE POLYTECHNIQUE DE MONTRÉAL

Ce mémoire intitulé:

SUBSTRATE INTEGRATED WAVEGUIDE E-PLANE COUPLING DUAL-MODE CAVITY FILTER SYNTHESIZED WITH ARRAYS OF METALLIC VIA SLOTS

présenté par : XIAOMA JIANG

en vue de l'obtention du diplôme de : Maîtrise ès sciences appliquées

a été dûment accepté par le jury d'examen constitué de :

M. BOSISIO Renato G., M. Sc. A, président

M. WU Ke, Ph. D., membre et directeur de recherche

M. BOURRY Mathieu, Ph. D., membre

DEDICATION

To my wife Danfen Yu

To my son Fan Frank Jiang

To my parents, my sister and brothers

ACKNOWLEDGEMENTS

I would like to express my sincere gratitude to my supervisor, Prof. Ke Wu, for offering me the opportunity and financial support to pursue my master study in such a challenge and exciting research field, and for his invaluable guidance and encouragement throughout the work involved in this thesis. I also want to thank each member of my thesis committee, Prof. Renato G. Bosisio and Prof. Bourry Mathieu, for their comments and suggests on my thesis.

I am grateful to Mr. Jules Gauthier, Mr. Roch Brassard, Mr. René Archambault, Mr. Jean-Sebastien Décarie, Mr. Marsan Eric and other staffs of Poly-Grames Research Center for their skillful technical support and software assistance during the process of my SIW filter design, machining and measurement.

I would appreciate my colleagues, Zhongfang Jin, Feng Xu, Yves Cassivi, Ping Yang, Dominic Deslandes, Yanyang Zhao, Xidong Wu, Jijun Xu, Lin Li, Tang Yu, Wenxin Hou, Zhao long Li, Hui Zhang and Yan Ding for their helpful discussions and generous stimulations.

Finally my special thanks go to my wife, my son, and to my parents, my sister and my brothers for their endless support and understanding that drive me to go for success.

RÉSUMÉ

Avec l'expansion rapide des marchés des télécommunications, des efforts importants ont été consacrés à la miniaturisation et à la production de masse de filtres micro-onde et millimétriques ayant une sélectivité élevée, de faibles pertes d'insertion et un délai de groupe uniforme. Cette thèse traite du développement de filtres à cavités bimodales réalisés par des structures de couplage en plan E et fabriqués en guides d'onde intégrés à même le substrat (SIW) de sorte à satisfaire des critères de performance très strictes.

Une nouvelle version de circuits SIW synthétisés par des ensembles de fentes métallisées est développée. En plus de conserver toutes les propriétés des SIW fabriqués par perforations circulaires métallisées (via hole), cette méthode permet de varier le ratio de l'espacement à la longueur de la fente de sorte à rencontrer les dimensions physiques des filtres. Les règles de conception utilisées assurent des pertes de radiation SIW négligeables et permet une échelle de conversion 1 :1 entre les éléments guides d'onde rectangulaires et leur équivalent SIW. Un filtre innovateur à cavités bimodales TE_{m0n} est étudié et les résultats obtenus démontrent que le cadre de travail développé est convenable pour les applications SIW. Dans un but d'accroître les performances à haute fréquence, une nouvelle configuration d'insertions métalliques de couplage en plan E est introduite pour les cavités bimodales TE_{102}/TE_{301} et TE_{102}/TE_{201}. Une méthode de conception impliquant des inverseurs K et une matrice de couplage est également exploitée.

Trois filtres SIW à cavités bimodales et couplage en plan E possédant des zéros de transmission aux bandes de coupure inférieure et supérieur sont fabriqués. Les résultats de simulation, de mesure et de conception concordent fortement pour les trois filtres SIW à cavité bimodale proposés.

Cette nouvelle technologie SIW peut facilement être étendue à une grande variété d'applications SIW.

ABSTRACT

With the rapid expansion of the communication system markets, tremendous efforts on the miniaturization and mass-production of microwave and millimeter wave filters along with high slope selectivity, low insertion loss and flat group delay have been made recently. Substrate Integrated Waveguide (SIW) filters have attracted extensive attention due to their features of high performance, compact size, low cost and tuning-free.

The objective of this thesis is to develop and design SIW E-plane coupling dual-mode cavity filters to satisfy some extraordinary requirement.

Two different approaches are proposed to achieve microwave and millimeter wave filter compactness. The first approach leads to the development of a novel version of SIW synthesized with arrays of metallic via slots. While preserving all properties of SIW synthesized with metallic via holes, it takes advantage of allowing the ratio of gap size to slot length to be varied to fit the physical dimensions of the filters. Two design rules are then conducted to ensure SIW radiation loss is kept at a negligible level and to make the structure mapping from the rectangular waveguide (RW) to the SIW with scale factor near 1:1, which means no physical size change results. Since filters are built in the dielectric substrate, they are highly compact and much shorter than conventional air filled RW filters.

The second approach leads to the design of E-plane dual-mode cavity filters with pseudo elliptic function responses, which possesses of small size, low insertion loss and high frequency selectivity. New TE_{mon}-like family degenerate mode RW cavities are

investigated and the result shows that their developed frameworks are only few suitable for SIW applications due to the nature of SIW structures. An innovative coupling method based on source/load multiple coupled network is presented and analytical expressions of the coupling matrix is derived. The designed E-plane coupling configurations for TE_{102}/TE_{301} and TE_{102}/TE_{201} dual-mode cavities ensure the realization of negative couplings which bring transmission zeros to finite frequency.

Finally, the design and implementation of SIW E-plane coupling dual-mode cavity filters synthesized with arrays of metallic via slots are depicted in detail. Utilizing a precise laser cutting technology in fabrication guarantees excellent mechanical tolerances and mass production. For applications of Substrate Integrated Circuits (SICs), a stepped transition of SIW to microstrip is exploited for impedance match and mode conversion in a wider band and applied to SIW filter designs. It has been verified for three designed SIW dual-mode cavity filters that excellent agreement among measured, simulated and designed results is achieved.

This new SIW technology can be easily extended to a variety of SIW applications.

CONDENSÉ EN FRANÇAIS

FILTRES À CAVITÉS BIMODALES INTÉGRÉS AU SUBSTRAT ET SYNTHÉTISÉS PAR DES RÉSEAUX DE FENTES MÉTALLIQUES

0.1. INTRODUCTION

En raison du développement rapide des systèmes de communication modernes, il est crucial que les filtres micro-ondes et millimétriques aient une bonne sélectivité en haute fréquence, de faibles pertes d'insertion et un délai de groupe uniforme pour minimiser les interférences et distorsions du signal. De plus, un haut niveau de miniaturisation, un faible coût et un niveau de performance élevé sont essentiels pour que ces filtres soient viables commercialement.

Les filtres guide d'onde bimodale sont la solution conventionnelle pour satisfaire ces critères de performance en raison de leur facteur de qualité élevé, de leur faibles pertes de transmission et de leur réjection hors bande élevée. Cependant, ces structures métalliques sont dispendieuses, volumineuses et requièrent des ajustements mécaniques précis pour obtenir la performance désirée. Les filtres bimodales planaires tel que les filtres microrubans sont également possibles en raison de leurs petites dimensions, leur faible coût et de leur facilité de manipulation. Cependant, un faible facteur de qualité naturel et des pertes d'insertion élevées ne permettent pas leur utilisation dans plusieurs applications. Une solution hybride entre les structures guide d'onde et les structures planaires devient alors une alternative plus intéressante.

La motivation de cette thèse provient du désir de satisfaire les critères de viabilité par le développement d'une nouvelle technologie de guides ingérés au substrat (SIW) et la poursuite du développement de filtres guide d'onde à cavité bimodales de sorte à créer un cadre propice à la réalisation de filtres SIW à cavité bimodale rencontrant les critères de performances énoncés.

0.2. FILTRES GUIDE D'ONDE À CAVITÉ BIMODALE

Les caractéristiques des filtres bimodales sont fondées sur la localisation arbitraire des zéros de transmission (TZ) ou des pôles d'atténuation situés à des points de fréquences déterminés en contraste avec les réponses tous pôles de types Chebyshev ou Butterworth et leur atténuation monotone croissante. L'avantage des filtres ayant des zéros de transmission à des fréquences déterminées peut être illustré par une comparaison avec un filtre Chebyshev tout pôle ayant une bande passante à ondulation constante identique. Par exemple, la rejection hors bande requise peut être obtenue par un filtre bimodal à deux cavités alors qu'une caractéristique tout pôle Chebyshev équivalente pourrait nécessiter un filtre à huit cavités. Cela signifie que la réjection requise peut être réalisée avec un filtre d'ordre inférieur, une perte d'insertion réduite et des dimensions minimales.

Pour débuter, les filtres à cavités guide d'onde seront étudiés et comparés à différents modes dégénérés orthogonaux et d'autres techniques variées de transformation de modes résonnants. Il est connu que les cavités bimodales supportent deux modes orthogonaux dégénérés et que le couplage intra-cavité entre ces deux modes est réalisé pour des vis de

couplages, la coupure carrée des coins ou d'autres éléments similaires. Quant au couplage inter-cavité, celui-ci se fait par des fentes en forme de croix ou de petites sections de guide à mode évanescent. Particulièrement, l'arrangement des sections de couplage de ces filtres comporte toujours un chemin principal où les résonateurs i et $(i+1)$ sont fortement couplés et où les résonateurs i et $(j>i+1)$ sont plus faiblement couplés, généralement de façons croisée. Depuis quelques dizaines d'années, plusieurs efforts de recherche on été consacrés à identifier des méthodes plus ingénieuses pour réaliser le couplage intra-cavité de sorte à minimiser les ajustements expérimentaux, accroître la production de masse et améliorer la réponse aux interférences. Malgré tout le progrès réalisé, le couplage intra-cavité demeure le paramètre requérant le plus d'attention lors de la conception de filtres à cavité bimodale.

Une nouvelle structure de filtres bimodale en guide rectangulaire (RW) et sans couplage intra-cavité a été rapportée en 2001. Une caractéristique importante de ce filtre est que la cavité ne supporte que le mode dégénéré TE_{m0n} et que le mode TE_{01n} ne peut exister puisque la hauteur de la cavité est identique à celle du guide d'onde rectangulaire conventionnel utilisé pour l'alimenter. Le nouvel arrangement de sections de couplage implique de coupler la source et la charge à plusieurs résonateurs créant ainsi plusieurs chemins de propagation du signal entre la source et la charge mais n'implique en aucun cas le couplage intra-cavité entre deux modes dégénérés.

Or, il est plus approprié de convertir les filtres à cavité bimodale en guide d'onde rectangulaire sans couplage intra-cavité sous la forme SIW puisque seulement la famille de modes dégénérés TE_{m0n} est utilisée. De plus, toutes les procédures existantes et le

cadre de travail théorique pour ce type de filtre s'applique directement à la synthèse de leur équivalent SIW sans toutefois permettre de guider les modes TM_{mn} et TE_{mn} ($n \neq 0$) en raison de la nature de la structure SIW.

0.3. COUPLAGE DU FILTRE ET SA SYNTHÈSE

En général, les couplages d'un filtre à cavité bimodale comprennent non seulement des couplages intra- et inter-cavités mais aussi des couplages aux interfaces. Le choix d'une structure de couplage appropriée se fait en fonction de plusieurs variables tels que le mode excité, le type de ligne de transmission utilisé et le niveau de couplage désiré. Aux fréquences micro-ondes et millimétriques, un filtre à cavités couplées en cascade peut être modélisé par un réseau de N résonateurs à deux ports représentés par des circuits en éléments localisés équivalents aux cavités et leurs interconnexions, par couplage intra- ou inter-cavité. Nous assumons que le couplage ne varie pas en fonction de la fréquence et ceci n'est valide que sur une largeur de bande étroite. De plus, une résistance R_i est introduite au modèle pour tenir compte des pertes de la cavité et les résistances R_S et R_L représentent respectivement les impédances de la source et de la charge.

Si le vecteur I représente le courant de boucle au sein des résonateurs et que E représente l'excitation, l'équation de boucle du réseau peut s'écrire sous forme matricielle tel que

$$\left[-j[R]+\omega'[U]+[M]\right][I]=[Z][I]=-j[E]$$

où $[R]$ est une matrice nulle de dimension $(n+2)\times(n+2)$ à l'exception près que seules les entrées d'impédance normalisée $R_{11} = R_{n+2,n+2} = 1$. ω' représente la fréquence normalisée par rapport à la fréquence d'opération ω et la largeur de bande $\Delta\omega$ selon

$$\omega' = \frac{\omega_0}{\Delta\omega}\left(\frac{\omega}{\omega_0} - \frac{\omega_0}{\omega}\right)$$

$[U]$ est une matrice identité de dimensions $(n+2)\times(n+2)$ où $U_{11} = U_{n+2,n+2} = 0$. Notez que $[M]$ est la matrice de couplage de dimensions $(n+2)\times(n+2)$ où les éléments diagonaux représentent le couplage propre non obligatoirement nul des résonateurs ce qui permet de prendre en compte les écarts de fréquence par rapport à la fréquence centrale ω_0.

Le courant de boucle $[I]$ peut s'exprimer par

$$[I] = -j[Z]^{-1}[E].$$

En utilisant cette équation, les paramètres S d'entrée/sortie du réseau prototype à deux ports sont donnés par

$$S_{21} = 2\sqrt{R_S R_L}\, I_{n+2} = -2j\sqrt{R_S R_L}\left[Z^{-1}\right]_{n+2,1}$$

$$S_{11} = 1 - 2R_S I_1 = 1 + 2jR_S\left[Z^{-1}\right]_{11}$$

Par exemple, un filtre à cavité bimodale unique ayant deux pôles et un seul zéro de transmission et aucun couplage intra-cavité aura la matrice de couplage

$$M = \begin{bmatrix} 0 & M_{S1} & M_{S2} & 0 \\ M_{S1} & M_{11} & 0 & M_{1L} \\ M_{S2} & 0 & M_{22} & M_{2L} \\ 0 & M_{1L} & M_{2L} & 0 \end{bmatrix}$$

où $M_{ij} = M_{ji}$ and $M_{12} = M_{21} = 0$.

0.4. SYNTHÈSE SIW AVEC FENTES METALLIQUES ET TRANSITIONS INTÉGRÉES

Récemment, plusieurs recherches ont portées sur le développement de nouvelles plateformes de lignes de transmission pour réduire les dimensions, simplifier la fabrication et diminuer les coûts de production. La technologie SIW est très intéressante à cet effet car elle permet de combiner les avantages du guide d'onde rectangulaire à ceux des lignes de transmission planaires de sorte à contourner leurs points faibles respectifs. De plus, l'intégration de cette technologie aux substrats standards est relativement aisée en utilisant des interfaces de transition entre les différents types de lignes de transmission.

La techniques de réalisation des SIW utilisant des perforations circulaires à la masse (via) a été utilisé avec succès dans plusieurs applications micro-ondes et millimétriques. Cependant, puisque les relations équivalentes définitives de ces conceptions SIW ne sont pas disponibles, quelques difficultés peuvent faire surface lorsque l'approche de conception est utilisée pour produire l'équivalent de petites structures guide d'onde en technologie SIW.

Une nouvelle structure SIW est développée dans cette thèse. Des fentes métallisées sont alors utilisées en remplacement des perforations circulaires pour synthétiser les éléments d'un guide d'onde rectangulaire à même le substrat. Le guide d'onde rectangulaire est alors composé du diélectrique et des deux couches métalliques (supérieure et inférieure) du substrat et de fentes métalliques discrètes. L'espacement g entre les deux fentes marque la portion de guide synthétisé et sa dimension permet de minimiser les ondes de fuite jusqu'à les rendre négligeables.

Malgré le fait que cette structure hérite de toutes les propriétés des circuits SIW utilisant les perforations circulaires métallisées, à savoir la possibilité d'intégration, un facteur de qualité élevé et la tolérance à de haute puissance, elle possède néanmoins l'avantage que la largeur du guide équivalent a_{eff} est approximativement égale à l'espacement a entre deux ensembles de fentes lorsque l'espacement g est suffisamment petit. Il est crucial de concevoir des circuits intégrés au substrat pour possiblement transférer les conceptions en guides d'onde rectangulaires vers des conceptions SIW sans en modifier les dimensions.

La réalisation des circuits SIW consiste à produire à même le substrat des structures équivalentes aux structures physiques des circuits guide d'onde en utilisant des ensembles de fentes métallisées. Ces circuits tirent avantage de la variation du ratio d'espacement par rapport à la longueur de la fente g/s de sorte à rencontrer les dimensions physiques du composant guide d'onde. Deux règles de conception provenant à la fois de la théorie et de résultats simulés s'expriment par

$g/s < 1/10$, $g/a < 1/20$.

Ces règles assurent que les pertes par radiation ou les fuites de la structure SIW sont négligeables et les équivalents guide d'onde et SIW aient un ratio de dimension 1:1. Pour tenir compte de l'effet de l'espacement entre deux fentes sur la fréquence de résonance SIW, une cavité résonante est simulée en utilisant la méthode FDFD (logiciel HFSS) de sorte à déduire les relations entre ces deux paramètres.

Les transitions entre les éléments SIW et microrubans sont explorés en détails. La procédure de conception des transitions à deux transformateurs quart d'onde est donnée et deux exemples sont conçus pour une fréquence centrale de 24 GHz sur différents substrats démontrent de parfaits résultats.

0.5. CONCEPTION ET RÉALISATION DE FILTRES SIW À CAVITÉS BIMODALE DANS LE PLAN E

Les principaux problèmes reliés à la conception des filtres proposés s'énoncent comme suit:

1. les cavités bimodale en guide d'onde rectangulaire et sans couplage intra-cavité sont préférées puisque seul les modes TE_{mop} sont utilisés et que ceux-ci s'harmonisent bien avec la nature des circuits SIW;
2. une structure à deux cavités cascadées est désirée pour générer quatre pôles et deux zéros de transmission symétriquement situés de chaque côté de la bande

passante de sorte à accroître la sélectivité en fréquence et rencontrer des critères de bande de réjection plus strictes;

3. la structure de couplage en plan E des insertions métalliques est précédé de l'iris en plan H en raison sa flexibilité pour réaliser le couplage requis simultanément aux deux modes de la cavité et ses bonnes performances aux longueurs d'onde millimétriques.
4. la réalisation de faibles pertes d'insertion sera assurée par trois facteurs essentiels: un facteur de qualité élevé de la cavité bimodale SIW (près de 500), les dimensions compactes de filtre SIW (2 cavités pour 4 pôles), et un substrat à faible dissipation (tan δ = 0.0012 à 10 GHz du Duroid 6002) ;

La conception débute avec le concept de la cavité résonante bimodale SIW et son facteur de qualité sans charge correspondant. Dans une cavité bimodale, les deux modes dégénérés résonnent à la même fréquence. Nous avons donc

$$f_{mnp} = f_{ijk},$$

$$\left(\frac{m\pi}{a}\right)^2 + \left(\frac{n\pi}{b}\right)^2 + \left(\frac{p\pi}{l}\right)^2 = \left(\frac{i\pi}{a}\right)^2 + \left(\frac{j\pi}{b}\right)^2 + \left(\frac{k\pi}{l}\right)^2$$

où les indices *m, n, p* font référence au premier mode TE_{mnp} alors que *i, j, k* font référence au second mode TE_{ijk}. Pour la paire de modes TE_{102} et TE_{201}, nous obtenons de l'équation ci-haut un ratio $a/l = 1$ et la solution pour déterminer la dimension *a* peut être dérivée par

$$a = \frac{13.2}{f_0(GHz)\sqrt{\varepsilon_r}} \text{ (pouce)}$$

où f_o est la fréquence centrale du filtre et ε_r est la constante diélectrique du matériau de remplissage (e.g. le diélectrique).

Pour la paire de modes TE_{102} et TE_{301}, le ratio devient $a/l = \sqrt{8/3}$ et la dimension a peut être calculée par

$$a = \frac{20.2}{f_0(GHz)\sqrt{\varepsilon_r}} \text{ (pouce)}.$$

Nous pouvons alors estimer le facteur de qualité de la cavité bimodale SIW dont les dimensions géométriques sont déterminées à la fréquence de résonance attendue f_0 = 24,15 GHz.

Dans le cas de la cavité des modes TE_{102}/TE_{201} sur le substrat ® 996 ayant les paramètres a =173,7 mil, b = 10 mil, and l = 173,7 mil, le facteur de qualité non chargé de chaque mode se situe autour de 350 et la perte d'insertion de l'ordre de 1.5 dB sur toute la bande passante peut être ajustée pour réaliser le filtre à cavité bimodale d'ordre quatre proposé.

La procédure traditionnelle pour déterminer les dimensions géométriques des insertions métalliques de couplage dans le plan E est fondée sur les inverseurs K définis par les paramètres d'un filtre passe-bas. Une nouvelle méthode alternative décrite ci-dessous utilise plutôt une matrice de couplage M représentant à la fois les couplages

directes et croisés de sorte qu'elle est plus facilement applicable aux filtres bimodales elliptiques.

1 . concevoir les chemins de couplage du filtre pouvant générer des zéros de transmission pour satisfaire les exigences,

2 . extraire la matrice de couplage M en se fondant sur les spécifications du filtre pendant sa synthèse,

3 . trouver les paramètres de chaque inverseur K en utilisant les relations en la matrice de couplage M et les inverseurs,

4 . calculer les paramètres S par la pertinence des inverseurs K caractérisés pour chaque structure de couplage. Pour les réseaux réciproques et sans perte cela conduit à

$$|S_{11}| = |S_{22}| = \left| \frac{\left(K/Z_0\right)^2 - 1}{\left(K/Z_0\right)^2 + 1} \right|, \qquad |S_{21}| = |S_{12}| = \left| \frac{2K/Z_0}{\left(K/Z_0\right)^2 + 1} \right|.$$

5 . utiliser HFSS pour simuler les paramètres S de chaque structure physique de couplage en comparant avec les résultats calculés et en ajustant la dimension de l'élément jusqu'à l'obtention d'une bonne adaptation.

0.6. FABRICATION ET MESURE

Trois filtres à cavités bimodales sont fabriqués; le premier avec deux pôles et un zéro de transmission au dessus de la bande passante, le second avec deux pôles et un zéro de transmission en dessous de la bande passante et le troisième avec quatre pôles et deux

zéros de transmission respectivement situés en dessous et au-dessus de la bande passante. La caractéristique de translation en fréquence des zéros de transmission d'un filtre à cavité bimodale unique est étudiée de sorte à permettre de déplacer le zéro d'un côté à l'autre de la bande passante par un simple ajustement de la dimension de la cavité sans effet sur les coefficients de couplage. Donc, la cavité SIW bimodale peut probablement servir de bloc d'assemblage de filtres cascadés d'ordre supérieur. La validation de cette propriété est réalisée par l'implémentation de deux filtres à cavité simple TE_{102}/TE_{201} ayant une structure de couplage identiques mais différentes dimensions de cavité. Finalement, une filtre SIW à cavités bimodales cascadées est fabriqué et possède quatre pôles et deux zéros de transmission respectivement situés de part et d'autre de la bande passante.

Les fentes SIW sont taillées par un laser de microfabrication du centre de recherche Poly-Grames. La tolérance mécanique de fabrication de l'ordre de ±0.5 mil a été ajustée directement sur les dessins de fabrication. Ainsi, une précision finale inférieure à ±0.3 mil peut être obtenue. Les résultats de simulation, de mesure et de conception concordent fortement pour les trois filtres SIW à cavités bimodales proposés.

TABLE OF CONTENTS

TABLE OF FIGURES

TABLE OF TABLES

CHAPTER 1

INTRODUCTION

The rapid development of modern communication systems has made it crucial for microwave and millimetre-wave filters to possess high frequency selectivity, low insertion loss and flat group delay for minimizing communication cross talk and distortion. Furthermore, low-cost and facility of fabrication along with high performance are essential for microwave and millimetre-wave filters to be commercially viable.

Dual-mode waveguide filters remain the conventional solution for satisfying such challenging demands due to their high Q factor, low transmission loss and high out-of-band rejection. However, such matured metallic structures are bulky and expensive, and precise mechanical tuning is required to obtain desired performance. Planar form dual-mode filters such as microstrip-like filters are a feasible choice for their small size, low cost and ease-of-handling, but its connatural low Q factor and high insertion loss prohibit it from being used in many applications. As such, hybrid schemes of waveguide structure and planar structures become a more attractive alternative.

The motivation for this thesis therefore stems from a desire to satisfy such attractive and challenging demands by synthesizing both the ground-breaking development of new generation technology of substrate integrated waveguide (SIW) and the continuous development of improved conventional dual-mode waveguide filters, and to create a framework to implement SIW dual-mode cavity filters which meet the requirements above.

We start with a brief review of the developed waveguide dual-mode cavity filters in Chapter 2 for comparison of different dual orthogonal degenerate modes and various techniques of resonant mode transformation. It may be concluded that the framework developed for the rectangular waveguide (RW) dual-mode cavity which employs TE_{mon}-like family degenerate modes is directly applicable to their synthesized SIW counterparts, but TM_{mn} and TE_{mn} ($n \neq 0$) modes used in the other waveguide structures cannot be propagated due to the nature of the SIW structure.

In Chapter 3, a general approach for the accurate modeling and synthesis of the equivalent circuit of the multimode cavity filter is studied. The key feature of the approach is that both source and load are coupled to more than one resonator and possibly to one another described by frequency-independent coupling coefficients respectively. The coupling matrix is then derived in matrix form. With extraordinary requirement for high selectivity, the coupling matrix becomes more important for determining and generating the desired finite transmission zeros (TZ) of the filter. For an SIW dual-mode filter, it is required to use non-intracavity coupling cavity so that a precise analysis of the electromagnetic fields of the resonator and accurate computation of the coupling matrix has to be explored.

Chapter 4 addresses a new version of SIW synthesized using metallic via slots instead of via holes. It takes advantage of allowing the ratio of gap size to slot length to be varied to fit the physical dimensions of waveguide circuit components. Two design rules are conducted from both theory and simulation results to ensure SIW radiation loss is kept at a negligible level and to make the structure mapping from the rectangular

waveguide to the SIW with scale factor 1:1, that is no physical size change results. Finite Difference Frequency Domain method (FDFD) is then used to compute the frequency shift that may be caused by the gaps in a SIW resonant cavity. Both results are in an excellent agreement and no distinct frequency shift appears. At the later part of this chapter, the design procedure for a transition between SIW and microstrip formed by two section stepped quarter-wave transformer is given and two examples designed at center frequency 24 GHz on different substrates are demonstrated with excellent results.

In Chapter 5, the design and implementation of SIW dual-mode cavity filters with TZs (transmission zeros) are depicted. It starts with calculating the unloaded Q_u value of an SIW resonant cavity to estimate its insertion loss. It is found that dissipated power on conducting wall has the primary effect on the unloaded Q_u. Coupling configurations providing positive or negative coupling are then discussed. Conventional design procedure based on K inverters and coupling equivalent circuits is introduced at first, and then an alternate way to determine physical dimensions of the inductive coupling structures is involved. It is concluded that the procedure based on K inverters and coupling matrix is more applicable to the SIW dual-mode cavity filters, since coupling matrix presents both direct coupling and cross coupling,.

Chapter 6 demonstrates that a very good agreement among measured, simulated and designed results is achieved. The TZ-shifting characteristic of single dual-mode cavity structure is investigated and the validation of this property is made by implementation of two single TE_{102}/TE_{201} cavity filters with the same coupling structure dimensions but different cavity sizes. Therefore, the single SIW dual-mode cavity probably can be used

as design building block in design of higher order cascaded filters. Finally an SIW dual-mode cavity filter is manufactured with four poles and two TZs at upper and lower stopbands and very good performance is observed.

CHAPTER 2

WAVEGUIDE DUAL-MODE CAVITY FILTERS

Generally, the complete transmission bands in a communication system are divided into several communication channels. The combination or selection of the individual channels aims at lowest-possible insertion loss, flat passband frequency response and high selectivity between adjacent channels [1]. All these demands can be accommodated by employing dual-mode or multimode cavity filters in which a physical cavity can provide more than one resonance [2].

The characteristics of dual-mode filters are based on the arbitrary location of transmission zeros or attenuation poles at finite frequencies in contrast to the all-pole Chebyshev or Butterworth response with their monotonically increasing attenuation [1], [3, 4]. The advantage of the filters with transmission zeros at finite frequencies is illustrated by a comparison of an all-pole Chebyshev filter with the same equal-ripple passband [5]. For example, a required near-out-of band rejection can be obtained by a two-cavity four pole dual-mode filter, while an all-pole Chebyshev characteristic may need an eight cavity eight pole filter [25]. This means that the required out-of-band rejection can be achieved with lowest possible filter order, resulting in lowest possible insertion loss and smallest physical size.

Microwave and millimetre-wave dual-mode filters, in general, can be realized either on waveguide structure in [6]-[10] or on planar structure in [11]-[12], such as microstrip resonator structures.

2.1 Circular Waveguide Dual-mode Filters

A typical circular waveguide dual-mode filter known as an elliptic dual-mode filter is shown in Fig.2.1. The circular waveguide cavities are widely used for feed system application [13, 14] due to their higher Q factor as compared to rectangular ones. This structure incorporates with top wall cascaded (longitudinal) circular cavities which support dual orthogonal degenerate modes, mainly TE_{11n} modes, and uses longitudinal end-coupled input and output cavities for excitation, although side coupled configuration has been reported but is not seen often probably because of the difficulties of design and poor spurious performance. The modes in each cavity are coupled together via coupling screws which are oriented at 45° to the normal electric field polarization [15], while adjacent inter-cavity coupling is provided by cross-shaped slots on the cavity top walls to corresponding horizontally and vertically polarized modes. The vertically polarized mode in the first cavity is excited by the horizontal slot in the input. The energy in the horizontal mode of the first cavity is then coupled from the vertical mode in the same cavity by the coupling screws. The horizontal mode and the vertical mode are together coupled to the adjacent cavity through respective thin horizontal and vertical slots on the cavity top wall. To balance the phase of the two modes in the cavity, vertical or

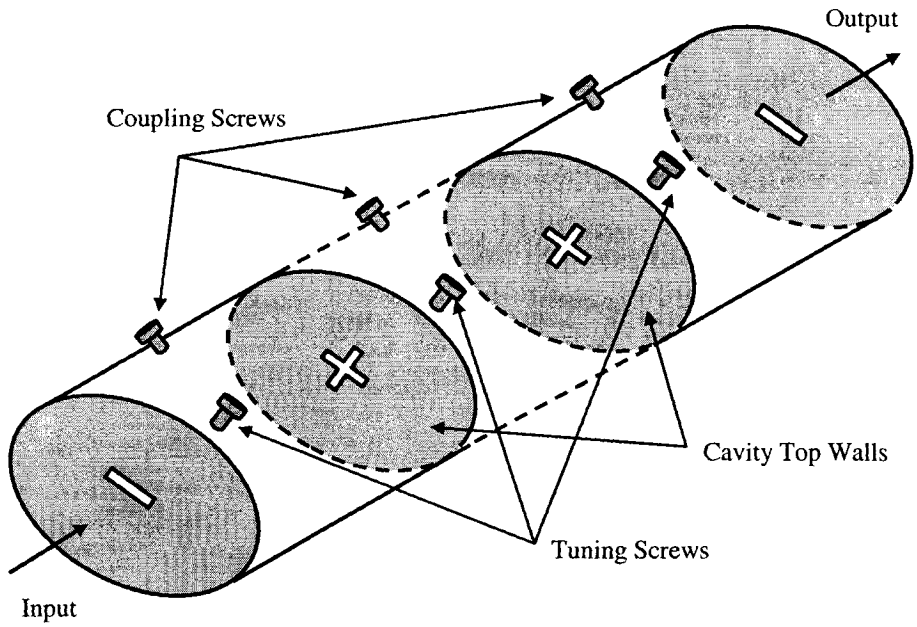

Fig.2.1. Longitudinal Circular Waveguide Dual-mode Filter

horizontal tuning screws are necessary. A recursive tuning process for obtaining a good performance is required. The resonances of the filter are in pairs sequentially assigned to the cavities, namely resonance1 and 2 to cavity 1; resonance 3 and 4 to cavity 2; and so on. However, cross coupling can only be performed between adjacent cavities resulting in reduced flexibility in the design of proper filter characteristics. This means that two adjacent dual-mode cavities can produce one pair of poles of the characteristic function, in other words, elliptic function can be realized for a filter with maximum number of pole pairs n_p (4, 6, 8 poles and so on) and $n_p / 2$ maximum zeros in this configuration,

(where $n_p = N/2$ and N is the number of physical cavities). For this reason, the term "pseudo elliptic" filter is used for this kind of filter to distinguish from full elliptic function filters that have possibility of utilizing all possible poles and zeros.

2.2 Rectangular Waveguide Dual-mode Filters

Rectangular waveguide (RW) dual-mode filters are widely utilized in satellite communications [16] because of their higher selectivity, smaller size and lower insertion losses than conventional single mode direct coupled filters. Its longitudinal prototype is of the same structural form with the circular waveguide dual-mode filters in Fig.2.1. Therefore the conventional approaches for rectangular waveguide dual-mode filters require tuning screws to provide coupling between pairs of orthogonal degenerate modes in the cavity and cross-shaped slots for coupling corresponding horizontally and vertically polarized modes in adjacent cavities. Due to interactions between coupling slots and tuning screws, a significant characterization effort is needed for experimental tuning. Recently many contributions have been made to replace tuning screws with suitable discontinuities [17], [18]. Another most novel approach of rectangular waveguide filter is employing one family of orthogonal degenerate modes without intra-coupling in the cavity in order to eliminate completely coupling screws [19], [20]. So rectangular waveguide dual-mode filters may be divided into two groups based on the coupling arrangement of cavity modes: intracavity coupling and non-intracavity coupling.

2.2.1 Dual-mode Filters with Intracavity Coupling in Rectangular waveguide

Fig. 2.2 depicts a configuration of a 4th pole rectangular waveguide dual-mode filter which is proposed to substitute the coupling screws by square corner cuts on the cavities [21]. A section of evanescent mode rectangular waveguide between cavities is to replace the cross-shaped coupling slot in order to provide a wide range of coupling values with minor reduction of cavity power handling capability together. The square corner cut on the cavity offers intracavity coupling of dual orthogonal degenerate modes which are TE_{101} and TE_{011} in this case.

Relating the coupling and routing schematic of the filter in Fig.2.3, mode 1 (TE_{101}) is exited by input waveguide dominant mode (TE_{10}) and mode 2 (TE_{011}) is coupled from mode 1 via the square corner cut in the first cavity. M23 and M14 are the couplings determined by the small evanescent waveguide between cavities. Mode 3 and mode 4 in the second cavity are similar to the mode 1 and mode 2. It is clear that main couplings are those M_{12}, M_{23} and M_{34} but there is only one weaker cross coupling M_{14}. It has to be noted that mode1 and mode 4 may be coupled each other either in phase or out of phase depending on arrangement of the square corner cuts. This is important for designing the filter because negative coupling can bring transmission zeros from infinity to finite frequency.

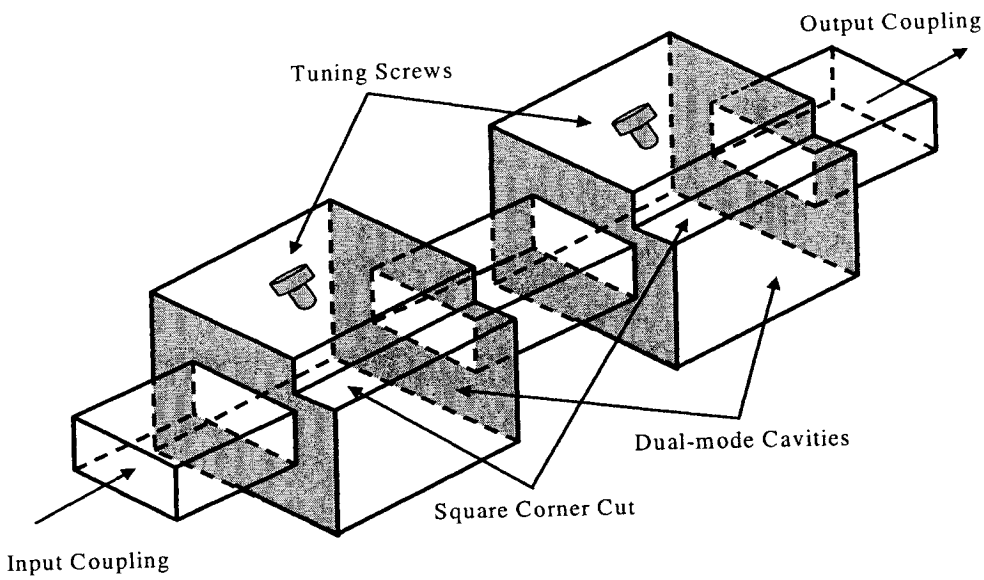

Fig.2.2. Four-Pole Rectangular Waveguide Dual-mode Filter

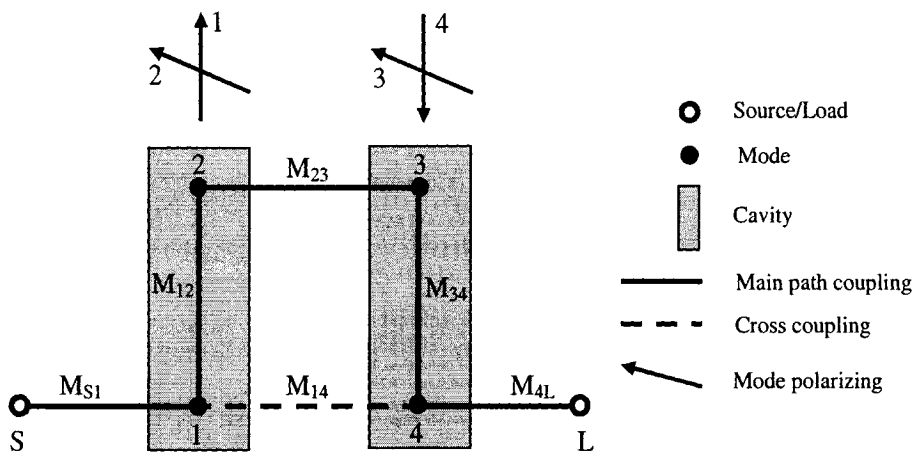

Fig.2.3. Coupling and routing Schematics of a 4th order dual-mode filter

2.2.2 Dual-mode Filters without Intracavity Coupling in Rectangular Waveguide

Based on the introduction of various dual-mode filters in previous sections, it is known that a dual-mode cavity supports two orthogonal degenerate modes and the intracavity coupling is implemented by coupling screws, square corner cuts or other similar elements while coupling between cavities is in terms of intercavity coupling via cross-shaped slots or small evanescent mode waveguides. In particular, the coupling and routing scheme of these filters always include a main path in which ith and $(i+1)$th resonators are directly coupled with relatively strong coupling and the coupling between ith and jth ($j > i+1$) resonators takes the form of cross or bypass coupling which is relatively weak. For decades, many researchers' efforts have been focused on more ingenious ways of achieving the coupling scheme and in particular intracavity coupling to minimize experimental tuning, improve spurious response and reduce size. Despite all this progress, the intracavity coupling is still the most demanding parameter in the design of dual-mode cavity filters.

A novel structure of rectangular waveguide dual-mode filters without intracavity couplings has been reported in 2001 [19]. Fig.2.4 illuminates a structure of single cavity dual-mode filter fed by standard rectangular waveguides. One important feature of the filter is that the cavity supports only TE_{m0n}-like degenerate modes but TE_{01n} mode can not exist since physical height of the cavity is same as the height of feed-in standard rectangular waveguides. The new coupling scheme shown in Fig.2.5 which may involve coupling the source and load to more than one resonator and contain more than one main path for signal between the source and load is investigated and applied to design dual-

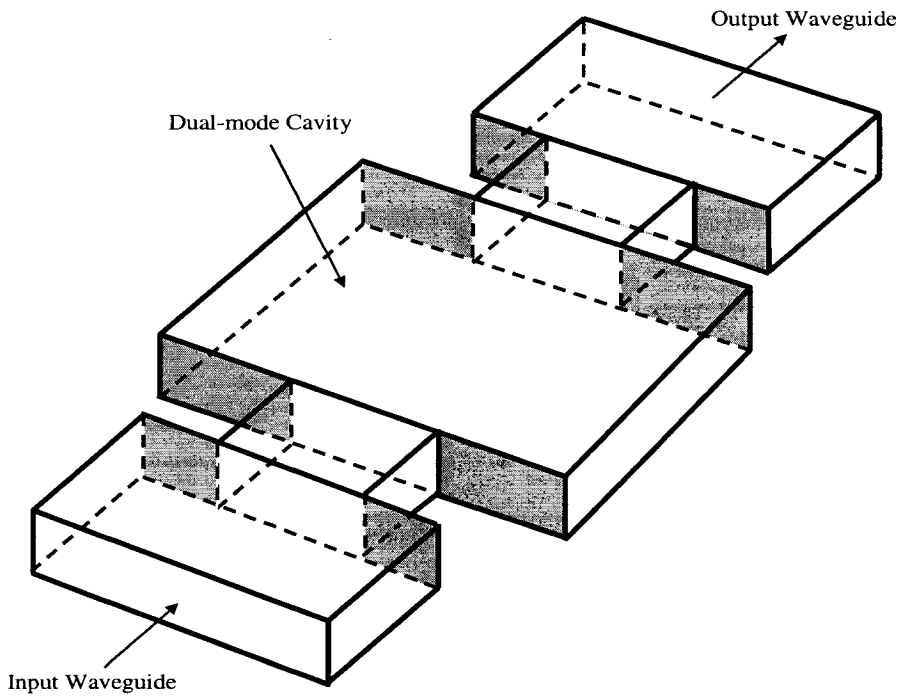

Fig.2.4 Single TE_{102}/TE_{301} Dual-mode Cavity Filter

mode filters [22]. Fig.2.5 (a) shows the basic coupling and routing scheme for a single dual-mode cavity without intracavity coupling which a pair of degenerated modes TE_{102}/TE_{301} is used and Fig.2.5 (b) offers the scheme solution for two cascaded cavity dual-mode filter employing waveguide degenerated modes TE_{102}/TE_{201}. Form Fig.2.5, it is observed that both orthogonal degenerate modes in the cavity are introduced from input iris simultaneously (M_{S1}/M_{S2}) or coupled to output iris (M_{1L}/M_{2L} and M_{3L}/M_{4L}) and direct coupling between the two modes is not present, such as M_{12} and M_{34}. One key point related to realizing higher order dual-mode filters with such coupling topology is

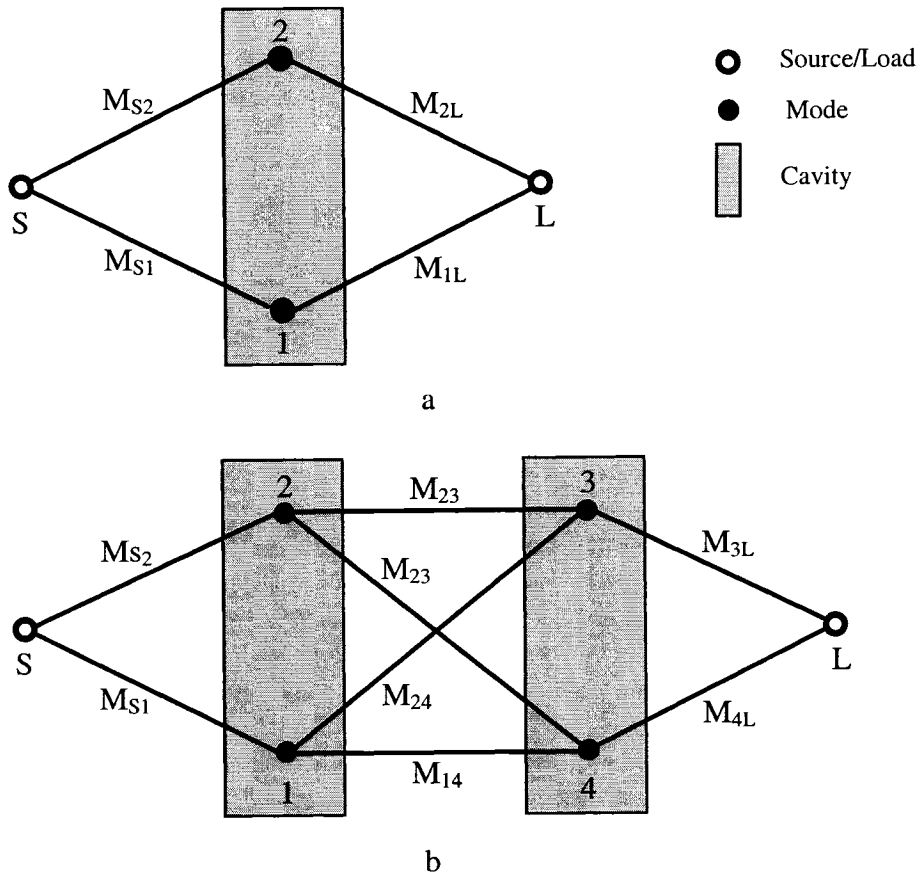

Fig.2.5 Coupling and Routing Scheme of Dual-mode Filters without Intracavity Coupling. a. Two Poles with one Zero. b. Four Poles with Two Zeros

to allow designers to break the filter down to separate paths or sections and focus on each of them one at a time. The responses of the complete filter can be yielded in a proper superposition of the performance of each individual path (section) that is designed and tuned separately.

Another approach for realizing non-intracavity coupling dual-mode filter involves TM_{110}/TE_{10} mode cavity structure. Fig.2.6 describes the implementation of elliptic and pseudo-elliptic function of the filters. All couplings are basically realized by magnetic field of the respective modes in the cavity and interface waveguides. It is noticed that the TE_{10} mode from interface waveguide is propagating through the cavity, but non-resonating while the TM_{110} mode in the cavity is excited directly by TE_{10} mode in input interface waveguides and directly coupled to output interface waveguide without any iris. So there is no intracavity coupling between TM_{110} and TE_{10} modes. The TM_{110} mode will not be excited in a centered structure of which interface waveguides are connected at the middle of the cavity, because the horizontally polarized magnetic field of the TM_{110} mode there is zero. Therefore, coupling of the TM_{110} mode with TE_{10} modes of the interface waveguides is obtained by employing proper centerline offsets between the waveguides and cavity as shown in Fig.2.6. Such a single cavity can generate one transmission pole by TM_{110} mode and bring one transmission zero by bypassing the resonator as shown in Fig.2.7. The position of transmission zero can be either at upper side of passband or at lower side of passband depending on different arrangement of the interface waveguides which results a relative sign change of direct coupling coefficient. The structure in F.2.6 (a) brings a transmission zero at upper stopband while that in Fig.2.6 (b) leads a transmission zero at lower stopband. To determine the sign of bypass coupling at the input and output interface waveguides, the phase of the propagating TE_{10} mode has to be considered. If the magnetic field reverses its direction at the output with respect to its direction at the input, a negative sign results

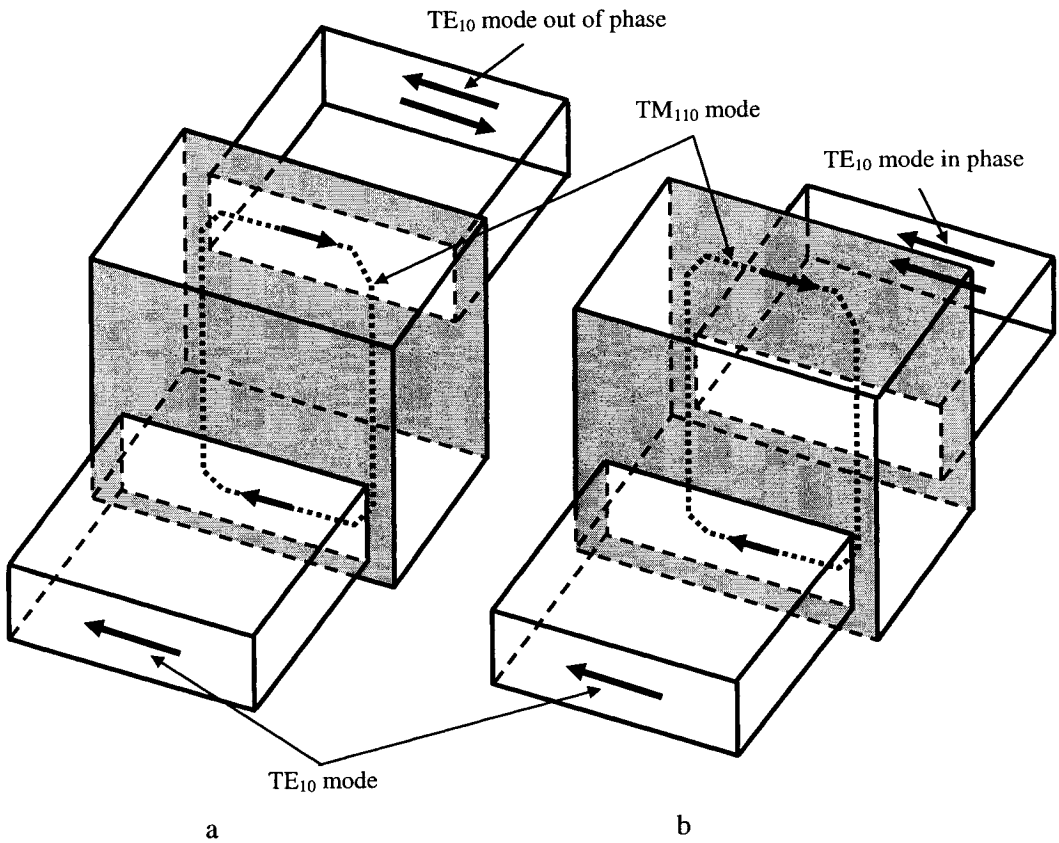

Fig.2.6 Coupling Mechanism Using Transverse Magnetic Fields. a. Direct and Bypass Coupling out of Phase. b. Direct and Bypass Coupling in Phase

in the coupling coefficient at the output. The transmission zeros are generated by exploiting non-resonating modes TE_{10} to provide additional paths for the power flow between adjacent resonators. By properly adjusting the coupling to these modes and their relative paths, the response of the dual-mode pseudo-elliptic filter with arbitrarily

positioned transmission zeros can be implemented in a rather simple geometry of rectangular waveguide.

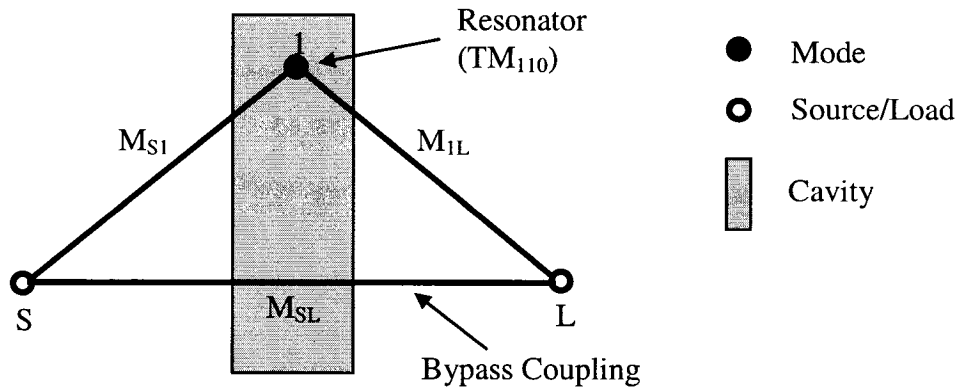

Fig.2.7 Coupling and Routing Scheme of Single Cavity with One Resonator and One Transmission Zero

2.3 Conclusion

It can be concluded that the rectangular waveguide dual-mode cavity without intracavity coupling is most suitable for mapping into SIW form since only TE_{m0n}-like family degenerate modes are employed. All existing procedures and theoretical frameworks developed for this rectangular waveguide dual-mode cavity are directly applicable to their synthesized SIW counterparts, but TM_{mn} and TE_{mn} ($n \neq 0$) modes cannot be guided due to the nature of the SIW structure.

CHAPTER 3

FILTER SYNTHESIS AND COUPLINGS

3.1 Introduction

In general, coupling for a higher order filter involves both intercavity coupling that represents wave energy exchange between adjacent resonators and interface coupling where the desired mode is excited at an end resonator from the input port or extracted to the output port. Elliptic and pseudo-elliptic filters are commonly implemented by introducing cross coupling between non-adjacent resonators to generate the required finite transmission zeros. In this case, intercavity coupling is also in terms of direct coupling. The coupling of a dual-mode cavity filter comprises of not only interface coupling and intercavity coupling but also of intracavity coupling which is exchanging wave energy between different modes in a cavity. The choice of an appropriate coupling structure depends on several variables, the mode excited; the transmission line used and the amount of the coupling desired. The necessary couplings of resonances in different cavities are performed by equal field components of normal electric field, or/and magnetic field that interact through probes, loops, small apertures, cross-shaped slots or small evanescent mode waveguides within the adjacent cavity walls.

3.2 General Coupling Representation and Coupling Matrix

At microwave and millimeter wave frequencies, it is natural to utilize the tuned cavity as one of basic resonating circuit elements in narrow band applications for which basic

two port model has been introduced in [23]. In this case, a two-port network will consist of equivalent resonator circuits of cavity and interconnections between cavities, where interconnection can represent a means of intercavity coupling, intracavity coupling and cross coupling. The coupling is assumed to be frequency invariant, which is valid for a narrow bandwidth. In addition, an ohmic resistor R_i will also be introduced for cavity loss. Further R_S and R_L are the source and load impedances respectively.

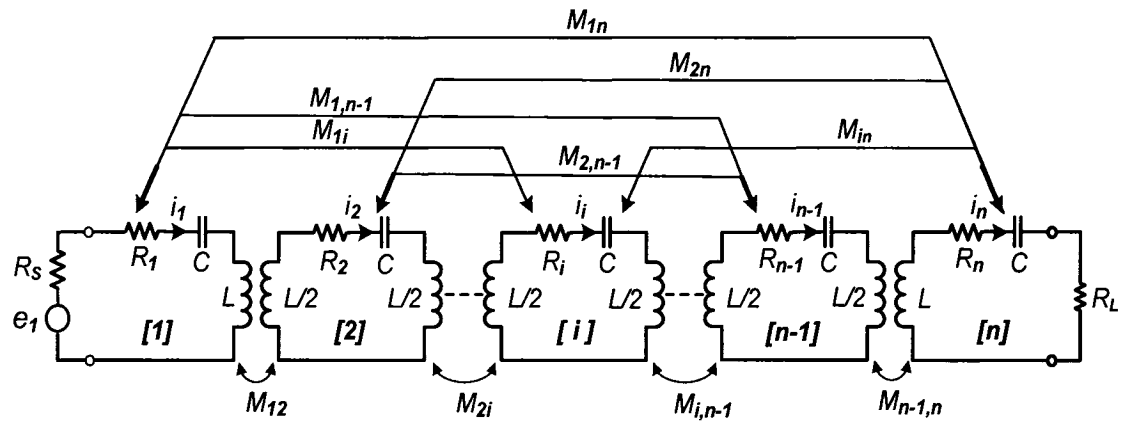

Fig.3.1 A General N-resonator Network Composed of Synchronously Tuned Coupled Cavities

Fig.3.1 shows a general network composed of multiple inductive coupled *N*-resonators, where all resonators are assumed identical and tuned to the same center frequency ω_0. The resonators are numbered 1, 2, ... n with the input applied to resonator *1* and the output taken from resonator *n*. The coupling between the *i*th and *j*th resonators is denoted M_{ij} whose values are real independent numbers.

Let the loop current in the resonator i be i_i, then the loop equation can be written as

$$\begin{aligned}
&i_1\left[R_S+R_1+j\left(\omega L-\frac{1}{\omega C}\right)\right]+ji_2\omega M_{12}+\cdots+ji_i\omega M_{1i}+\cdots+ji_n\omega M_{1n}=e_1\\
&ji_1\omega M_{21}+i_2\left[R_1+j\left(\omega L-\frac{1}{\omega C}\right)\right]+\cdots+ji_i\omega M_{2i}+\cdots+ji_n\omega M_{2n}=0\\
&\qquad\qquad\bullet\\
&\qquad\qquad\bullet\\
&\qquad\qquad\bullet\\
&ji_1\omega M_{n1}+ji_2\omega M_{n2}+\cdots+ji_i\omega M_{ni}+\cdots+i_n\left[R_L+R_n+j\left(\omega L-\frac{1}{\omega C}\right)\right]=0
\end{aligned} \tag{3.1}$$

where e_1 is the input voltage and $M_{ij}=M_{ji}$ since the couplings are reciprocal.

Using definitions of $\omega_0=\frac{1}{\sqrt{LC}}$ and $Z_0=\sqrt{\frac{L}{C}}$, the following abbreviation can be expressed as

$$\left(\omega L-\frac{1}{\omega C}\right)=Z_0\left(\frac{\omega}{\omega_0}-\frac{\omega_0}{\omega}\right)=\lambda \tag{3.2}$$

where ω is operating frequency.

Now the loop equations (3.1) can be placed in the matrix form as

$$\left[-j[R]+\lambda[U]+\omega[M]\right][I]=[Z][I]=-j[E] \tag{3.3}$$

where $[R]$ is an $n\times n$ matrix whose elements are all zero, except the (i, i) entry which is equal to $R_{11}=R_{nn}$ etc. respectively

$$[R]=\begin{bmatrix} R_S+R_1 & 0 & \cdots & 0 & \cdots & 0 & 0 \\ 0 & R_2 & \cdots & 0 & \cdots & 0 & 0 \\ \vdots & \vdots & \ddots & & & \vdots & \vdots \\ 0 & 0 & & R_i & & 0 & 0 \\ \vdots & \vdots & & & \ddots & \vdots & \vdots \\ 0 & 0 & \cdots & 0 & \cdots & R_{n-1} & 0 \\ 0 & 0 & \cdots & 0 & \cdots & 0 & R_n+R_L \end{bmatrix} \tag{3.4}$$

and $[U]$ is an identity matrix. $[M]$ is an $n\times n$ real symmetric coupling matrix in which (i, j) entry is M_{ij} for $i\neq j$, and 0 for $i = j$..

$$[M]=\begin{bmatrix} 0 & M_{12} & \cdots & M_{1i} & \cdots & M_{1,n-1} & M_{1n} \\ M_{21} & 0 & \cdots & M_{2i} & \cdots & M_{2,n-1} & M_{2n} \\ \vdots & \vdots & \ddots & & & \vdots & \vdots \\ M_{i1} & M_{i2} & & 0 & & M_{i,n-1} & M_{in} \\ \vdots & \vdots & & & \ddots & \vdots & \vdots \\ M_{n-1,1} & M_{n-1,2} & \cdots & M_{n-1,i} & \cdots & 0 & M_{n-1,n} \\ M_{n1} & M_{n2} & \cdots & M_{ni} & \cdots & M_{n,n-1} & 0 \end{bmatrix} \tag{3.5}$$

and $[I]$ is the current vector whose elements represent individual loop current,

$$[I]=\begin{bmatrix} i_1 \\ i_2 \\ \vdots \\ i_i \\ \vdots \\ i_{n-1} \\ i_n \end{bmatrix} \tag{3.6}$$

and $[E]$ is termed excitation vector whose elements are all zero, except $E_1 = e_1$

$$[E]=\begin{bmatrix} e_1 \\ 0 \\ \vdots \\ 0 \\ \vdots \\ 0 \\ 0 \end{bmatrix} \tag{3.7}$$

By further assuming all resonators are tuned to the same normalized center frequency, $\omega_0 = 1\ rad/\sec$ and normalized impedance $Z_0 = 1\Omega$, equation (3.2) becomes

$$\lambda == \left(\omega - \frac{1}{\omega}\right) \tag{3.8}$$

As mentioned before, if the filter is operated in a narrow bandwidth, the coupling is independent of frequency. In this way, the following simplification is reasonable for

$$j\omega M_{ij} \approx j\omega_0 M_{ij} \approx jM_{ij} \tag{3.9}$$

Now expression (3.3) can be rewritten as

$$[E]=\big[[R]+j\lambda[U]+j[M]\big][I] \qquad J^2=-1 \tag{3.10}$$

or

$$[E]=[Z][I] \tag{3.11}$$

where $[Z]$ stands for the impedance matrix

$$[Z]=[R]+j\lambda[U]+j[M]=$$

$$\begin{bmatrix}
R_s+R_1+j\lambda & jM_{12} & \cdots & jM_{1i} & \cdots & jM_{1,n-1} & jM_{1n} \\
jM_{21} & R_2+j\lambda & \cdots & jM_{2i} & \cdots & jM_{2,n-1} & jM_{2n} \\
\vdots & \vdots & \ddots & & & \vdots & \vdots \\
jM_{i1} & jM_{i2} & & R_i+j\lambda & & jM_{i,n-1} & jM_{in} \\
\vdots & \vdots & & & \ddots & \vdots & \vdots \\
jM_{n-1,1} & jM_{n-1,2} & \cdots & jM_{n-1,i} & \cdots & R_{n-1}+j\lambda & jM_{n-1,n} \\
jM_{n1} & jM_{n2} & \cdots & jM_{ni} & \cdots & jM_{n,n-1} & R_L+R_n+j\lambda
\end{bmatrix} \tag{3.12}$$

Although Fig.3.1 depicts a general two-port n-resonator network of an inline coupled single-mode cavity filter, it also can be used to analyze dual-mode cavity filters with intracavity coupling, such as circular waveguide dual-mode filters shown in Fig1.1, or

rectangular waveguide dual-mode filters introduced in Fig1.2. In such cases, M_{12} can be described as direct coupling or intracavity coupling between two degenerated modes in the same cavity while M_{14} is cross coupling or non-adjacent cavity coupling even though two cavities may be physically cascaded. There are some restrictions imposed by this network model. Since the source feeds only one resonator, resonator *1* mostly, and the load is also connected to only one resonator, resonator *n*, it is established that the filter only can generate at most $n-2$ finite transmission zeros with *n* resonators. Furthermore, it is not applicable to the filtering structures either with additional coupling between the source and the load, or with source/load-multiresonator coupling, for example the filter shown in Fig.1.4. A universal and comprehensive synthesis technique of the coupled resonator filters with source/load-multiresonator coupling has been developed to overcome the drawbacks above [24].

3.3 Source/Load-Multiresonator Couplings

The analysis is based on the presentation in section 3.2 above with proper extension to handle the presence of source/load-multiresonator coupling. Fig.3.2 illustrates the coupling and routing scheme of a universal two-port network of coupled resonators with source/load-multiresonator coupling. The attractive feature of the filter is that both source and load are coupled to more than one resonator and possibly to one another by frequency-independent coupling coefficients M_{si}, M_{Li} and M_{SL} respectively.

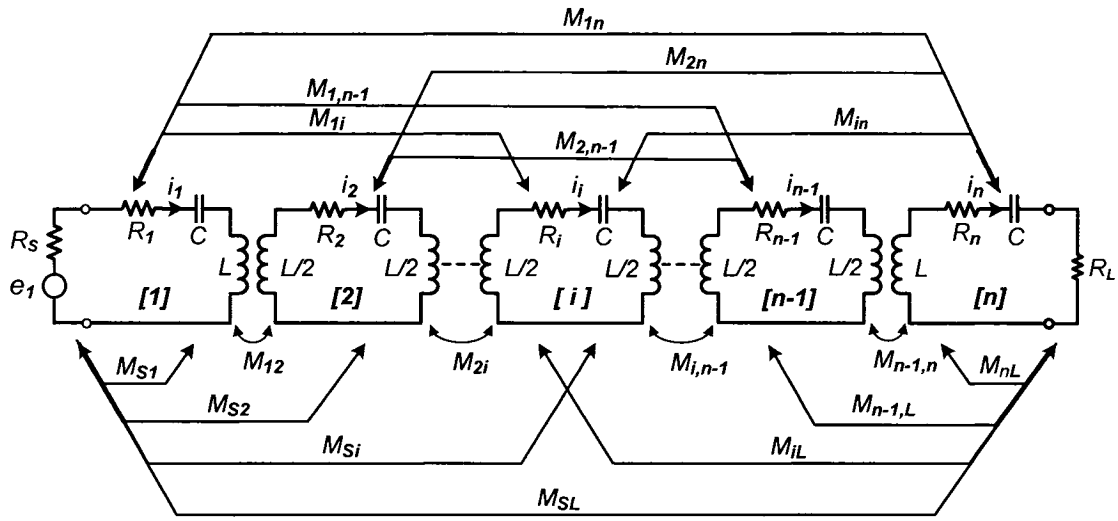

Fig.3.2 N-Coupled Cavity Network with Source/Load Multiple Couplings

Following the same analysis method of loop currents of the network used to conduct equation (3.3), then the loop equations can written as

$$\left[-j[R]+\omega'[U]+[M]\right][I]=[Z][I]=-j[E] \qquad j^2=-1 \qquad (3.13)$$

here by assuming all resonators are lossless, $[R]$ is a null $(n+2)\times(n+2)$ matrix except that only nonzero entries $R_{11} = R_{n+2,n+2} = 1$ which are the normalized impedances.

$$[R]=\begin{bmatrix} 1 & 0 & \cdots & 0 & 0 \\ 0 & 0 & \cdots & 0 & 0 \\ \vdots & \vdots & \ddots & \vdots & \vdots \\ 0 & 0 & \cdots & 0 & 0 \\ 0 & 0 & \cdots & 0 & 1 \end{bmatrix} \tag{3.14}$$

ω' is normalized frequency and is related to the actual operating frequency ω by

$$\omega' = \frac{\omega_0}{\Delta\omega}\left(\frac{\omega}{\omega_0} - \frac{\omega_0}{\omega}\right) \tag{3.15}$$

where ω_0 is the center frequency of the filter and $\Delta\omega$ is its bandwidth. Note that both ω_0 and $\Delta\omega$ can be set to unity since they act only as scaling parameters.

$[U]$ is similar to the $(n+2)\times(n+2)$ identity matrix in which $U_{11} = U_{n+2,n+2} = 0$. Note that $[M]$ is the $(n+2)\times(n+2)$ coupling matrix whose diagonal elements represented for self couplings may be not zero anymore, which account for frequency offsets from center frequency ω_0.

$$M = \begin{bmatrix} 0 & M_{S1} & \cdots & M_{Si} & \cdots & M_{Sn} & M_{SL} \\ M_{1S} & M_{11} & \cdots & M_{1i} & \cdots & M_{1n} & M_{1L} \\ \vdots & \vdots & \ddots & \vdots & & \vdots & \vdots \\ M_{iS} & M_{i1} & & M_{ii} & & M_{in} & M_{iL} \\ \vdots & \vdots & \vdots & & \ddots & \vdots & \vdots \\ M_{nS} & M_{n1} & \cdots & M_{ni} & \cdots & M_{nn} & M_{nL} \\ M_{LS} & M_{L1} & \cdots & M_{Li} & \cdots & M_{Ln} & 0 \end{bmatrix} \tag{3.16}$$

Then matrix $[Z]$ is defined by (3.17)

$$[Z] = [R] + j\omega'[U] + j[M] =$$

$$\begin{bmatrix} 1+j\omega' & jM_{S1} & \cdots & jM_{Si} & \cdots & jM_{Sn} & jM_{SL} \\ jM_{1S} & j(\omega'+M_{11}) & \cdots & jM_{1i} & \cdots & jM_{1n} & jM_{1L} \\ \vdots & \vdots & \ddots & & & \vdots & \vdots \\ jM_{iS} & jM_{i1} & & j(\omega'+M_{ii}) & & jM_{in} & jM_{iL} \\ \vdots & \vdots & & & \ddots & \vdots & \vdots \\ jM_{nS} & jM_{n1} & \cdots & jM_{ni} & \cdots & j(\omega'+M_{nn}) & jM_{nL} \\ jM_{LS} & jM_{L1} & \cdots & jM_{Li} & \cdots & jM_{Ln} & 1+j\omega' \end{bmatrix} \tag{3.17}$$

Having characterized the model this way, it is then possible to use the filter specifications to determine the unknown filter parameters such as the coupling coefficients M_{ij}. To do this, a mathematical filter function has to be derived from the filter specifications. The process of using target function to find unknown parameters by optimization is termed filter synthesis.

3.4 Filter Synthesis

A simple analysis for the network of the two-port inline resonator filter is described by equation (3.13) in terms of loop currents $[I]$ which can be expressed as

$$[I] = -j[Z]^{-1}[E] \tag{3.18}$$

Using this equation, the scattering parameters for input and output of the prototype network are given by

$$\begin{aligned} S_{21} &= 2\sqrt{R_S R_L}\, I_{n+2} = -2j\sqrt{R_S R_L}\left[Z^{-1}\right]_{n+2,1} \\ S_{11} &= 1 - 2R_S I_1 = 1 + 2jR_S\left[Z^{-1}\right]_{11} \end{aligned} \tag{3.19}$$

As an example, consider a single dual-mode cavity filter whose coupling and routing scheme is shown in Fig.3.3. It is clear that the filter has two poles and one transmission zero without intracavity coupling. Therefore its coupling matrix is exhibited as

$$M = \begin{bmatrix} 0 & M_{S1} & M_{S2} & 0 \\ M_{S1} & M_{11} & 0 & M_{1L} \\ M_{S2} & 0 & M_{22} & M_{2L} \\ 0 & M_{1L} & M_{2L} & 0 \end{bmatrix} \tag{3.20}$$

where $M_{ij} = M_{ji}$ and $M_{12} = M_{21} = 0$.

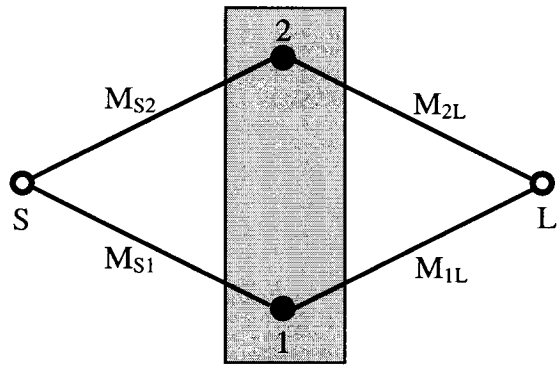

Fig.3.3 Single Cavity Dual-Mode filter with Souce/Load-Multiresonator Coupling

For this given matrix $[M]$, the inverse of the matrix $[Z]$ in equation (3.19) can be calculated analytically by assuming normalized impedance $R_S = R_L = 1$ and network coefficients are yielded as

$$S_{21} = \frac{a\omega' + b}{\det}$$

$$S_{11} = \frac{\omega'^2 + c\omega' + d}{\det} \tag{3.21}$$

where the constants *a, b, c, d* and determinant *det* are given as

$$
\begin{aligned}
a &= -M_{2L}M_{S2} - M_{S1}M_{1L} \\
b &= -M_{2L}M_{S2}M_{11} - M_{S1}M_{1L}M_{22} \\
c &= M_{11} + M_{22} + j\left(M_{S1}^2 - M_{2L}^2 + M_{S2}^2 - M_{1L}^2\right) \\
d &= M_{11}M_{22} - 2M_{S1}M_{2L}M_{S2}M_{1L} + M_{S1}^2M_{2L}^2 + M_{S2}^2M_{1L}^2 \\
&\quad + jM_{11}\left(M_{S2}^2 - M_{2L}^2\right) + jM_{22}\left(M_{S1}^2 - M_{1L}^2\right) \\
\det &= -\omega'^2 + e\omega' + f \\
e &= -\left(M_{11} + M_{22}\right) + j\left(M_{S1}^2 + M_{2L}^2 + M_{S2}^2 + M_{1L}^2\right) \\
f &= -M_{11}M_{22} - 2M_{S1}M_{2L}M_{S2}M_{1L} + M_{S1}^2M_{2L}^2 + M_{S2}^2M_{1L}^2 \\
&\quad + jM_{11}\left(M_{S2}^2 + M_{2L}^2\right) + jM_{22}\left(M_{S1}^2 + M_{1L}^2\right)
\end{aligned}
\tag{3.22}
$$

A proposed two-pole filter is based on the coupling scheme shown in Fig.3.3. Two separate paths between the source and load comprise two resonators respectively without intracavity coupling. And for two resonator structures, cross coupling will bring one transmission zero. The required filter parameters are

center frequency f_o 24.06 GHz

bandwidth Δf 320 MHz

inband return loss 24 dB

transmission zero 23.38 GHz

By examining the extraction of coupling matrix according to the coupling scheme in Fig.3.3, the result is

$$M = \begin{bmatrix} 0 & 1.221 & 0.74 & 0 \\ 1.221 & -1.88 & 0 & -1.221 \\ 0.74 & 0 & 1.999 & 0.74 \\ 0 & -1.221 & 0.74 & 0 \end{bmatrix} \tag{3.23}$$

It is apparent that the coupling coefficients are not prohibitively large in this case and non-zero diagonal elements are only frequency shift in the resonant frequency. The frequency response of the coupling matrix is calculated by equation (3.21) and plotted in Fig.3.4. It is obvious that all the specifications are met well.

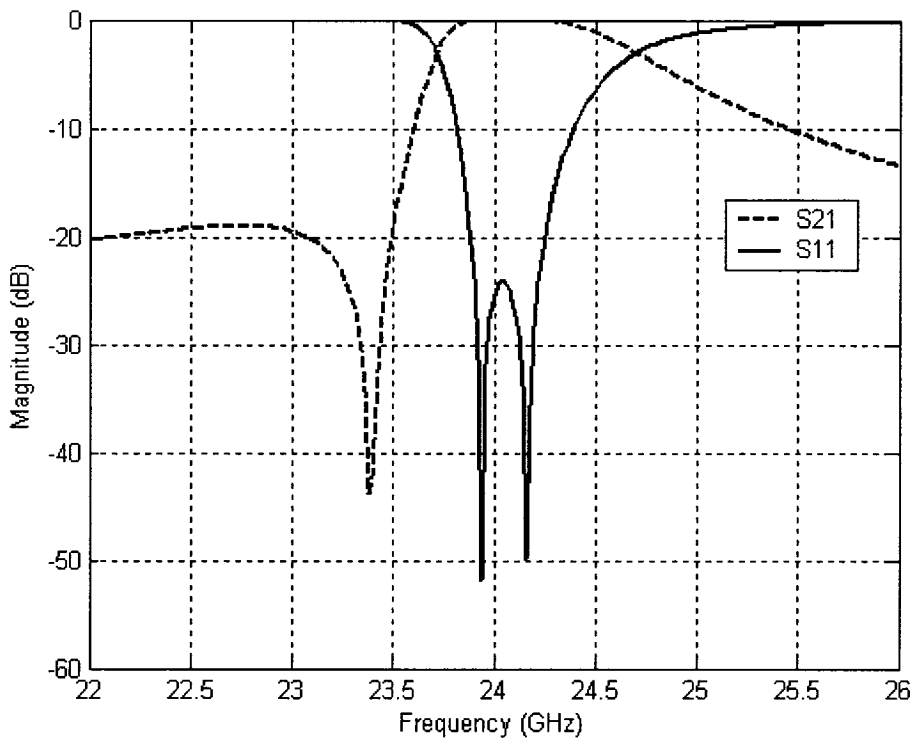

Fig.3.4 Frequency Response of the coupling matrix in (3.23)

A MATLAB code which describes the above calculation principle is attached in the Appendix.

CHAPTER 4

SIW SYNTHSIZED WITH METALLIC VIA SLOTS AND INTEGRATED TRANSITIONS

4.1 Introduction

Design principles for classical waveguides as one of the earliest type transmission lines remain the mainstream today for designing high-performance millimeter wave systems and high-precision detecting systems. A large variety of components such as filters, diplexers, couplers, detectors, phase shifters, and splitters/combiners are commercially available for various standard bands from 1 GHz to 320 GHz. It is known that these matured waveguide components feature properties of low loss and high power handling. But their bulky structures and the complex tuning processes required might be prohibitive in most practical applications and difficult to achieve in mass production. For decades, due to the trends toward miniaturization and integration of microwave devices, planar transmission lines, such as microstrip and stripline are utilized to fabricate many microwave circuit components, rather than waveguides. Microstrip line is the most popular type of planar transmission lines, primarily because it can be realized by photolithographic processes and is easily integrated with other passive and active microwave devices. However, microstrip line cannot support a pure TEM wave, since dielectric does not fill the air region above the strip so that the phase velocity of TEM filed in the dielectric region would be $c/\sqrt{\varepsilon_r}$, but the phase velocity of TEM filed in the air region would be c. Thus, a phase match at the dielectric-air interface is impossible to

obtain for a TEM wave. More importantly, microstrip line has a completely different current distribution from the waveguide. A very high current density at the edge of the strip induces high conductor loss and low Q value of microstrip line. Furthermore, the radiation loss of the microstrip is also significant.

Recently, many researches have been focusing on developing new platforms of transmission lines to reduce the size, simplify the manufacture process, lower the production cost and maintain high performance [26]. Hybrid schemes of waveguide and planar transmission line have become more attractive because they are able to combine the advantages of both transmission line types to overcome their drawbacks. Substrate Integrated Waveguide (SIW) technology is the most popular and the most developed platform as it is quite easy to integrate conventional rectangular waveguide into standard PCB or substrates with interfaces of transition between waveguide and microstrip line [27].

4.2 Rectangular Waveguide and Its Modes

The most common propagation medium among all types of waveguides is the rectangular waveguide which is a closed metal rectangle filled with dielectric to transport electromagnetic energy over short or long distances [25]. A typical rectangular waveguide in the coordinate system is illustrated in Fig.4.1. The conducting walls are structured such that the inner surfaces form a rectangular cross section with dimensions a and b along X and Y coordinate axes, respectively. Transmission is along the Z

direction. As shown in Fig.4.2, an electromagnetic wave travels in the rectangular waveguide by bouncing between two broad sidewalls with an incident angle θ. It can be

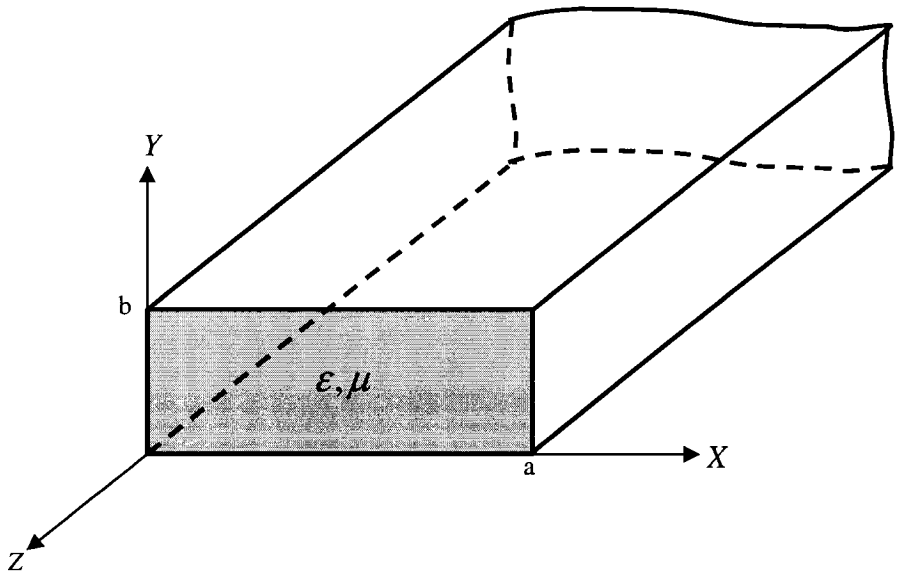

Fig.4.1 Geometry of a Rectangular Waveguide

imaged that when θ is increased up to $\pi/2$, the wave will reflect up and down with no motion in Z axis. Therefore the wave is cutoff. As frequency of the incident wave decreases or wavelength of the wave increases, the angle θ is increased and approached to $\pi/2$. From such a viewpoint, waveguide performs as a high pass filter.

The rectangular waveguide can establish an infinite number of distinct electromagnetic field configurations that can transmit electromagnetic energy from one point to another. Each of these configurations is referred to as waveguide mode. As already stated, waveguide can support the propagating mode only above its cutoff

frequency, which is a function of the waveguide geometry. The types of modes that can be propagated in the rectangular waveguide are transverse electric (TE) modes and transverse magnetic (TM) modes which are characterized respectively by $E_z = 0, H_z \neq 0$ and $H_z = 0, E_z \neq 0$, but not TEM mode, since only one conductor is present.

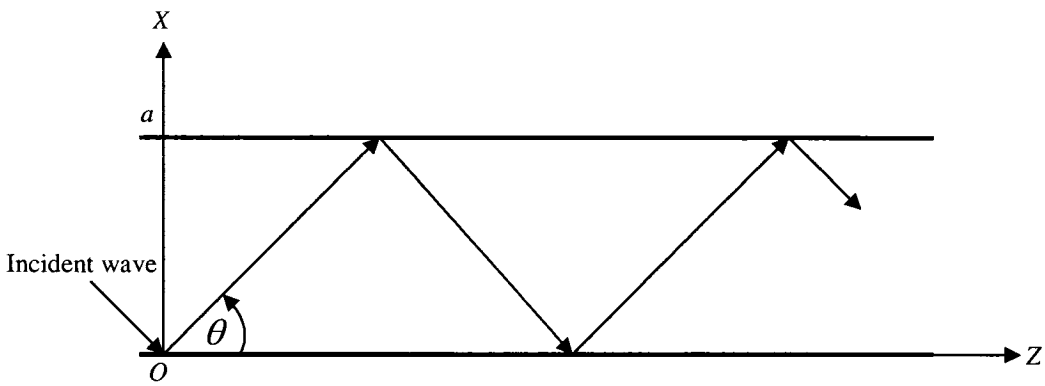

Fig.4.2 Electromagnetic Wave Traveling in a Rectangular Waveguide

4.2.1 TE Modes

The geometry of a rectangular waveguide shown in Fig.4.1 is conventionally defined to have the longest side of the waveguide along the X axis, namely $a > b$. And it is standard to assume that the guide wall is perfectly conduction and the filled dielectric material is lossless. The transverse field components of the TE_{mn} modes can be found by

$$
\begin{aligned}
E_z &= 0 \\
H_z &= A_{mn}\cos\frac{m\pi x}{a}\sin\frac{n\pi y}{b}e^{-j\beta z} \\
E_x &= \frac{j\omega\mu n\pi}{k_c^2 b}A_{mn}\cos\frac{m\pi x}{a}\sin\frac{n\pi y}{b}e^{-j\beta z} \\
E_y &= \frac{-j\omega\mu n\pi}{k_c^2 a}A_{mn}\sin\frac{m\pi x}{a}\cos\frac{n\pi y}{b}e^{-j\beta z} \\
H_x &= \frac{j\beta m\pi}{k_c^2 a}A_{mn}\sin\frac{m\pi x}{a}\cos\frac{n\pi y}{b}e^{-j\beta z} \\
H_y &= \frac{j\beta n\pi}{k_c^2 b}A_{mn}\cos\frac{m\pi x}{a}\sin\frac{n\pi y}{b}e^{-j\beta z}
\end{aligned}
\tag{4.1}
$$

where A_{mn} is an amplitude constant and integer m and n describe the number of variation of the fields along the two transverse coordinates and

$$
k_c^2 = k_x^2 + k_y^2 = \left(\frac{m\pi}{a}\right)^2 + \left(\frac{n\pi}{b}\right)^2 \tag{4.2}
$$

and propagation constant is

$$
\beta = \sqrt{k^2 - k_c^2} = \sqrt{\omega^2\mu\varepsilon - \left(\frac{m\pi}{a}\right)^2 + \left(\frac{n\pi}{b}\right)^2} \tag{4.3}
$$

It is seen from equation (4.1) that β should be real corresponding to a propagating mode.

$$
k > k_c = \sqrt{\left(\frac{m\pi}{a}\right)^2 + \left(\frac{n\pi}{b}\right)^2}
$$

When $\beta = 0$, The TE mode cannot propagate along the Z axis or the modes are cutoff.

$$k = k_c = \sqrt{\left(\frac{m\pi}{a}\right)^2 + \left(\frac{n\pi}{b}\right)^2}$$

then

$$k = \omega\sqrt{\mu\varepsilon} = \sqrt{\left(\frac{m\pi}{a}\right)^2 + \left(\frac{n\pi}{b}\right)^2} \tag{4.4}$$

Equation (4.4) implies that each TE mode has associated with a characteristic cutoff frequency $f_{c.m.n}$, below which the mode does not propagate. From equation (4.4) get

$$f_{c.m.n} = \frac{k_c}{2\pi\sqrt{\mu\varepsilon}} = \frac{1}{2\pi\sqrt{\mu\varepsilon}}\sqrt{\left(\frac{\pi m}{a}\right)^2 + \left(\frac{\pi n}{b}\right)^2} \tag{4.5}$$

The cutoff frequency $f_{c.m.n}$ is a geometrical parameter dependent on the waveguide cross section dimensions. The cutoff wavelength is defined as

$$\lambda_c = \frac{2\pi}{k_c} = \frac{2\pi}{\sqrt{\left(\frac{\pi m}{a}\right)^2 + \left(\frac{\pi n}{b}\right)^2}} \tag{4.6}$$

Each of TE_{mn} modes has its own guide wavelength λ_g which is defined as the distance between two equal phase planes along the waveguide and is equal to

$$\lambda_g = \frac{2\pi}{\beta} = \frac{2\pi}{\sqrt{\omega^2\mu\varepsilon - \left(\frac{m\pi}{a}\right)^2 + \left(\frac{n\pi}{b}\right)^2}} \tag{4.7}$$

The mode with the lowest cutoff frequency is called the domain mode which also is the most commonly used mode. In rectangular waveguide, the lowest f_c occurs for the TE_{10} (m = 1, n = 0) mode when assumed $a > b$:

$$f_{c10} = \frac{1}{2a\sqrt{\mu\varepsilon}}$$

and

$$\lambda_{c10} = 2a \tag{4.6}$$

$$\lambda_{g10} = \frac{\lambda}{\sqrt{1 - \left(\frac{\lambda}{2a}\right)^2}} \tag{4.7}$$

where λ is the wavelength of the wave in the dielectric medium.

In Fig.4.3 the magnetic and electric field of the TE_{10} mode in a rectangular waveguide is illustrated. It is observed that electromagnetic field of the TE_{10} mode is constituted by only three components due to $E_z = E_x = H_y = 0$, namely

$$E_y = E_{yo} \sin\left(\frac{\pi x}{a}\right) e^{-j\beta z}$$

$$H_x = H_{xo} \sin\left(\frac{\pi x}{a}\right) e^{-j\beta z} \tag{4.8}$$

$$H_z = H_{zo} \cos\left(\frac{\pi x}{a}\right) e^{-j\beta z}$$

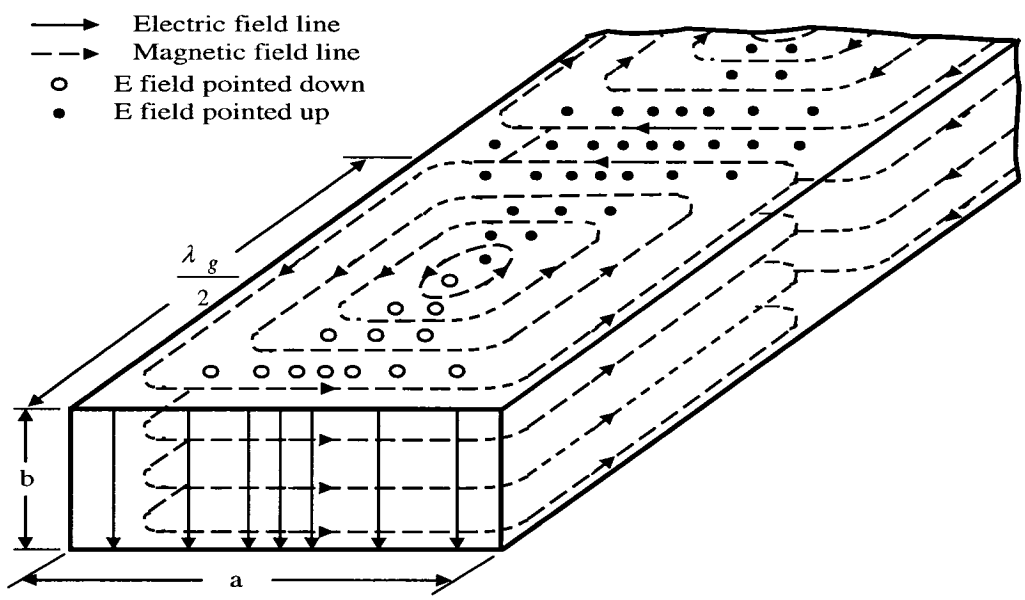

Fig.4.3 Magnetic and Electric Field Distribution for the TE_{10} Mode

The second lowest order TE_{mn} modes is TE_{20} when waveguide dimension $a = 2b$ which is typical. From the equations (4.5), (4.6) and (4.7), the cutoff frequency, cutoff wavelength and guide wavelength of TE_{20} mode are given as

$$f_{c20} = \frac{1}{a\sqrt{\mu\varepsilon}}$$

$$\lambda_{c20} = a$$

$$\lambda_{g20} = \frac{\lambda}{\sqrt{1-\left(\frac{\lambda}{a}\right)^2}} \tag{4.9}$$

Fig.4.4 shows magnetic and electric field distributions of the TE_{20} mode in a rectangular waveguide.

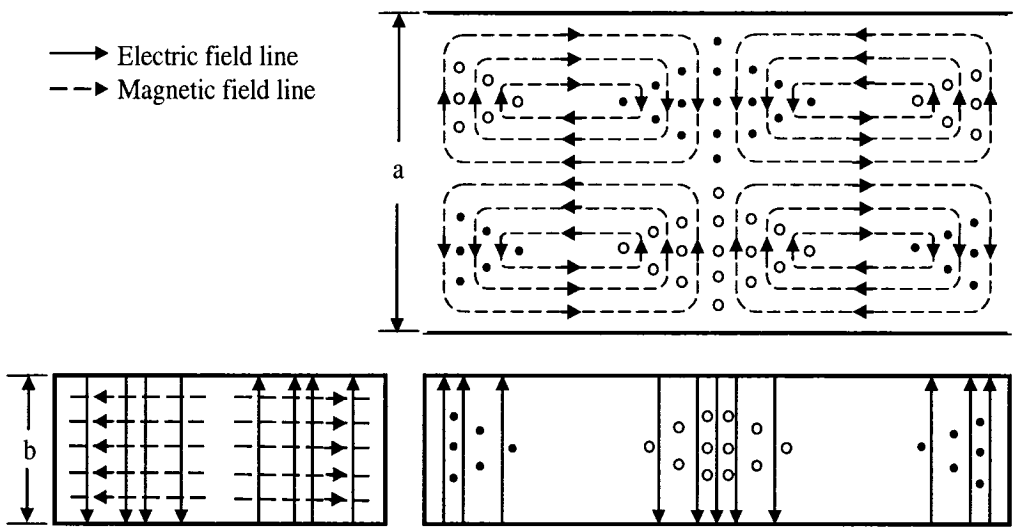

Fig.4.4 Magnetic and electric field patterns of TE_{20} Mode

Note that TE_{10} and TE_{20} modes are two lowest order propagating modes if waveguide dimension $a > 2b$. This pair of modes is often used in dual-mode waveguide filters described in section 2.2.2. When $a = b$, then TE_{10} and TE_{01} modes have the same lowest cutoff frequency and they are degenerate since they posses the same propagation

constant. It is a typical pair chosen for the dual-mode waveguide filters depicted in section 2.2.1.

4.2.2 TM Modes

The TM modes are characterized by field with $H_z = 0$ and E_z plays the role of a potential function from which the remaining field components may be derived. The transverse field components for the TM_{mn} mode are

$$
\begin{aligned}
H_z &= 0 \\
E_z &= B_{mn} \sin\frac{m\pi x}{a} \sin\frac{n\pi y}{b} e^{-j\beta z} \\
E_x &= \frac{j\beta m\pi}{k_c^2 a} B_{mn} \cos\frac{m\pi x}{a} \sin\frac{n\pi y}{b} e^{-j\beta z} \\
E_y &= \frac{-j\beta n\pi}{k_c^2 b} B_{mn} \sin\frac{m\pi x}{a} \cos\frac{n\pi y}{b} e^{-j\beta z} \\
H_x &= \frac{j\omega\varepsilon n\pi}{k_c^2 b} B_{mn} \sin\frac{m\pi x}{a} \cos\frac{n\pi y}{b} e^{-j\beta z} \\
H_y &= \frac{-j\omega\varepsilon m\pi}{k_c^2 a} B_{mn} \cos\frac{m\pi x}{a} \sin\frac{n\pi y}{b} e^{-j\beta z}
\end{aligned}
\tag{4.9}
$$

As for the TE modes, the propagation constant of the TM mode is real for propagation modes, and imaginary for evanescent modes. The cutoff frequency and cutoff wavelength for TM_{mn} modes is also the same as that of the TE_{mn}, as given in equation (4.3), (4.5), (4.6) and (4.7).

The lowest order TM mode to propagation is the TM_{11} mode with a lowest cutoff frequency of

$$f_{c11} = \frac{1}{2\pi\sqrt{\mu\varepsilon}}\sqrt{\left(\frac{\pi}{a}\right)^2 + \left(\frac{\pi}{b}\right)^2} \tag{4.10}$$

which is seen to be larger than f_{c10}. And its cutoff wavelength is

$$\lambda_{c11} = \frac{2ab}{\sqrt{a^2 + b^2}} \tag{4.11}$$

TM_{11} mode associated with TE_{10} mode is employed in the dual-mode waveguide filter illustrated in section 2.2.2.

4.3 SIW Using Metallic Via-hole Arrays

In general, Substrate Integrated Waveguide (SIW) is the synthesized rectangular waveguide built in the standard PCB or dielectric substrate by placing two discrete metallic via-hole arrays. A typical geometry is shown in Fig. 4.5 in which metallic via-hole arrays fence as narrow walls of the waveguide while the substrate's metal cover and ground plane form the waveguide broad walls. The wave propagation is well confined between two arrays of the metallic via holes which can be considered as non-radiating electric walls from the microwave point of view. Each gap between two via holes can be viewed as a holder to support and prevent the waveguide from falling down from the substrate. An appreciative gap size is critical to minimizing lateral radiation loss or wave leakage [28].

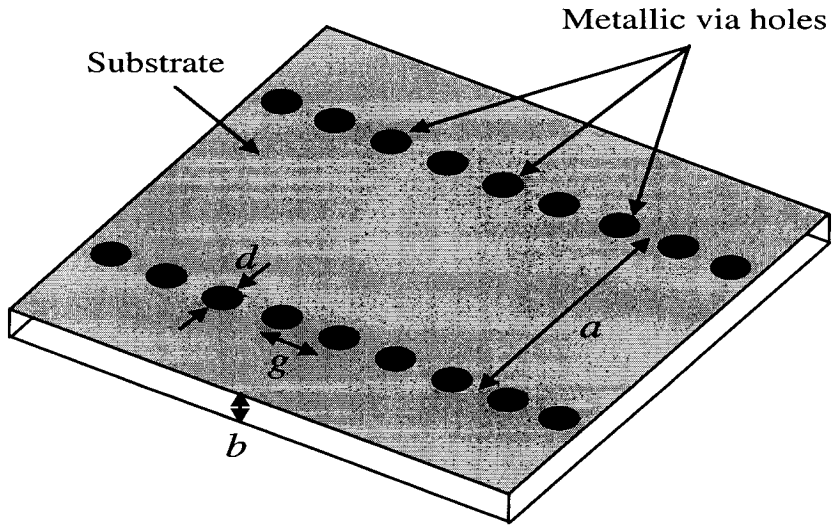

Fig. 4.5 Configuration of the SIW synthesized by metallic via-hole arrays

SIW structures can largely preserve the well-known advantages of conventional three-dimensional metallic rectangular waveguide, namely, a high Q factor and high power capability. On the other hand, its planar structure which offers the merit of reduced size and less complexity makes it easily integrated into microstrip circuits together with other types of passive and active components on the single substrate, which generalize a new concept termed "Substrate Integrated Circuits (SICs)"

4.3.1 Characteristics of SIW

Since SIW actually performs as conventional rectangular waveguide [29], it also can be characterized by a propagation constant, waveguide modes, cutoff frequency and guide wavelength etc.

From equation (4.3), (4.5) and (4.7), it is seen that waveguide characteristics such as β, f_c and λ_g are determined by waveguide geometries a and b of its width and height respectively. There still are discriminations for waveguide geometries between SIW and conventional waveguide although both structure have similar properties. First, comparing with $b/a = 1/2$ in a typical rectangular waveguide, the SIW geometrical parameter a is much larger than b, ($b << a$) since b actually is thickness of the substrate and usually is very thin. In this case, the cutoff frequency f_{cm0} of TE_{m0} is much smaller than that of TE_{mn} ($n \neq 0$) and TM_{mn}, which means TE_{mo} may be the only modes that could propagate in SIW. Second, equivalent waveguide width of SIW a_{eff} is not equal to a or (a-d). Experiments and simulations have verified that value of a_{eff} is between a and (a-d). In [28], an accurate empirical equation is proposed for a_{eff}

$$a_{eff} = a - 1.08\frac{d^2}{g} + 0.1\frac{d^2}{a} \tag{4.12}$$

where a, d and g are the dimensions depicted in Fig. 4.5 and when $d/g < 1/3$ and $d/a < 1/5$. And third, the gap g is subject to conducting wave leakage and make SIW insertion loss increased when g getting bigger. This issue has been focused on, and many researches have proven that by choosing proper ratio of d/g, such wave leakage can be minimized or may be negligible [28]. As a rule, SIW can be modeled by a rectangular

waveguide with an equivalent width and remained radiation loss at a negligible level, when its geometry parameters meet

$$\begin{aligned} d &< \lambda_g / 5 \\ g / d &\leq 2 \end{aligned} \tag{4.13}$$

where λ_g is the guide wavelength related to a_{eff} and it is suggested that λ_g is chose as of the lowest frequency of the band.

4.4 SIW Using Metallic Via-slot Arrays

The technique of SIW using via holes is successfully utilized in many applications of microwave and millimeter wave designs, such as filters, power combiners and circulators in [30] [31] and [32]. However, in these SIW designs the definite equivalent relationships are not given. Since the dispersion characteristics of SIW can be presented by an equivalent rectangular waveguide, a common design procedure is to model a design in real rectangular waveguide structure to an SIW structure by determining equivalent waveguide width a_{eff} and propagation constant β_{eff}. When using this approach, some difficulties may arise when mapping tiny waveguide elements to SIW, like coupling irises and metal inserts whose geometries typically are comparable to the size of a single via hole. From another standpoint, based on equation (4.13) it is known that with very high operating frequency, d of the via hole is greatly reduced. Currently,

fabrication of a metallic via hole involves drilling a hole, inserting a metal pin into the hole and soldering the pin together with substrate metal plates or directly metalizing via holes. Therefore, it becomes more crucial to have via holes positioned precisely to obtain desired performance at very high frequency. As a result, the design and implementation of SIW using metallic via holes much depend on the experience of the designers and many adjustments may be involved.

A novel SIW structure is developed in this work. Instead of via holes, metallic via slots are used to synthesize a rectangular waveguide in the substrate as seen in Fig. 4.6. Similar to SIW using via holes, substrate's metal cover and ground plane, and discrete metallic slots compose of a dielectric rectangular waveguide. The gap g between two slots as a holder sustains the synthesized waveguide on the substrate and appropriate size g will greatly minimize wave leakage or make it negligible.

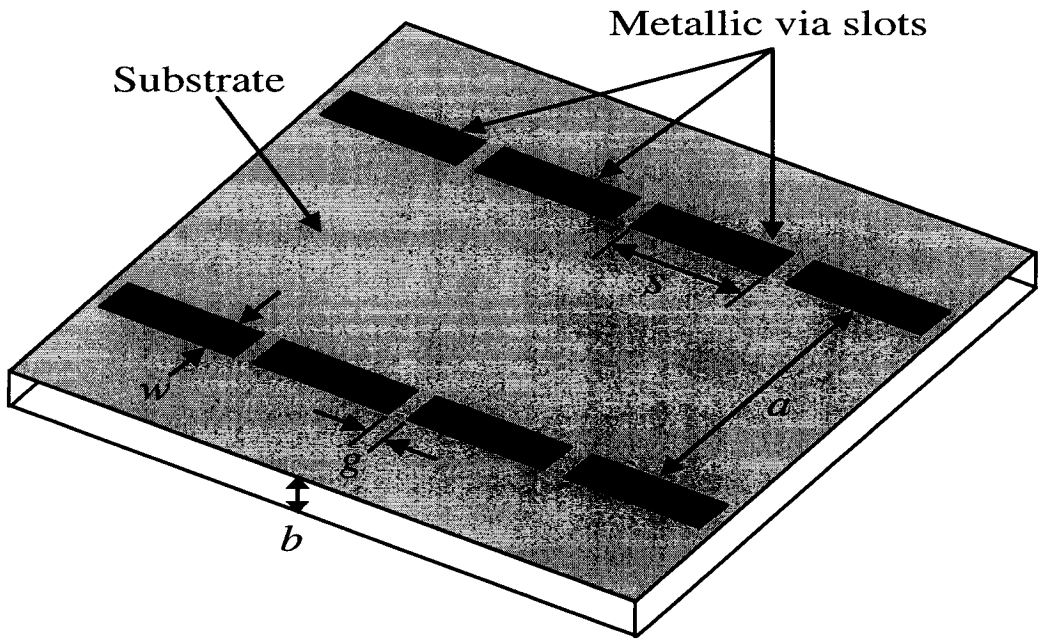

Fig.4.6 Configuration of the SIW synthesized by metallic via-slot arrays

It is obvious that such an SIW structure inherits all properties of the SIW using via holes, like the possibility of integration, small size, high Q factor and high power capacity. The additional advantages of this SIW structure are the facilitation of mechanical processes in which slots are cut by laser beam and then are metallized, capability of precisely mapping tiny waveguide elements to SIW structure without adjustment or very minimum, and simplification of design and implementation of SIW components due to waveguide equivalent propagation constant $\beta_{eff} \approx \beta$ of the rectangular waveguide.

4.4.1 Properties of SIW using Metallic Slots

The characteristics of SIW using metallic slot is also can be depicted by equivalent propagation constants, waveguide modes, cutoff frequency and guide wavelength etc. A unique feature of propagation characters is that when the gap g is small enough, the size of the equivalent waveguide width a_{eff} is approximately equal to the space a between two arrays of the slots in Fig.4.6. It is crucial to design SICs, especially for SIW cavity filters since there is no or very tiny frequency shift. In order to analyze this new SIW structure, a FDFD algorithm developed for modeling guide-wave properties of periodic structures in [33] is used. At the same time, we also apply the numerical calibration technique integrated with commercial simulators [28] to this SIW structure in order to compare the results.

First, a simulation of the SIW structure, as illustrated in Fig.4.6, is performed by FDFD method [33] and numerical calibration technique [28] respectively. The sizes of the SIW are chosen as

s = 3 mm,

w = 0.8 mm,

a = 6.4 mm, and

g = 1.2mm, 0.6mm, and 0.3mm is taken separately.

Fig.4.7, Fig.4.8 and Fig.4.9 show the propagation constants of TE_{10} mode from above proposed simulations and associate a comparison with that of a conventional rectangular waveguide which its width is 6.4 mm.

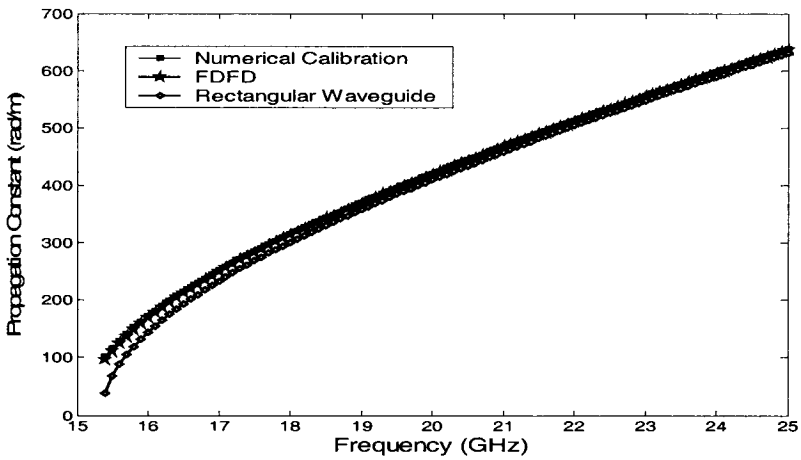

Fig.4.7 Comparison of the TE_{10} mode propagation constant generated by employing the numerical calibration method, the FDFD method and the calculation for a rectangular waveguide which a = 6.4 mm. The gap g = 1.2 mm.

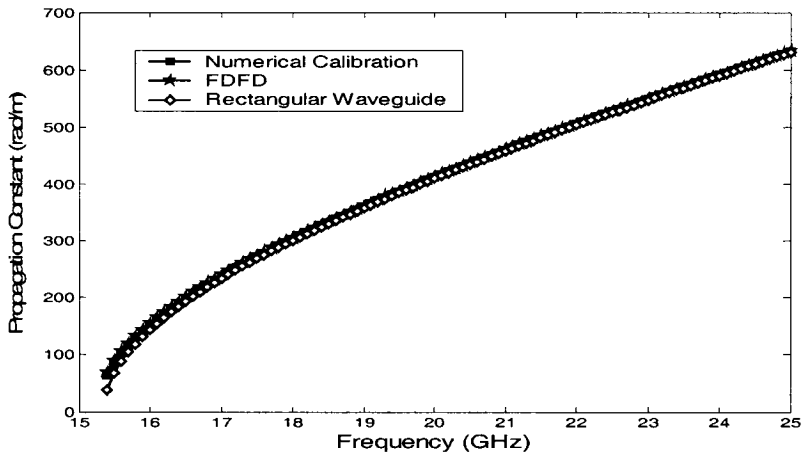

Fig.4.8 Comparison of the TE_{10} mode propagation constant generated by employing the numerical calibration method, the FDFD method and the calculation for a rectangular waveguide which a = 6.4 mm. The gap g = 0.6 mm.

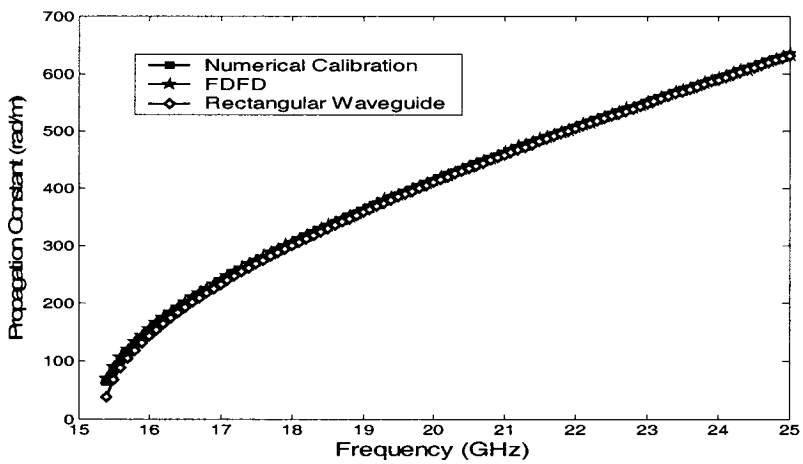

Fig.4.9 Comparison of the TE_{10} mode propagation constant generated by employing the numerical calibration method, the FDFD method and the calculation for a rectangular waveguide which a = 6.4 mm. The gap g = 0.3 mm.

It can be concluded that the propagation constants of the SIW become equal to that of the rectangular waveguide as the gap g is reduced. In other words, the phase bias approaches zero.

Second, we investigate the relation of propagation constants to slot length s while the gap g remains unchanged. For the simulations, the sizes of the SIW in Fig.4.6 is taken as

a = 6.4 mm,

w = 0.6 mm and 0.4mm, separately

s = varied

f = 20 GHz.

Note that it is unnecessary to consider influences of frequency change for dispersion characteristics since the SIW can be equivalent to a rectangular waveguide. From Fig.4.10 and Fig.4.11, it is demonstrated that with slot length s gradually increasing, the propagation constant of the SIW decreases and approximately trends stable which is the value of propagation constant of a rectangular waveguide with width a.

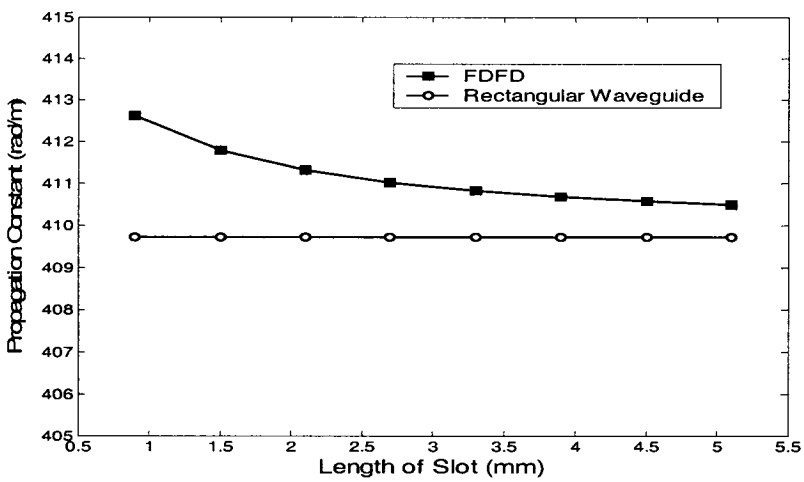

Fig.4.10 propagation constant versus slot length s, when g = 0.6 mm

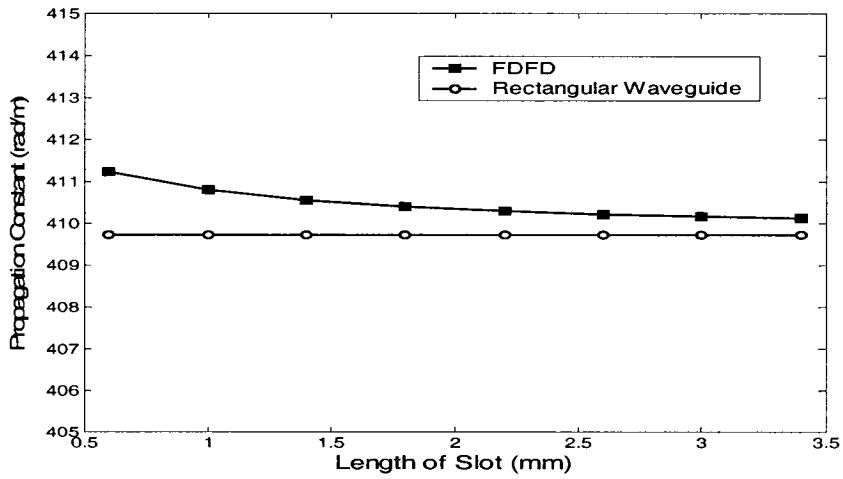

Fig.4.11 propagation constant versus slot length s, when g = 0.4 mm

Both theory and simulation suggest that it is a good choice of ratio $g/a < 1/20$ and $g/s < 1/10$. From a design point of view, such a SIW using metallic via slots can be treated as a conventional rectangular waveguide whose wide wall size a is equal to that space between two rows of slots in SIW. This means that a design in conventional waveguides can be directly transferred and mapped to a design in SIW using metallic via slots without any real waveguide dimension changed. It will greatly simplify designs of SICs.

4.4.2 Realization of SIW using Metallic Slots

Realization of the SIW is an operation of mapping physical structures of waveguide circuit components on a substrate by using metallic via-hole arrays or via-slots arrays. The process may involve enlarging or shrinking sizes of original design in waveguide

since SIW a_{eff} is not equal to the width a of the waveguide. Different from SIW using via holes whose a_{eff} is determined by the diameter of via holes and the space between two holes, the a_{eff} of the SIW using via slots is mainly related to the size of gap between two slots, when $g/s < 1/10$. To account for how gaps affecting SIW mapping scales, we were motivated to conduct a study on a resonant cavity by using FDFD method and HFSS simulation to determine the relationship of the gap size and position to the resonant frequency shift. As shown in Fig.4.12, two group of sizes of a SIW resonant cavity, a = 12 mm, b = 12 mm; and a = 16 mm, b = 12 mm, are calculated by FDFD algorithm. As the results, Table 4.1 and Table 4.2 give the comparison of resonant

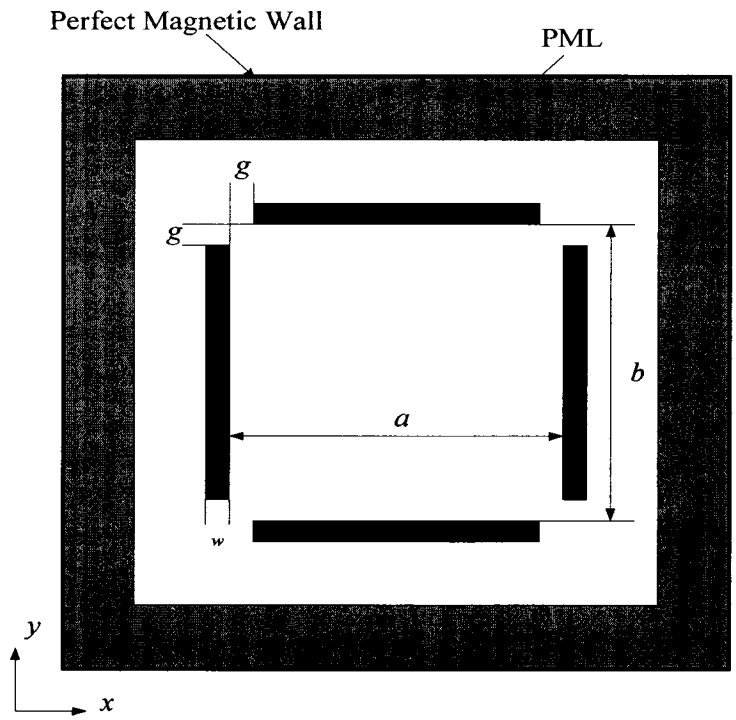

Fig.4.12 Configuration of FDFD Algorithm for SIW Resonant Cavity

frequency of SIW cavity with slots by using FDFD method with the data of rectangular resonant cavity in the same sizes of a and b.

Table 4.1 The Comparison of Resonant frequencies of TE_{101} mode of SIW resonant cavity and rectangular waveguide resonant cavity (a=12mm, b=12mm)

a=12mm b=12mm	Resonant Frequency of TE_{101} Mode (GHz)		
	Theoretical	SIW cavity	Error (%)
g=0.8mm	11.581 (no leakage)	11.578	2.59e-4
g=1.2mm		11.575	5.18e-4
g=1.6mm		11.564	1.47e-3

Table 4.2 The Comparison of Resonant frequencies of TE_{101} mode of SIW resonant cavity and rectangular waveguide resonant cavity (a=16mm, b=12mm)

a=16mm b=12mm	Resonant Frequency of TE_{101} Mode (GHz)		
	Theoretical	SIW cavity	Error (%)
g=0.8mm	10.236 (no leakage)	10.235	9.77e-5
g=1.2mm		10.233	2.93e-4
g=1.6mm		10.228	7.82e-4

From the tables, it is seen that the leakage from the gaps is minimal and the resonant frequency remains unchanged. We also notice that, even though $g/a > 1/20$, there still is no distinct frequency shift, of which the worst case is only 17 MHz ($g/a = 0.133$). This phenomenon is further explored by viewing distribution of electromagnetic field in

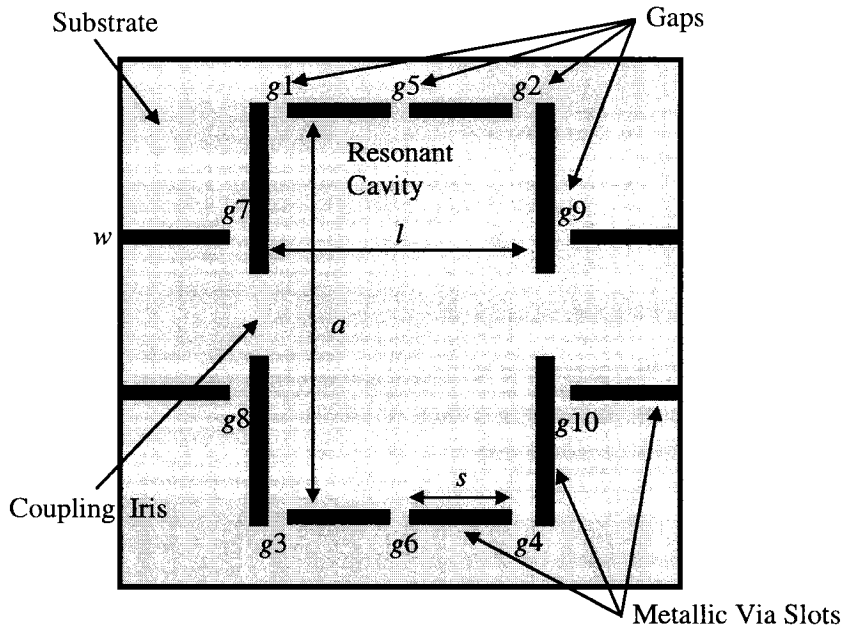

Fig.4.13 A Dual-mode SIW Cavity Filter Synthesized using Metallic Via Slots

a dual-mode resonant cavity as illustrated in Fig.4.13. The filter employs H-plane iris coupling structures and its dual-mode cavity supports a pair of TE_{102} and TE_{301} degenerate modes. Four gaps, $g1$, $g2$, $g3$ and $g4$ are placed at each corner of the rectangular cavity while gaps, $g5$ and $g6$ are settled at middle of the narrow walls where the field may be very strong. HFSS simulator then is used to picture the filed distribution in this SIW cavity and, for a purpose of comparison; the filed distribution in a cavity with the same sizes but without gaps is also drawn in Fig.4.14. Both resonant modes TE102 and TE301 in different cavities are captured. By viewing and comparing the figures with one another, we found that the gaps, $g1$ to $g4$ at the corner of the cavity do not lead wave leakage since strength of the field there is zero and the gaps, $g5$ and $g6$

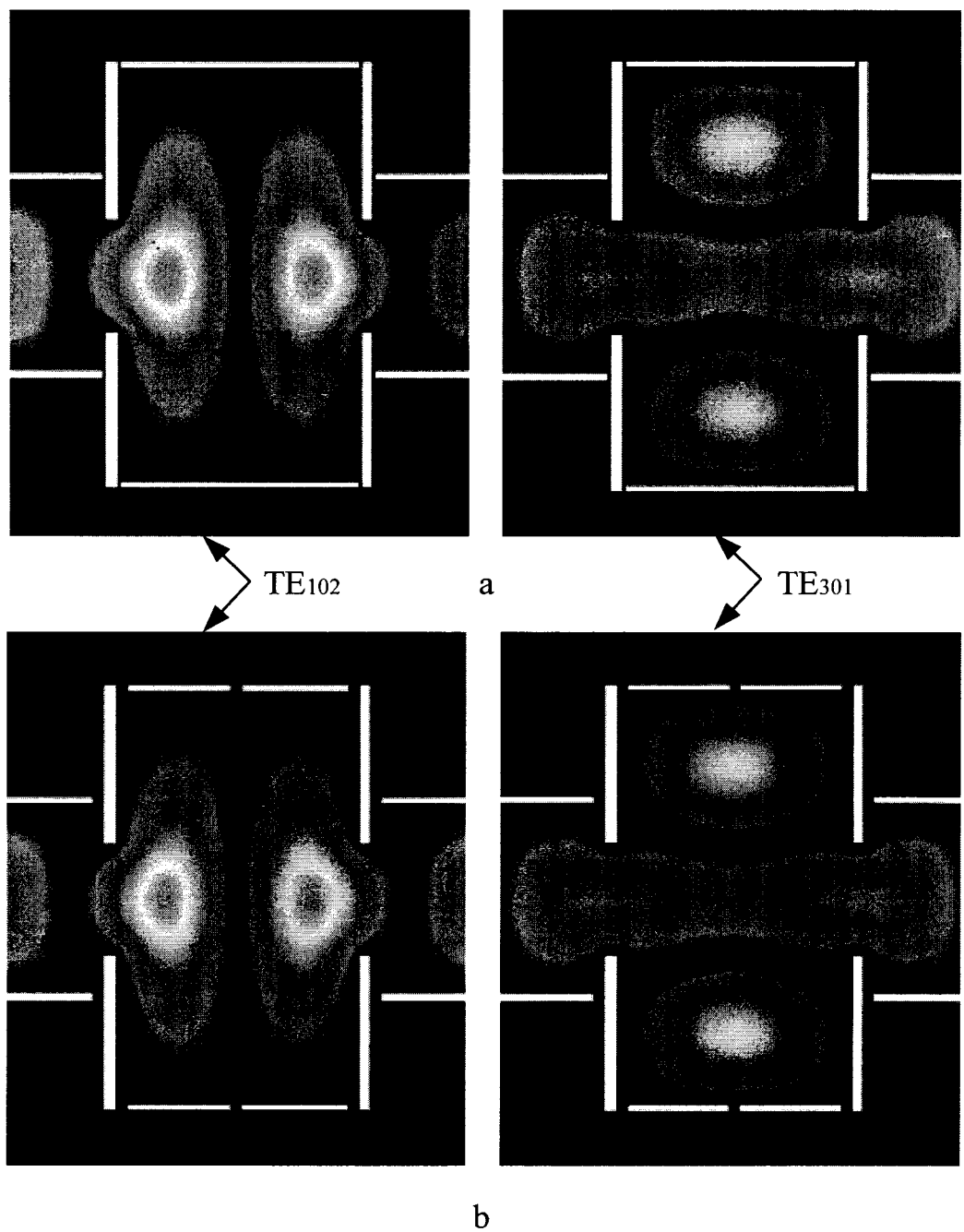

Fig.4.14 Field Distributions in the Dual-mode Cavities. a. TE_{102}/TE_{301} Modes in a Cavity without gaps, b. TE_{102}/TE_{301} Modes in a Cavity with gaps

should not disturb the mode TE_{102} much, where its fields are very weak. It is assumed that gaps of $g5$ and $g6$ may affect TE_{301} mode and conduct a shift of resonant frequency due to related strong field there. To further validate the resonant frequency shift, we perform simulations for the frequency response of the filter in three different groups of gaps settings by using HFSS simulator. The first group of gaps according to Fig.4.13 is set for

$g1 = g2 = g3 = g4 = 10$ mil,

$g5 = g6 = 0$,

$s = 126$ mil,

$a = 476.5$ mil,

$l = 272$ mil,

and the second group is

$g1 = g2 = g3 = g4 = 20$ mil;

$g5 = g6 = 0$;

$s = 116$ mil,

and the third is

$g1 = g2 = g3 = g4 = 30$ mil;

$g5 = g6 = 0$;

$s = 106$ mil.

The corresponding frequency responses for each group setting are presented in Fig.4.15 (b), (c) and (d), respectively. By comparing with Fig.4.15 (a) which shows the performance of that cavity without any gap, or $g1 = g2 = g3 = g4 = g5 = g6 = 0$, It seems

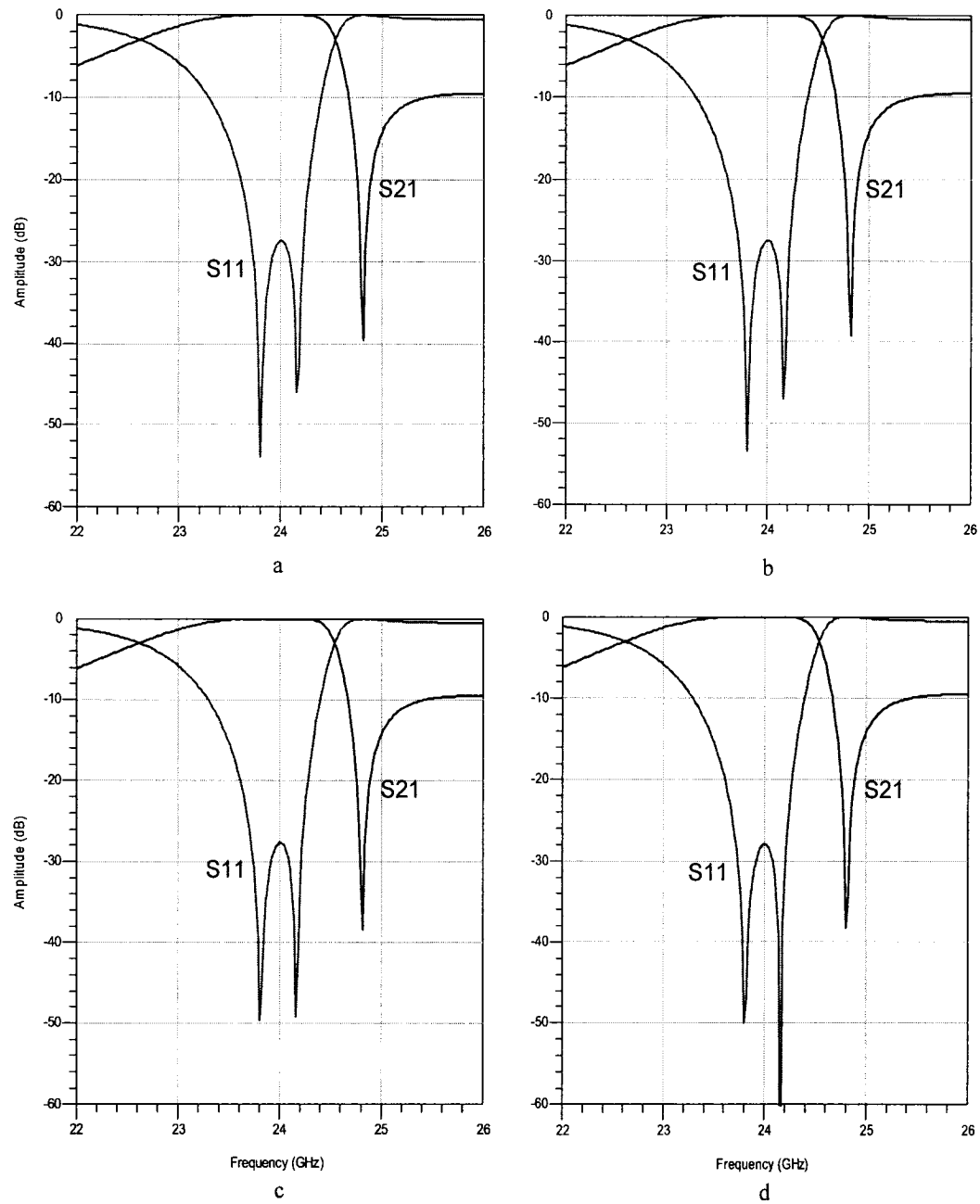

Fig.4.15 Responses of the Dual-mode Filter according to Fig.4.13. a. No gaps, b. Group I, 10 mil gaps. c. Group II, 20 mil gaps. d. Group III, 30 mil gaps.

that there is no distinct frequency shift among them. We confirmed this by plotting four responses simultaneously together in Fig.4.16. It may be clearly seen that all results coincide well with one another and frequency shift cannot be distinguished.

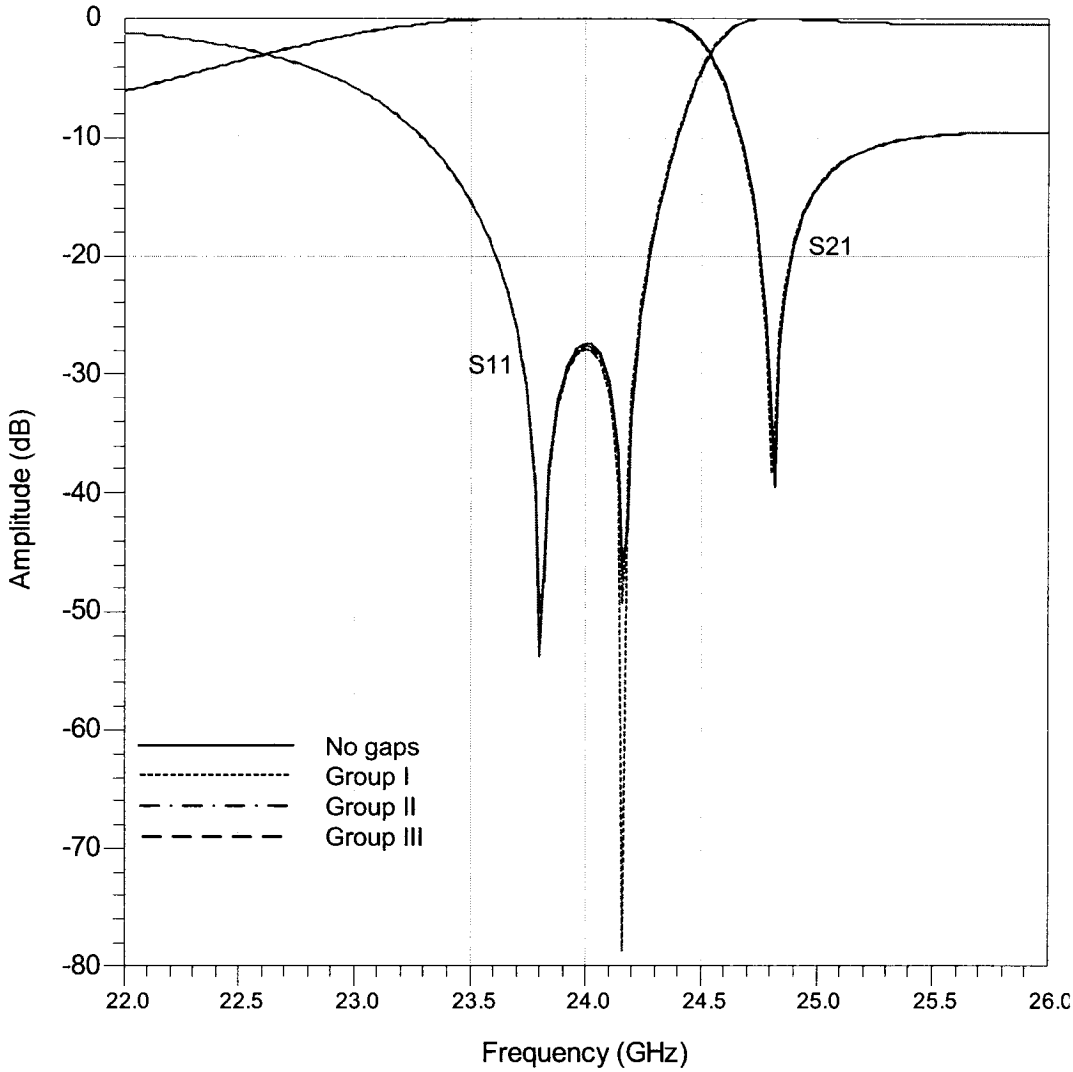

Fig.4.16 Comparison of the Frequency Responses from Four Different Gap Settings, Frequency shift cannot be Distinguished

Based on theoretical calculation and analytical simulation, these results clearly demonstrate that gaps at the corners of a resonant cavity do not lead to shift of resonant frequency, or are minimal enough to be ignored in engineering. Next we move our interests to the gap at the middle of the cavity, such as $g5$ and $g6$, where the field is the strongest along the cavity walls. To keep the gaps radiationless or leakage loss free, parametric effects of size g and s have to be studied. We start such an investigation by HFSS simulator for an initial gap setting according to Fig.4.13

$g1 = g2 = g3 = g4 = 0$,

g5 = g6 = 10 mil,

s = 131 mil,

a = 476.5 mil,

l = 272 mil,

and the next gap setting is

$g1 = g2 = g3 = g4 = 0$,

g5 = g6 = 20 mil,

s = 126 mil.

The frequency responses from these two different gap settings are shown in Fig.4.17.a as well as Fig.4.17.b, respectively and the results are compared in Fig.4.17.c and Fig.4.17.d with the frequency response of which cavity without gap. It can be observed from Fig.4.17.c that the cavity with the first gap setting in which $g5$ and $g6$ are equal to10 mil, has the performance agreed well with that of cavity without gaps, namely no distinguished frequency shift existed from Fig.4.17.c. This verifies the design

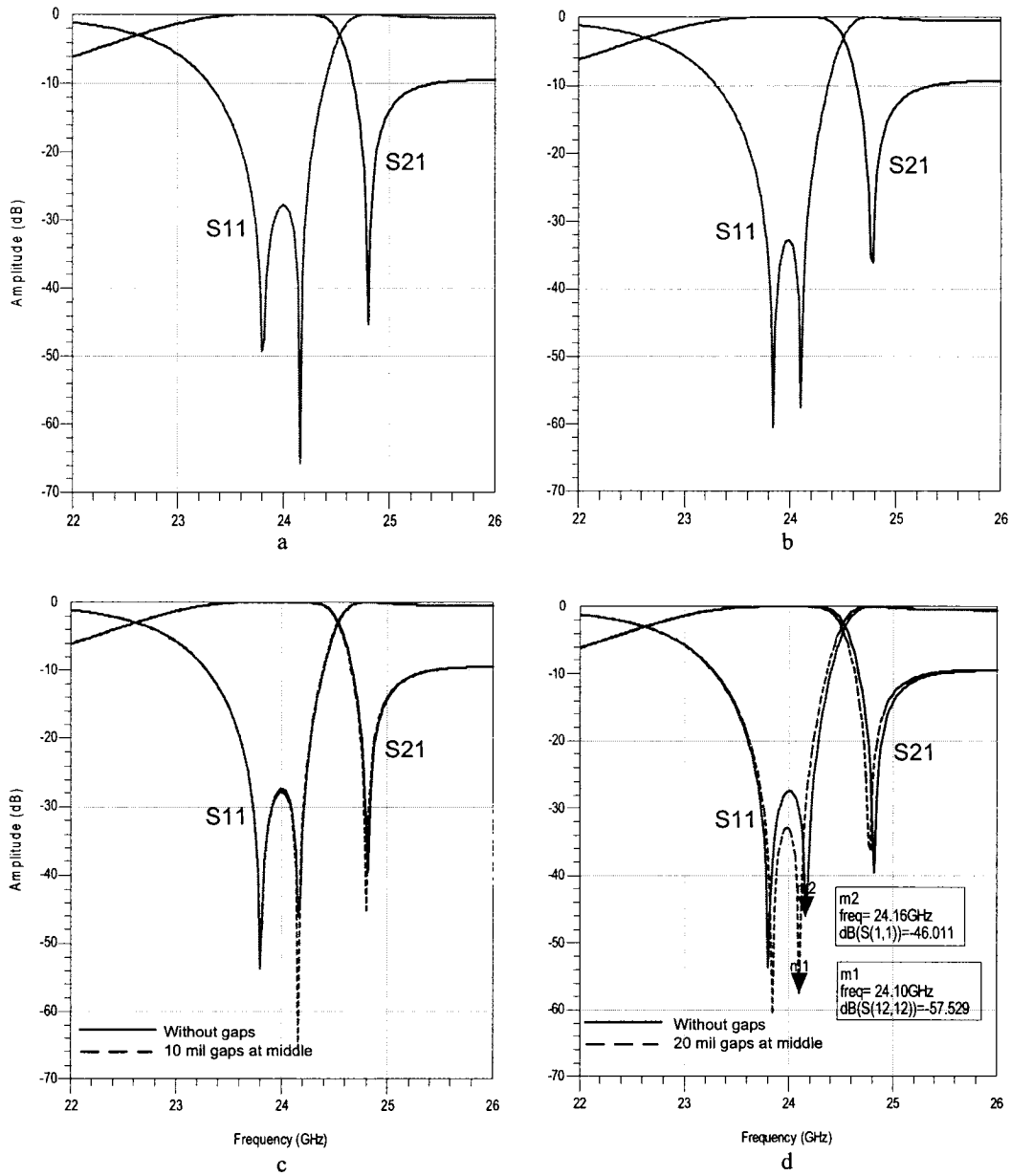

Fig 4.17 Responses of the Dual-mode Filter according to Fig.4.13. a. $g5 = g6 = 10$ mil, b. $g5 = g6 = 20$ mil, c. Comparison Response in Fig.4.17.a with which without gap, d. Comparison Response in Fig.4.17.b with which without gap

approach that requires the geometric parameters of gap size g, slot length s and waveguide width a have to be satisfied with $g/s < 1/10$ and $g/a = 1/20$, in this case, $g/s = 10/131$ and $g/a = 10/272$. For second gap setting which $g5 = g6 = 20$ mil and $s =$ 126 mil, we anticipate there may have frequency shift due to the ratio of $g/s = 20/126 > 1/10$ and it is validated by Fig.4.17.d in which maximal frequency shift reaches 60 MHz.

4.4.3 Summary and Design Examples

It is summarized that the technique of SIW synthesized using metallic via slots takes advantage of allowing the ratio of gap size to slot length g/s varied to fit in physical dimensions of waveguide circuit components. Two design rules are conducted from both theory and simulation results not only to ensure SIW radiation loss at a negligible level, or leakage, but, more importantly, to make structure mapping from the RW to the SIW nearly perfect with scale factor 1:1, or without any change of physical size .

$$g/s < 1/10 \tag{4.14}$$

$$g/a < 1/20 \tag{4.15}$$

These two rules are sufficient enough for placing slots with a gap at any section of SIW structure, but not always necessary. For instance, a gap at the corner of a cavity

larger than one tenth of slot length or one twentieth of guide width can be laid without shifting resonant frequency distinctly. Selecting gap locations in a SIW structure is flexible and gap size can be adjusted depending on the strength of electromagnetic field there. It is always advisable to avoid locating gap where the field is very strong while a corner is the first choose for setting a gap. The rule to follow is the stronger field, the smaller gap.

As a completely design example, a dual-mode SIW cavity filter according to Fig.4.13 is built in a substrate (Rogers RT/Duriod 6002, $\varepsilon_r = 2.94, \tan\delta = 0.0012$ at 10 GHz, thickness 10 mil) and its geometric dimensions are

a = 476.5 mil,

l = 272 mil,

$g1 = g2 = g3 = g4$ = 20 mil,

g5 = g6 = 10 mil,

g7 = g8 = g9 = g10 = 10 mil

s = 111 mil,

w = 10 mil,

coupling iris thickness 15.3 mil, coupling window width 127.4 mil and input/output waveguide width 218.7 mil. Simulation results from HFSS in Fig.4.18.a. show that the filter has a center frequency at 24 GHz with a bandwidth of 500MHz. There are two transmission poles corresponding to two degenerate modes and a transmission zero appeared at 24.8 GHz. The maximum return loss of the filter is -28 dB. A comparison of responses between this SIW filter and an RW filter with the same geometric dimensions

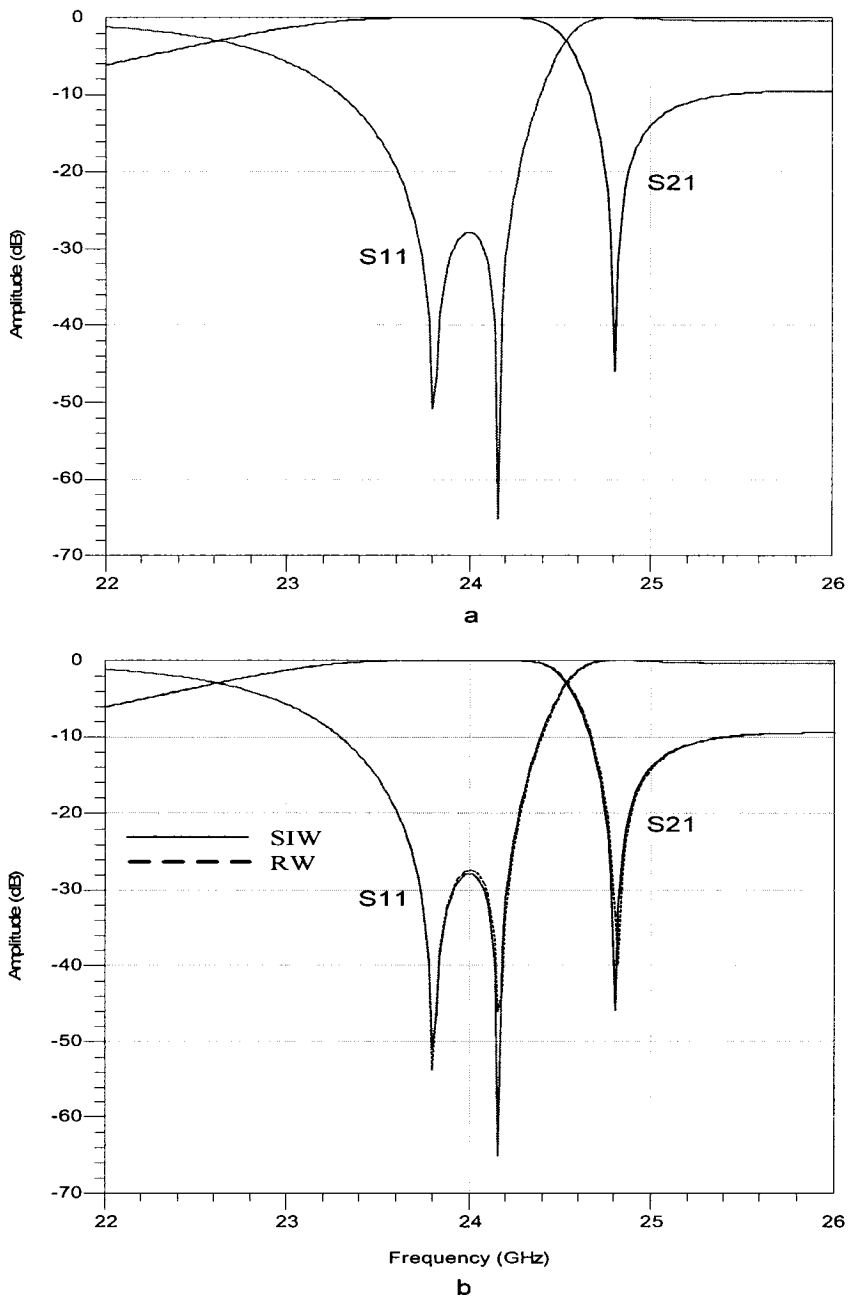

Fig.4.18. a. Response of the dual-mode SIW cavity filter. b. Comparison of the SIW filter with a RW filter having exact same structure and geometric dimensions except all gaps = 0.

except that all gaps are taken to become zero. As shown in Fig.4.18.b, the two results are in an excellent agreement with one another, and no distinct frequency shift emerges. It demonstrates a success in mapping an RW dual-mode filter to an SIW structure without any scaling of the physical dimensions.

4.5 Transitions of SIW to Microstrip

4.5.1 Introduction

In SICs concept, SIW circuit components can be easily connected with other planar passive or active devices by various transitions. This kind of transitions actually acts as a transformer for mode conversion and impedance match between the SIW and the planar

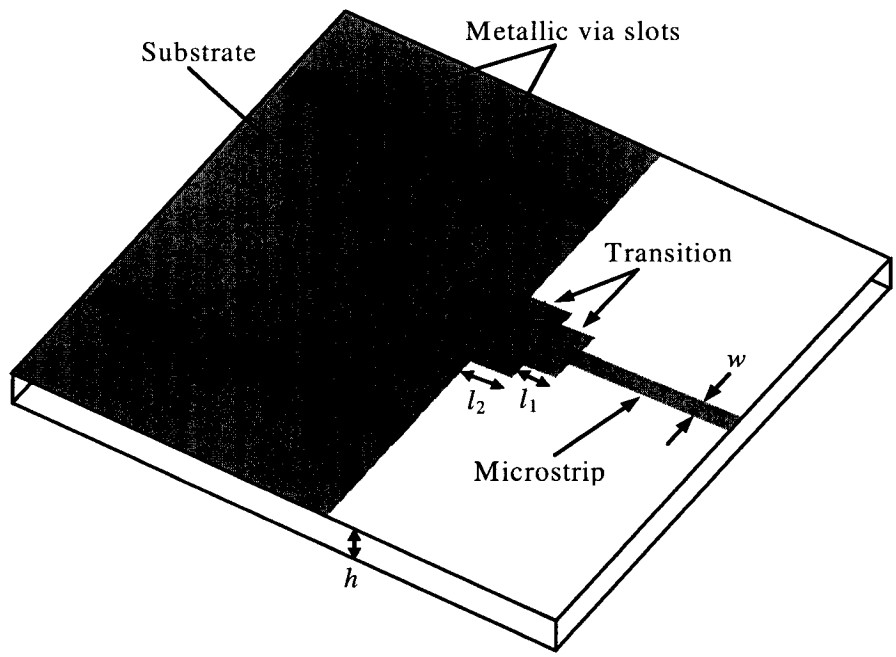

Fig.4.19 Schematic View of Proposed Transition between SIW and Microstrip

transmission line. The first transition reported in 2001 has involved use of a tapered microstrip line [27]. The other transitions presented can be classified by transformations of coplanar waveguide (CPW) and microstrip probes [34] [16]. In this thesis, a microstrip stepped transformer is preferred for transition of the SIW to microstrip as illustrated in Fig.4.19.

It is well known that stepped quarter-wave transformer is a useful and practical circuit for impedance matching with a quite simple transmission line structure [83]. Based on circuit theory, if a quarter-wave long transmission line section of characteristic impedance Z_1 is connected between the feed line of characteristic impedance Z_0 and the load Z_L, then a perfect match is achieved when

$$Z_1 = \sqrt{Z_0 Z_L} \tag{4.16}$$

However, the impedance match is perfect only at a single frequency, and thus it is insufficient in most applications. Therefore, a multi-section transformer is necessary to obtain a match over wider bandwidth. Fig.4.20 is presenting a model for a two-section stepped quarter-wave transformer corresponding to the transition structure in Fig.4.19. Z_0 stands for characteristic impedance of microstrip and Z_L represents characteristic impedance of SIW guide. Those two stepped microstrip transmission lines have a length $\lambda/4$ and characteristic impedance $Z_1$and Z_2, respectively. To make $\Gamma = 0$ looking into the $\lambda/4$ matching section, the equation (4.16) is extended as

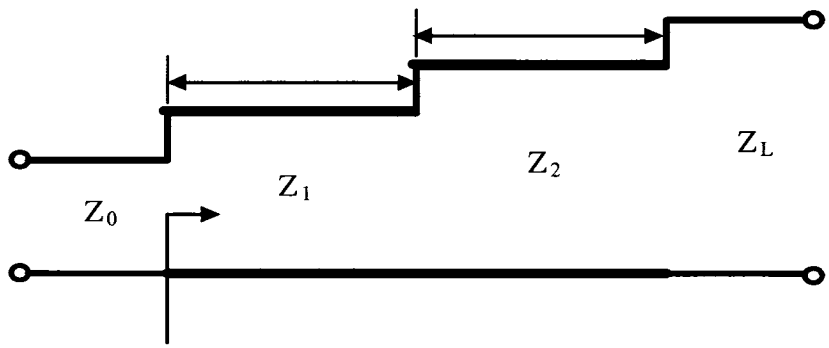

Fig.4.20 A Two-section Stepped Quarter-wave Matching Transformer

$$Z_1 = \sqrt{Z_0\left(Z_2^2 / Z_L\right)}$$

It can be rewritten as

$$Z_1 / Z_2 = \sqrt{Z_0 / Z_L} \tag{4.17}$$

It must be noticed that the results still only give a perfect impedance match at a single frequency, although this two-section stepped quarter-wave transformer has a binomial passband frequency response which is as flat as possible near the design frequency.

On the other hand, a transition is required for mode conversion. We mentioned in section 4.3.1 that SIW can only support the TE modes propagation while TM modes cannot be guided due to the nature of the SIW structure. This property will benefit transferring exited microstrip mode to waveguide TE_{10} mode through the stepped

microstrip sections, or vice versa, because both modes have the same vertical polarization on electric fields.

4.5.2 Transition Design

Two transitions of SIW to microstrip are designed at center frequency 24 GHz on different substrates whose specifications are listed in Table 4.3 and Table 4.4, respectively.

Table 4.3 Substrate Specification I

RT / Duroid ® 6002	Typical Values (10GHz / 23°)
Dielectric constant	2.94 ±0.04
Dissipation factor	0.0012
Magnetic constant	1
Coefficient of thermal expansion in X and Y	16 ppm/°C
Coefficient of thermal expansion in Z	24 ppm/°C
Thickness	0.254 mm

Table 4.4 Substrate Specification II

Substrate ® 996	Typical Values
Dielectric constant	9.9
Dissipation factor	0.001
Alumina Content	99.6% (Weight %)
Coefficient of thermal expansion	7.0 ppm/°C
Hardness	87
Thickness	0.254 mm

The procedure for designing the proposed synthesized transitions according to Fig.4.19 involves the following steps:

1. computing the width w of microstrip line with $50\,\Omega$ characteristic impedance on selected substrate,
2. determining characteristic impedance Z_L of the SIW guide by HFSS simulator, which is power-current definition of the characteristic impedance Z_{pi}..
3. calculating Z_1/Z_2 from equation (4.17), and then choosing Z_1 and Z_2 for a binomial response.
4. determining microstrip steps w_1 and w_2 by Z_1 and Z_2. Initial values of l_1 and l_2 can be a quarter-wavelength of the microstrip mode.
5. using HFSS to simulate and optimize the transformer for desired responses.

The first synthesized transition is built on Rogers RT / Duroid 6002 substrate of thickness 10mil with dielectric constant ε_r 2.94. By following the design procedure 1 to 5, we finally get the transition geometric parameters as

a = 218.7 mil, Z_L = 17.7 Ω (Z_{pi} definition),

Z_0 = 50 Ω , w = 25.4 mil,

Z_1 =35.5 Ω , w_1 = 42 mil,

Z_2 =28.5 Ω , w_2 = 56.4 mil,

l_1 = 48.6 mil, l_2 = 29.6 mil,

and relevant simulated S parameters of a back to back transition are shown in Fig.4.21 and Fig.4.22. A return loss of -42 dB at the center frequency and a maximum of -23 dB

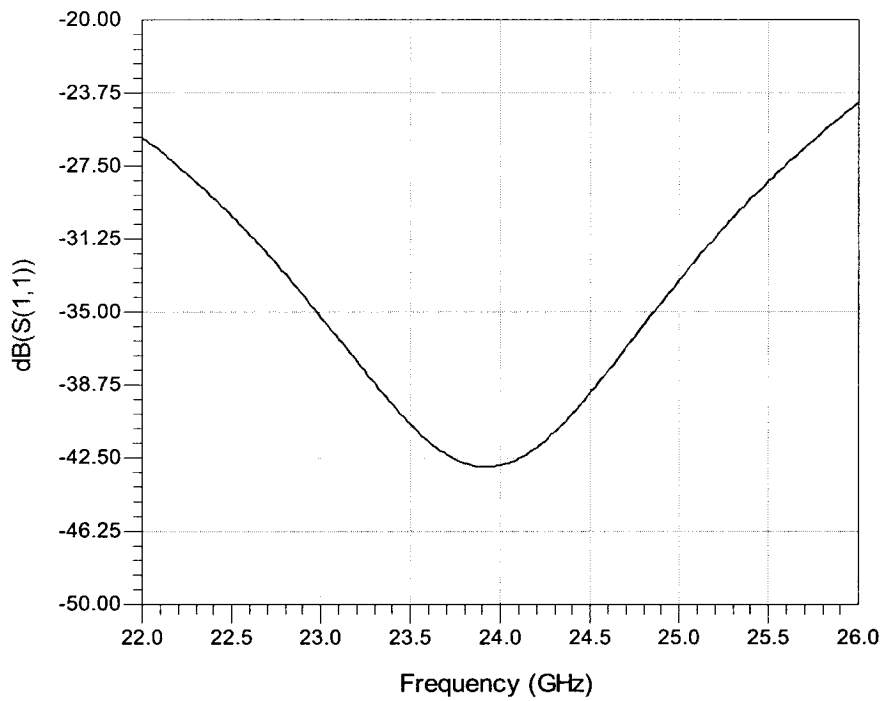

Fig.4.21 Return Loss of the Transition on Duroid 6002 Substrate

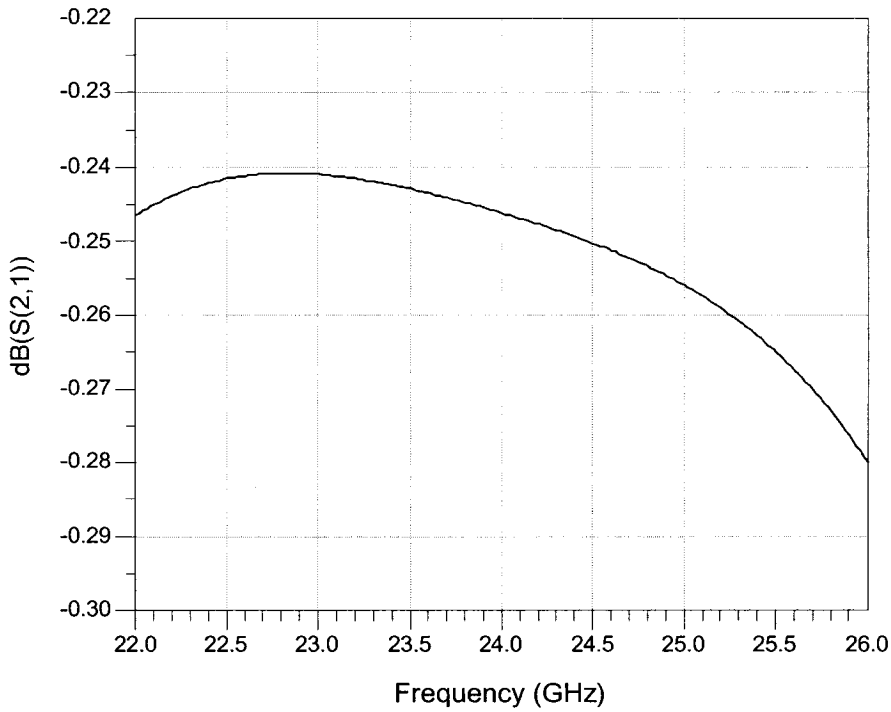

Fig.4.22 Insertion Loss of the Transition on Duroid 6002 Substrate

over a bandwidth of 22 GHz through 26 GHz, is obtained. The insertion loss in the passband is better than -0.28 dB.

The second designed transition is implemented on the ceramic 996 substrate of thickness 10 mil with dielectric constant $\varepsilon_r = 9.9$. Following the step 1 to step 5 of the design procedure, the geometric parameters of transition are found

$a = 119.2$ mil, $Z_L = 17.3\,\Omega$ (Z_{pi} definition),

$Z_0 = 50\,\Omega$, $w = 9.6$ mil,

$Z_1 = 35.6\,\Omega$, $w_1 = 18.1$ mil,

$Z_2 = 22.4\,\Omega$, $w_2 = 36.8$ mil,

$l_1 = 37.7$ mil, $l_2 = 19.7$ mil.

The frequency responses of the back to back transition are plotted in Fig.4.23 and Fig.4.24. A return loss of -49 dB at the center frequency and a maximum of -23 dB over a bandwidth of 22 GHz through 26 GHz, is achieved. The insertion loss in the passband is better than -0.58 dB.

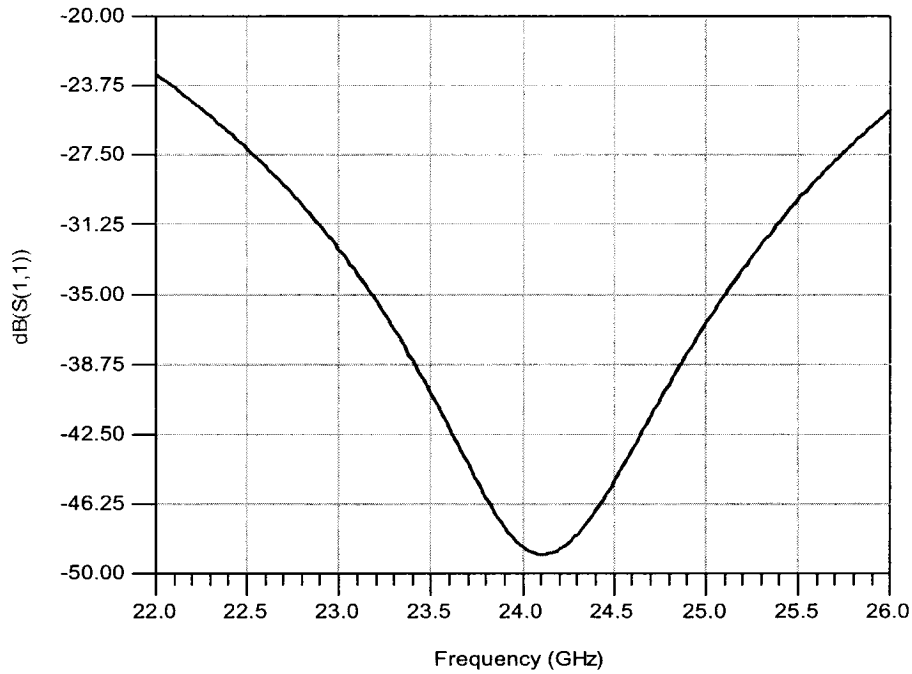

Fig.4.23 Return Loss of the Transition on ceramic 996 substrate

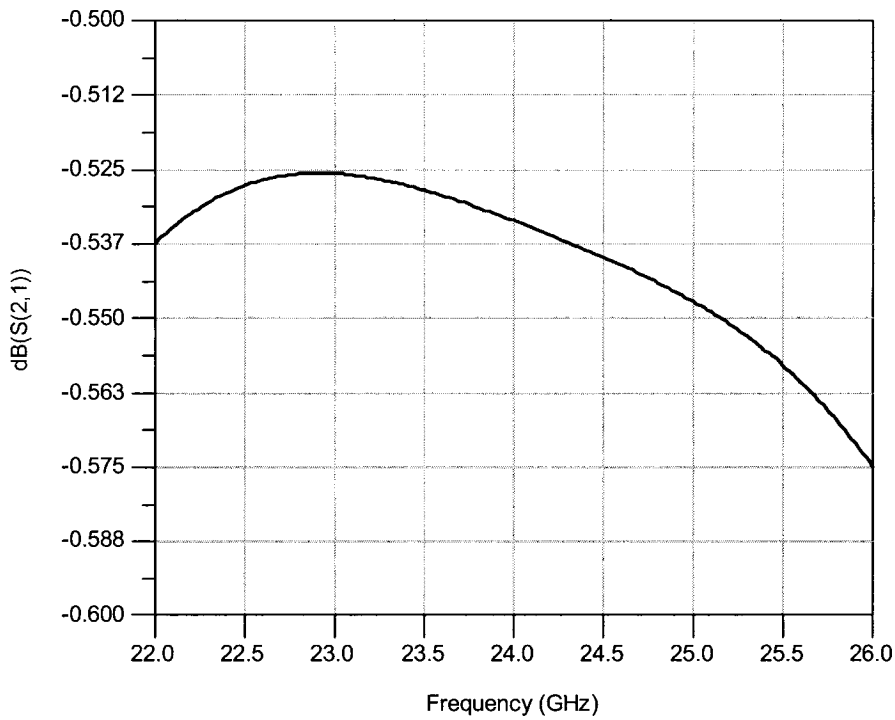

Fig.4.24 Insertion Loss of the Transition on Ceramic 996 substrate

CHAPTER 5

DESIGN AND IMPLEMENTATION OF SIW E-PLANE COULPING DUAL-MODE CAVITY FILTERS

5.1 Introduction

The main issues related to the design of the proposed filters consist of the following:

1. dual-mode RW cavity with non-intracavity coupling described in Chapter 1 is preferred due to its property of only TE_{mop} modes employed, which is the exclusive solution harmonizing with the nature of the SIW;
2. a two-cavity cascaded structure is desired to generate four poles and two TZs which will be symmetrically located at each side of the passband to increase frequency selectivity and meet the demand of stopband rejections;
3. performance of low insertion loss will be ensured by three essential factors, high Q factor of SIW dual-mode cavity (around 500), compact size of the SIW filter (two cavities for four poles) and low dissipation substrate ($\tan\delta = 0.0012$ at 10 GHz of Duroid 6002),
4. coupling structure of E-plane metal insert is preceded with that of H-plane iris because of its flexibility of realizing required couplings to dual cavity modes simultaneously, and its good performance at millimeter wave frequency.

We start the first part of this chapter with the design concept of SIW dual-mode resonant cavity and its corresponding unloaded Q factor. The overall insertion loss in the passband is evaluated by determined Q factor. Then realization of negative

coupling with different coupling structures has been explored. At the end of the chapter, two procedures for designing dual-mode cavity filter using k inverters, coupling equivalent circuits or coupling matrix are given in details.

5.2 SIW Dual-mode Resonant Cavity and Its Q Factor

Microwave resonators are of great importance for filter circuits. Similar to the operation of the lumped element resonator circuit, the characteristics of resonators, such as resonant frequency, 3-dB bandwidth, Q factor and coupling coefficient, etc. are used to describe a microwave resonator. But the great difference exists between their structures that microwave resonators can be constructed from closed metallic sections of waveguide. The most common type of different microwave resonators is rectangular waveguide resonator, or rectangular resonant cavity, which is illustrated in Fig. 5.1.

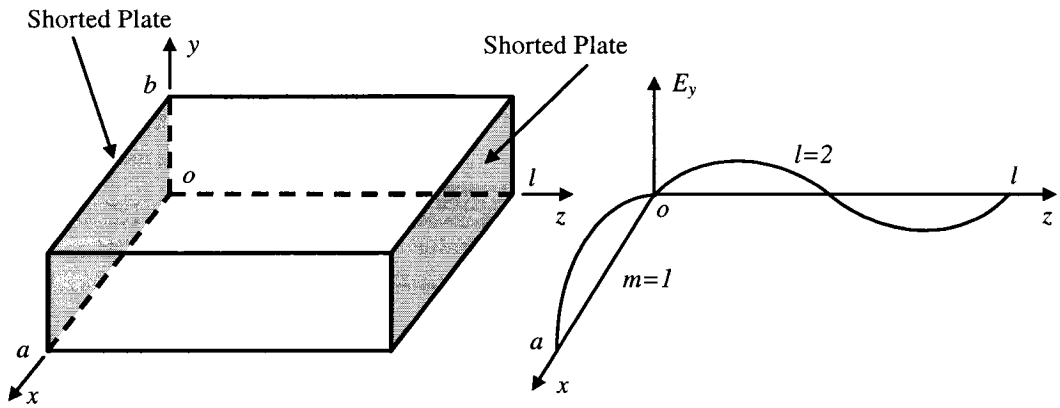

Fig.5.1. A Rectangular Resonant Cavity, and Electric Field Distribution for the TE_{102} Resonant Mode

The geometry of a rectangular resonant cavity includes a height b, width a, and length l. It may be considered as a section of rectangular waveguide terminated with shorted plates at both ends ($z = 0$, $z = l$). If l is a multiple of a half guide wavelength, λ_g long at the frequency f, the electromagnetic wave will be reflected by the shorted plate at $z = l$, which results a standing wave, and makes a null of electric field at $z = o$. As an example, electric field distribution for the TE_{102} resonant mode can be viewed in Fig. 5.1. It would not changed the original field distribution when a shorted plate is introduced at $z = {}^{n\lambda_g}/_{2}$, where n is an integer number. The rectangular cavity is thus a waveguide version of the short-circuited ${}^{\lambda_g}/_{2}$ transmission line resonator. The sides a and b of the cavity also can be extended and then multiple higher order modes will be excited simultaneously. For SIW cavity, all the resultant solutions deducted for the rectangular cavity can be directly applicable to its SIW counterpart except that SIW cavity supports TE_{mnp} modes only since TM modes cannot be resonated due to the nature of very small height b.

5.2.1 SIW Dual-mode Cavity Design and Its Resonant Frequency

To a rectangular resonant cavity, field solutions corresponding to the TE modes with respect to the x, y and z axes can be deducted as in [25]

$$\overline{E}_t(x,y,z) = \bar{e}(x,y)\left[A^+ e^{-j\beta_{mn}z} + A^- e^{-j\beta_{mn}z}\right] \tag{5.1}$$

where $\bar{e}(x,y)$ is the transverse variation of the mode, and A^+, A^- stand for arbitrary amplitudes of the forward and backward traveling waves. For the *m, n*th TE mode, the propagation constant is given by

$$\beta_{mn}^2 = k^2 - \left(\frac{m\pi}{a}\right)^2 - \left(\frac{n\pi}{b}\right)^2 \tag{5.2}$$

where $k = \omega\sqrt{u\varepsilon}$, and u, ε are the permeability of permittivity the material filling the cavity.

Note that $\overline{E}_t = 0$ at $z = 0$ to equation (5.1) suggests $A^+ = A^-$ because of reflection from a perfectly conducting plate. Thus the condition that $\overline{E}_t = 0$ at $z = l$ brings the equation

$$\overline{E}_t(x,y,l) = -\bar{e}(x,y)A^+ 2j\sin\beta_{mn}l = 0 \tag{5.3}$$

since $A^+ \neq 0$, solution thus occurs for

$$\beta_{mn}l = p\pi, \qquad p = 1,2,3,\cdots \tag{5.4}$$

which impose that the cavity must be a multiple of a half guide wavelength long.

Substituting equation (5.4) for (5.2), the corresponding cutoff wavenumber for the rectangular cavity is given

$$k_{mnp} = \sqrt{\left(\frac{m\pi}{a}\right)^2 + \left(\frac{n\pi}{b}\right)^2 + \left(\frac{p\pi}{l}\right)^2} \tag{5.5}$$

where m, n, p are indexes of the TE_{mnp} modes and refer to the number of half standing wave in the respective x, y and z directions. These particular values of k_{mnp} bring the resonator frequencies of the cavity

$$f_{mnp} = \frac{ck_{mnp}}{2\pi\sqrt{\mu_r\varepsilon_r}} = \frac{c}{2\pi\sqrt{\mu_r\varepsilon_r}}\sqrt{\left(\frac{m\pi}{a}\right)^2 + \left(\frac{n\pi}{b}\right)^2 + \left(\frac{p\pi}{l}\right)^2} \tag{5.6}$$

In a dual-mode cavity, both degenerated mode resonate at the same frequency. The equation (5.7) can be found from equation (5.6) as

$$f_{mnp} = f_{ijk},$$

$$\left(\frac{m\pi}{a}\right)^2 + \left(\frac{n\pi}{b}\right)^2 + \left(\frac{p\pi}{l}\right)^2 = \left(\frac{i\pi}{a}\right)^2 + \left(\frac{j\pi}{b}\right)^2 + \left(\frac{k\pi}{l}\right)^2 \tag{5.7}$$

where the subscripts m, n, p refer to the first resonant mode TE_{mnp} while i, j, k refer to the second TE_{ijk}. In SIW cavity, as explained previously that only TE_{mop} exist, thus equation (5.7) is simplified to

$$\left(\frac{m\pi}{a}\right)^2 + \left(\frac{p\pi}{l}\right)^2 = \left(\frac{i\pi}{a}\right)^2 + \left(\frac{k\pi}{l}\right)^2 \tag{5.8}$$

Equation (5.8) leads to the following expression for the initial choice of the ratio a/l in relation of the chosen mode pair:

$$\frac{a}{l} = \sqrt{\frac{m^2 - i^2}{k^2 - p^2}} \tag{5.9}$$

In a SIW rectangular cavity, as proved previously, if gap g and slot length s satisfy equation (4.14) and (4.15), SIW $a_{eff} = a$ of the rectangular waveguide. Thus all equations and conclusions above derived from the rectangular cavity are applicable to SIW cavity. For pair of TE_{102} and TE_{201} modes, we obtain the ratio $a/l = 1$ from equation (5.9). To the first mode TE_{102}, $l = \lambda_{g10}$ has been determined. A solution thus can be derived from equation (5.9) and (4.7) to determine size a of the TE_{102}/TE_{201} dual-mode cavity

$$a = \frac{13.2}{f_0(GHz)\sqrt{\varepsilon_r}} \text{ (inch)} \tag{5.10}$$

where f_o is the filter center frequency and ε_r is dielectric constant of filling material.

A single SIW dual-mode cavity using TE_{102} and TE_{201} modes will be built in the substrate @ 996 (ε_r=9.9, h = 10 mil) at center frequency 24.15 GHz. From equation (5.10), the initial cavity dimensions of the cavity can be chosen by

$a = l = 0.1737" = 173.7$ mil,

$b = 10$ mil.

It is important to ensure that modes whose order is higher than TE_{201} should not resonate in the cavity. We verify it by using equation (4.5) to calculate cutoff frequency f_{cmn} for each high order mode such that

f_{c20} = 21.6 GHz, f_{c30} = 32.4 GHz, f_{c40} = 43.2 GHz

It is clear that the modes of order higher than 2 cannot be propagated in such a waveguide.

For pair of TE_{102} and TE_{301} modes, the ratio $a/l = \sqrt{8/3}$ is given from equation (5.9). To the second TE_{301} mode, $l = \lambda_{g30}/2$ and $\lambda_{c30} = 2a/3$. Using equation (5.9) and (4.7), a expression for determining size a of the TE_{102}/TE_{301} dual-mode cavity is as

$$a = \frac{20.2}{f_0(GHz)\sqrt{\varepsilon_r}} \text{ (inch)} \tag{5.11}$$

A single SIW TE_{102}/TE_{201} mode cavity is synthesized on duroid 6002 substrate that ε_r =2.94, h = 10 mil at center frequency 24.15 GHz. From equation (5.11), the initial cavity dimensions of the cavity can be chosen by

a = 487.7 mil, l = 298.6 mil,

b = 10 mil.

Again, by verifying cutoff frequencies of high order modes such that

f_{c20} = 14.1 GHz, f_{c30} = 21.2 GHz, f_{c40} = 28.2 GHz.

It is guaranteed that the modes of order higher than 3 cannot be excited or coupled in the cavity except for TE_{201}. It is necessary to place coupling elements at the middle of

the transverse section of the cavity as shown in Fig.4.13 so that the even modes, such as TE_{201}, are not allowed to propagate.

5.2.2 Q Factor of SIW Cavity

The Q, or quality factor is an important figure of merit for a resonant circuit. A very general definition of Q factor applicable to all resonant circuits is

$$Q = 2\pi \frac{\text{maximum energy stored dyring a cycle}}{\text{average energy dissipated per cycle}} \tag{5.12}$$

Thus Q is a measure of the loss of a resonant circuit and lower loss means a higher Q. In a SIW rectangular resonant cavity, dissipated power consists of P_c, loss on the conducting walls, P_d, loss in the dielectric filling and P_r, radiation, or leakage from gaps between metallic slots. Therefore, the total power loss present in the SIW cavity is the sum of these individual internal components

$$P_u = P_c + P_d + P_r \tag{5.13}$$

where P_u is unloaded internal power dissipation. Then the unloaded Q_u is expressed as

$$Q_u = \frac{2\pi W}{(P_c + P_d + P_r)T} = \frac{\omega W}{P_c + P_d + P_r} = \left[\frac{1}{Q_c} + \frac{1}{Q_d} + \frac{1}{Q_r}\right]^{-1} \tag{5.14}$$

where W is stored energy and T is period.

Considering the radiation loss from a gap really at negligible level when equation (4.14) and (4.15) are met, Equation (5.14) becomes

$$Q_u = \left[\frac{1}{Q_c} + \frac{1}{Q_d}\right]^{-1} \tag{5.15}$$

Q_c of TE_{10l} resonant cavity with lossy conducting walls can be found from [25]

$$Q_c = \frac{(kad)^3 b\eta}{2\pi^2 R_s \left(2l^2a^3b + 2bd^3 + l^2a^3d + ad^3\right)} \tag{5.16}$$

where $k = 2\pi/\lambda$, $\eta = 377/\sqrt{\varepsilon_r}$ and $R_s = \sqrt{\omega\mu_0/2\sigma}$ is the surface resistivity of the metal with the properties of metal conductivity σ. The *a*, *b*, and *d* are the width, height and length of the cavity, respectively. The *l* refers the number of the half standing wave along length of the cavity.

Q_d of the cavity with lossy dielectric filling, but with perfect conducting wall, is

$$Q_d = \frac{1}{\tan\delta} \tag{5.17}$$

where $\tan\delta$ is the dielectric loss tangent.

Now we can estimate Q factors of the SIW dual-mode cavities that geometry sizes have been determined at expected resonant frequency f_0 = 24.15 GHz..

For TE_{102}/TE_{201} dual-mode cavity on Substrate ® 996, the well-defined parameters are:

a =173.7 mil, b = 10 mil, and d = 173.7 mil;

$\varepsilon_r = 9.9$, $\tan\delta = 0.001$, and $k = 1591.5\ m^{-1}$;

Conductivity of copper is $\sigma = 5.813\times10^{7}\ s/m$, $\mu_0 = 4\pi\times10^{-7}\ H/m$. Then the surface resistivity is equal to $R_s = 4.05\times10^{-2}\ \Omega/m$.

From equation (5.16) the Q due to conductor only is

for TE_{102} mode, Q_c = 536,

for TE_{201} mode, Q_c = 536.

Noted that TE_{201} mode can be treated as TE_{102} mode rotated 90° from the field distribution point of view.

From equation (5.17) the Q due to dielectric loss only is

for both TE_{102} and TE_{201} modes, $Q_d = 1/\tan\delta$ = 1,000.

Thus the unloaded Q can be obtained by equation (5.15) for both TE_{102} and TE_{201} modes

$$Q_u = \left[1/Q_c + 1/Q_d\right]^{-1} = 349$$

The overall passband insertion loss can be weighted by [36]

$$L_A = \frac{4.34n}{wQ_u} \tag{5.18}$$

where n is the filter order and w is of the fractional bandwidth of the filter.

A resulting insertion loss of 1.5 dB is get for proposed 4-order 2-dual-mode cavity filter. It meets the requirement of $IL < 2.2$dB.

For another choose of using the TE_{102}/TE_{301} mode cavity on Duroid 6002 substrate, we have

a =487.7 mil, b = 10 mil, and d = 298.6 mil;

$\varepsilon_r = 2.94$, $\tan\delta = 0.0012$, and $k = 867.3\ m^{-1}$;

Conductivity of copper is $\sigma = 5.813\times10^{7}\ s/m$, $\mu_0 = 4\pi\times10^{-7}\ H/m$, and the surface resistivity $R_s = 4.05\times10^{-2}\ \Omega/m$. From equation (5.16)

for TE_{102} mode, Q_c = 565,

for TE_{301} mode, Q_c = 573.

Again TE_{301} mode is treated as TE_{103} mode rotated 90° from the field distribution point of view.

And equation (5.17) gives the Q related to dielectric only

for both TE_{102} and TE_{301} modes, $Q_d = \frac{1}{\tan\delta} = 833$.

Thus the unloaded Q can be obtained by equation (5.15)

for TE_{102} mode, Q_u = 337,

for TE_{301} mode, Q_u = 339.

Using equation (5.18), we have evaluated that insertion loss IL is around 1.6 dB which is better than 2.2 dB of the filter specification.

It is concluded that in our case, dissipated power on conducting wall has the primary effect on the unloaded Q_u. The low Q_u results mainly from the small height b of the

cavity. Increasing the substrate thickness will achieve higher Q and lower the insertion loss of passband, but leads to an increase of radiation loss in the microstrip lines in SICs. The solution to overcome this problem is to use coplanar waveguide (CPW).

5.3 Coupling Elements and Configurations

Coupling involves both internal coupling and external coupling to make of bandpass filters. For a SIW dual-mode elliptic response filter, internal coupling can be divided into three types: direct coupling between two adjacent cavities along the main path, intracavity coupling between two degenerated resonators or modes in the same cavity and cross coupling between two nonadjacent cavities. External coupling occurs between the feeding microstrip transition and the first or last SIW cavity of the filter. To realize TZs, it is essential to create a coupling scheme which can realizing negative cross coupling.

5.3.1 Positive and Negative Coupling Coefficients

In modern filter design, negative coupling is introduced to generate TZs to improve filter selectivity. Using different configurations of coupling structures, RW cavities and resonant modes to control amplitude and phase of the coupling has been becoming a common practice.

To our proposed SIW dual-mode filter design, the source/load coupling route, as shown in Fig.1.5 has to be adopted since in SIW only TE_{mn} modes can propagate. Thus a challenge of realizing negative coupling arises because SIW coupling structures are all

of inductive elements and corresponding to positive polarity of the coupling phase. In this case the negative coupling is more difficult to achieve than that of conventional RW

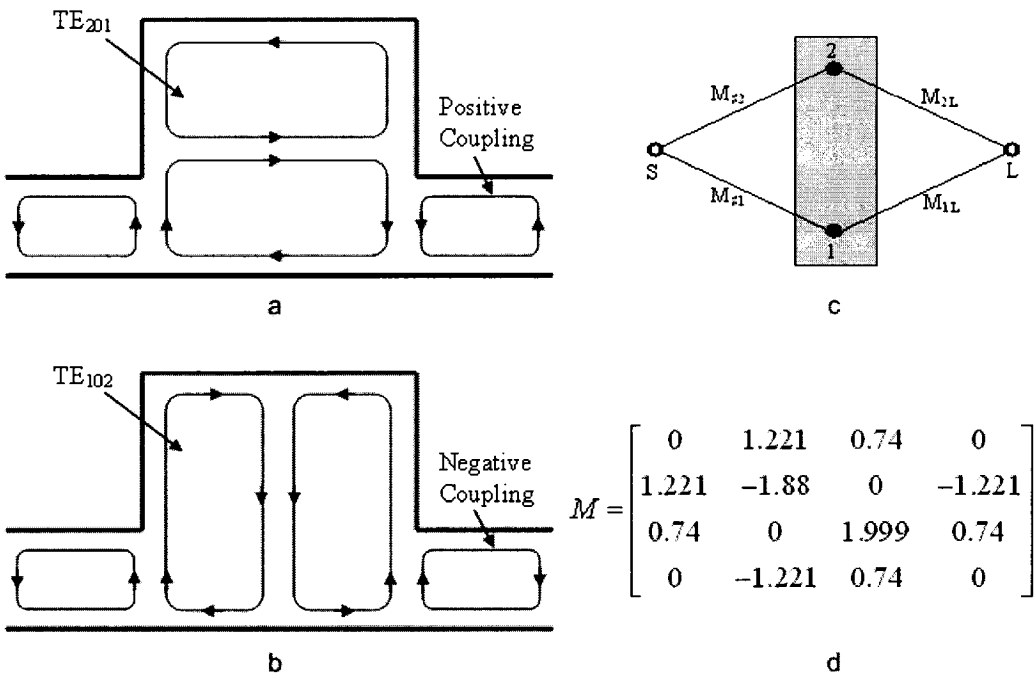

Fig.5.2 Coupling configuration of Single TE_{102}/TE_{201} Dual-Mode Cavity; a. TE_{201} Coupling Pattern Providing Positive Coupling, b. TE_{102} Coupling Pattern Providing Negative Coupling, c. Corresponding Coupling Scheme, d. Corresponding Coupling Matrix

dual-mode filter with field polarization degeneration. By imposing an additional constraint that the indexes m and p (or i and k) of mode in equation (5.8) must be different, namely, $m \neq p$ or $i \neq k$, one can affirm the field distributions of the pair of modes are orthogonal and may make a TZ appear. Fig.5.2 illustrates a magnetic coupling configuration of TE_{102}/TE_{201} dual-mode cavity providing a negative coupling.

The coupling matrix in Fig.5.2 shows that Coupling coefficients M_{1S}, M_{2S} and M_{2L} are positive, but M_{1L} is negative referred to a cross coupling, which is agreed well to the physical coupling configuration of Fig.5.2a and b. The external coupling positions are placed at the corners of the square cavity to excite or couple both TE_{102} and TE_{201} modes. It has to be noted that for a certain coupling scheme the corresponding coupling

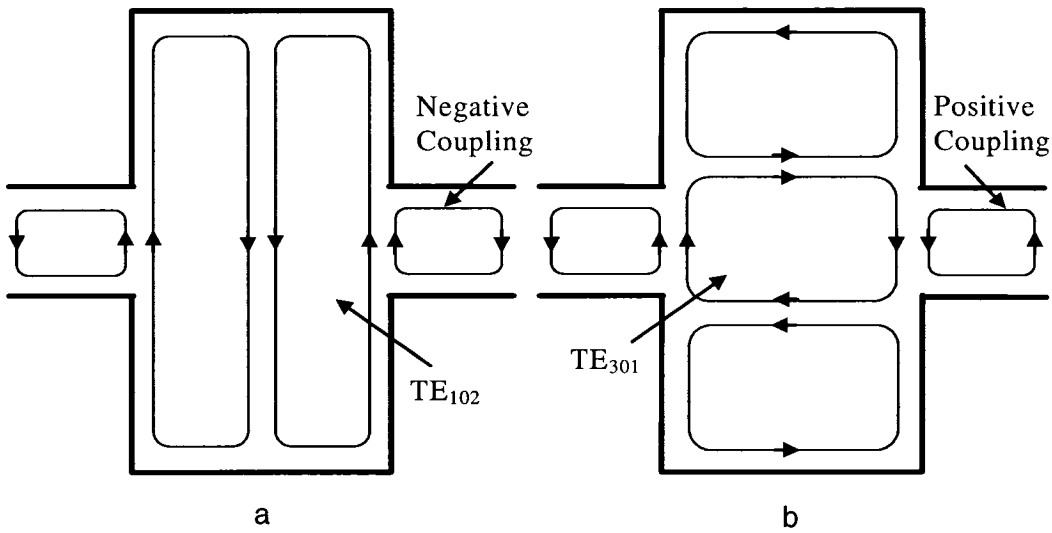

Fig.5.3 Coupling Configuration of Single TE_{102}/TE_{301} Dual-Mode Cavity; a. TE_{102} Coupling Pattern Providing Negative Coupling, b. TE_{201} Coupling Pattern Providing Positive Coupling,

matrix is not unique. Thus when a coupling matrix is obtained, the possibility of realization of a physical structure must be verified.

The next is another example of coupling structure for TE_{102}/TE_{301} dual-mode filter having the same coupling schematic as Fig.5.2 c. The coupling between resonator TE_{102} and the load is negative while others refer to positive ones.

5.3.2 Design of E-Plane Inductive Coupling Structures

The most popularly used RW coupling structures are E-plane metal insert type, iris type and post type as shown in Fig.5.4. A practical dual-mode bandpass filter is a cascade of coupling elements and resonators. In modern microwave filter design, such a filter can be modeled to a chain of inverters spaced along the resonators that are sections of waveguide one half-wavelength in length as shown in Fig.5.5. An impedance inverter

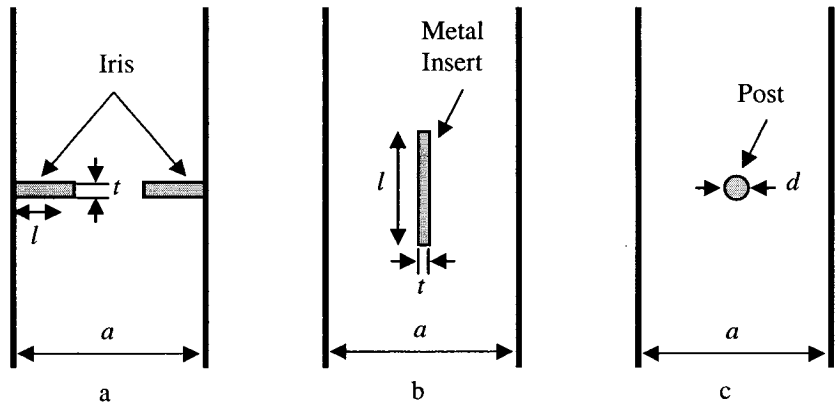

Fig.5.4 Top View of RW Filter Coupling Structures; a. Iris Coupling,

b. Metal Insert Coupling, c. Post Coupling

is a lossless, reciprocal and frequency-independent two-port network to substitute for the coupling structure. The K impedance inverter works actually as an impedance transformer and its conceptual operation can be defined by an ABCD matrix in Fig. 5.6 [37]. Thus input impedance is proportional to the inverse of the load

$$Z_{in} = \frac{AZ_L + B}{jZ_L/K} = \frac{K^2}{Z_L} \tag{5.19}$$

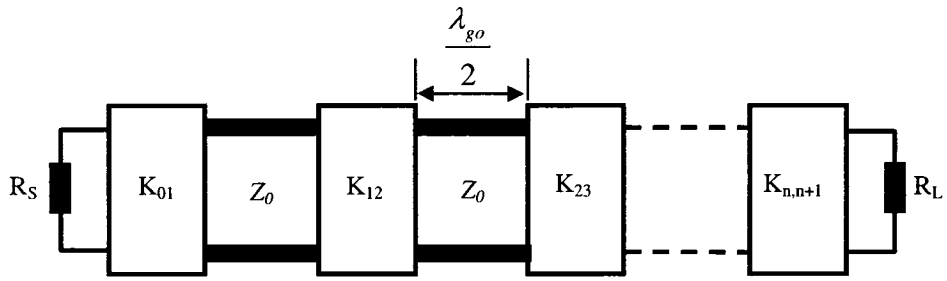

Fig.5.5 Bandpass Filter as a Cascade of Impedance Inverters and Resonators

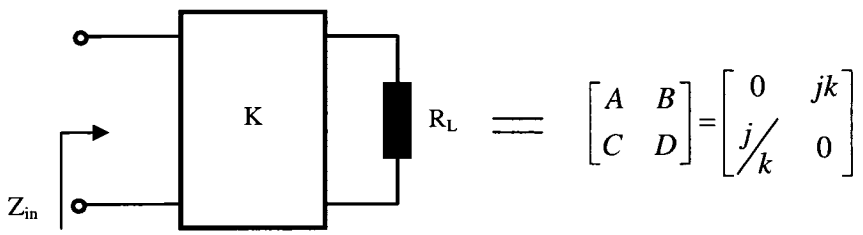

Fig.5.6 Impedance Inverter Terminated with a Load

Many RW coupling structures can be replaced by impedance inverters. Typical equivalent circuits of the RW iris coupling and metal insert coupling are illustrated in Fig.5.7 and the relations with K inverters are denoted [36] [38].

For an iris coupling

$$\frac{K}{Z_0} = \left|\tan\left(\frac{\phi}{2}\right)\right|$$
$$\phi = -\tan^{-1}\left(\frac{2X}{Z_0}\right)$$
$$\frac{X}{Z_0} = \frac{K/Z_0}{1-\left(K/Z_0\right)^2} \tag{5.20}$$

and for a metal insert coupling

$$\frac{K}{Z_0} = \left|\tan\left(\frac{\phi}{2} + \tan^{-1}\left(\frac{X_s}{Z_0}\right)\right)\right|$$
$$\phi = -\tan^{-1}\left(\frac{2X_p}{Z_0} + \frac{X_s}{Z_0}\right) - \tan^{-1}\left(\frac{X_s}{Z_0}\right) \tag{5.21}$$

where $Z_0 = \sqrt{Z_1 Z_2}$ and ϕ in two equations above is the electrical length of the corresponding K inverter and usually a negative number. This poses no problem and may turn out to be useful for implementations of filter resonant cavities in Fig.5.5 since

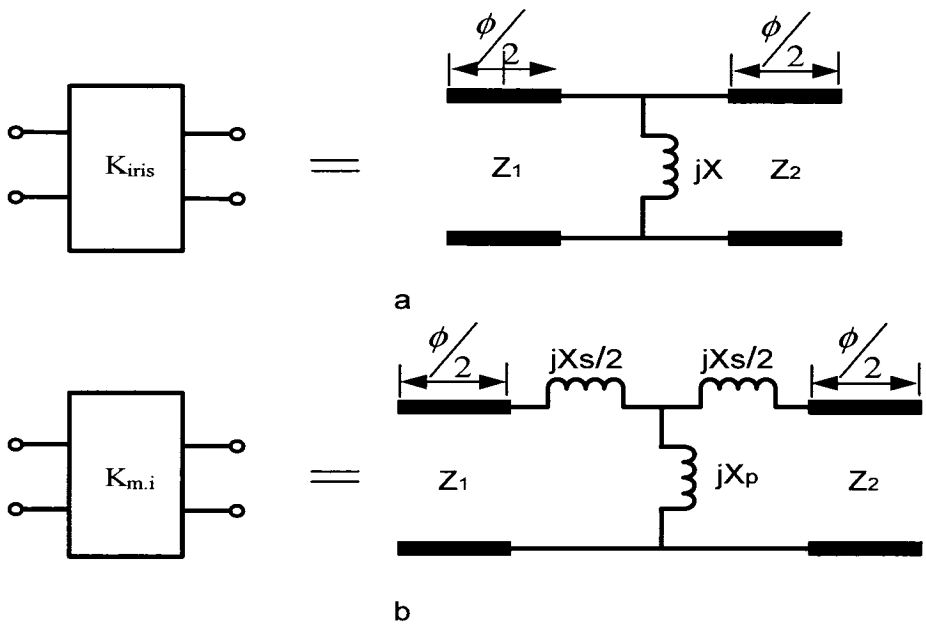

Fig.5.7 Impedance Inverter and Equivalent Circuit. a. Iris Coupling,

b. Metal Insert Coupling

the negative ϕ of transmission line can be merged into $\lambda_{go}/2$ transmission line of each resonator. Thus the physical length of j_{th} resonant cavity is reduced to

$$l_j = \frac{\lambda_{g0}}{2\pi}\left(\pi - \frac{1}{2}\left(\phi_{j-1,j} + \phi_{j,j+1}\right)\right) \qquad j = 1,2\cdots n+1 \qquad [5.22]$$

5.4 Geometric Dimensions of E-Plane Coupling Structures

There are many methods to determine geometric dimensions of inductive coupling structures. In our proposed filter design, both iris and metal insert structures employed. It is critical to transfer the designed coupling parameters, such as k inverters and M

coupling matrix, to actual coupling structure with geometric dimensions. Two transformation approaches are introduced in this section.

5.4.1 Procedure Based on *K* inverters and Coupling Equivalent Circuits

This traditional procedure is based on *K* inverters defined by prototype parameters of the low-pass filter when the resonant cavity is realized by $\lambda_{g0}/2$ transmission line.

1. determine elements, g_j, of the low-pass prototype according to specifications of the filter [36],
2. calculate parameters of each *K* inverter by

$$\frac{K_{01}}{Z_0} = \sqrt{\frac{\pi w}{2 g_0 g_1}} \left(\frac{\lambda_{g0}}{\lambda_0} \right)$$

$$\frac{K_{j,j+1}}{Z_0} = \frac{\pi w}{2\sqrt{g_j g_{j+1}}} \left(\frac{\lambda_{g0}}{\lambda_0} \right)^2 \qquad (5.23)$$

$$\frac{K_{n,n+1}}{Z_0} = \sqrt{\frac{\pi w}{2 g_n g_{n+1}}} \left(\frac{\lambda_{g0}}{\lambda_0} \right)$$

where *w* is fractional bandwidth of the filter, and λ_0, λ_{g0} are the wavelength and guide wavelength at center frequency, respectively,

3. compute the reactance *X* in equivalent circuits by equations (5.20) and (5.21) associated with the results of step 2.

4. determine physical dimensions of the irises or metal inserts with aid of the charts of reactance of inductive window in [39] [36].
5. evaluate actual length, l_j of each resonant cavity using equation (5.22).

5.4.2 Procedure Based on *K* inverters and Coupling Matrix

An alternate way to determine physical dimensions of the inductive coupling structures involves coupling matrix, *M,* which has been derived from filter synthesis in section 3.4. Since coupling matrix presents both direct coupling and cross coupling, the procedure described below is more applicable to the elliptic dual-mode filters.

1 design filter coupling route and scheme which may bring TZs for satisfying requirement of the filter,

2 extract the coupling matrix, *M,* relying on the specifications of the filter by operating filter synthesis,

3 find each of the inverters *K* from relations (5.24) between coupling matrix *M* and inverter *K* [17]

$$K_{01} = \sqrt{\frac{\pi w}{2}}\left(\frac{\lambda_{g0}}{\lambda_0}\right) M_{s1}$$

$$K_{pq} = \frac{\pi w}{2}\left(\frac{\lambda_{g0}}{\lambda_0}\right)^2 M_{pq} \tag{5.24}$$

$$K_{n,n+1} = \sqrt{\frac{\pi w}{2}}\left(\frac{\lambda_{g0}}{\lambda_0}\right) M_{l,n+1}$$

where w is fractional bandwidth of the filter, and λ_0, λ_{g0} are the wavelength and guide wavelength at center frequency, respectively,

4 compute the S parameters from the relevancy with K inverter characterized for each coupling structure according to Fig.5.8. For a reciprocal and lossless network, it leads to the following

$$|S_{11}| = |S_{22}| = \left|\frac{\left(K/Z_0\right)^2 - 1}{\left(K/Z_0\right)^2 + 1}\right|$$

$$|S_{21}| = |S_{12}| = \left|\frac{2K/Z_0}{\left(K/Z_0\right)^2 + 1}\right|$$

$$\phi_1 = -\frac{1}{2}\theta_1 + \frac{1}{2}\pi \ (\text{for } K > 1) \quad \text{or}$$

$$\phi_1 = -\frac{1}{2}\theta_1 \qquad (\text{for } K < 1)$$

$$\phi_2 = -\frac{1}{2}\theta_2 + \frac{1}{2}\pi \ (\text{for } K > 1) \quad \text{or} \tag{5.25}$$

$$\phi_2 = -\frac{1}{2}\theta_2 \qquad (\text{for } K < 1)$$

$$\phi_{12} = \frac{\theta_1 + \theta_2}{2} + \frac{1}{2}\pi$$

where $S_{11} = |S_{11}|e^{j\theta_1}$, $S_{22} = |S_{22}|e^{j\theta_2}$, $S_{21} = S_{12} = |S_{21}|e^{j\phi_{12}}$ and $Z_0 = \sqrt{Z_1 Z_2}$.

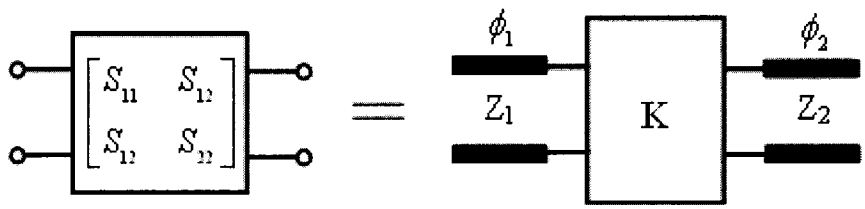

Fig.5.8 Scattering Matrix Representation of an Impedance Converter *K*

5 using HFSS to simulate the *S* parameters of each physical coupling structure. comparing with the corresponding computed *S* parameter values, adjust coupling element size until they are accurately matched.

6. evaluate actual length, l_j of each resonant cavity using equation (5.22) and (5.25).

CHAPTER 6

FABRICATION AND MEASUREMENT

6.1 Introduction

Implementation of SIW E-plane coupling dual-mode cavity filters consists of three major parts, first following the procedures described in Chapter 5 to design a RW dual-mode cavity filter relying on the specifications of pursued filter, then mapping the structure of RW design to the SIW form on the substrate and finally integrating the mapped SIW filter with stepped microstrip transitions on the same substrate.

We start with the implementation of a single TE_{102}/TE_{201} dual-mode cavity filter and then its TZ-shifting characteristic is demonstrated. Such a single dual-mode cavity filter can be utilized as a building block in design of higher order cascaded filters. Next we address a new equivalent circuit model of the dual-mode filter by the simulator of Advanced Design System (ADS) to verify coupling and routing schematic. At the end of the chapter, an SIW two-cavity dual-mode filter is given with all detailed dimensions.

6.2 Single SIW Dual-Mode Cavity Filter with a TZ above the Passband

Specifications for the filter are assigned as

center frequency: 24.08 GHz,

bandwidth: 250 MHz,

passband return loss: $\leq$ -25 dB,

passband insertion loss: $\leq$ 2 dB,

stopband rejections: > 30 dB at f = 24.78 GHz.

The coupling routing scheme is defined as same as shown in Fig.1.5 a and E-plane metal insert illustrated in Fig.5.4 b is chosen for coupling structures.

6.2.1 Verification of Coupling Topology by ADS Modeling

By following the filter synthesis procedure described in Chapter 3, we get the related coupling coefficients as follows

$M_{S1} = M_{1S} = 1.221$, $M_{S2} = M_{2S} = 0.74$, $M_{12} = M_{21} = 0$, $M_{11} = 1.88$, $M_{22} = 1.999$,

$M_{L2} = M_{2L} = 0.74$, $M_{L1} = M_{1L} = -1.221$.

Note that the nonzero coupling elements M_{11} and M_{22} account for differences in the resonant frequencies of the different resonators and M_{L1} and M_{1L} with minus values indicate a negative coupling. As mentioned before, there are many solutions of coupling matrix for a designed coupling routing and structure, but only one can be realized in practice. A new circuit model, therefore, is created by ADS to verify the coupling routing schematic. As shown in Fig.6.1, lumped LC resonant circuits are used to express each resonant mode in the cavity and quarter wavelength transmission lines are introduced as coupling elements, in which Z_{s1} stands for M_{s2}, Z_{s2} for M_{s1}, Z_{l1} for M_{l2} and Z_{l2} for M_{l1}. By optimizing the circuit, we found when characteristic impedance Z_{l2} = -806 Ω while others remain positive impedances, a TZ appears. Thus it can be understood that a transmission line with negative characteristic impedance creates a

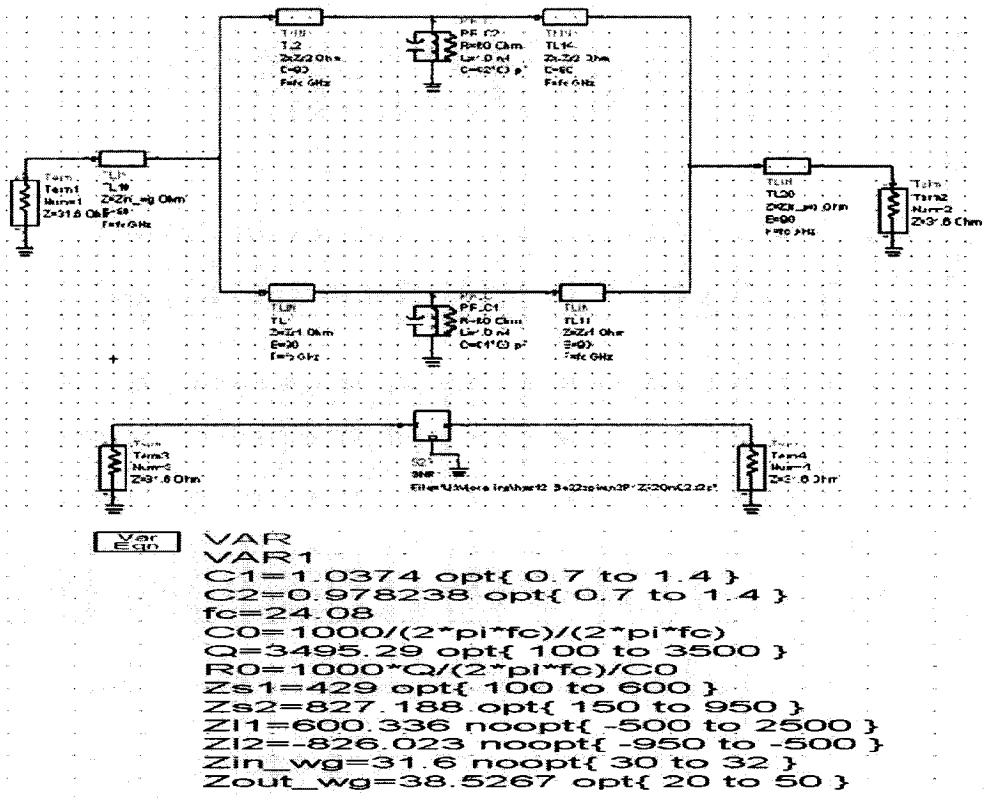

Fig.6.1 Equivalent Circuit Model of Single Cavity Dual-Mode Filter

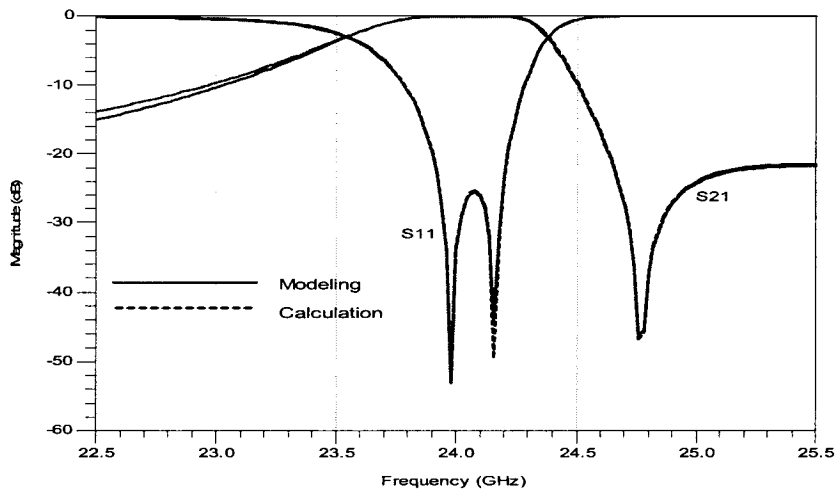

Fig.6.2 Comparison of Frequency Responses from Simulation of Circuit Model and Calculation of Coupling Matrix

negative coupling. Fig.6.2 shows a comparison of results from simulation of circuit model and calculation of coupling matrix. They cannot be distinguished from one another except at low frequency end, which may be caused by frequency dispersion.

6.2.2 Measurement

The SIW single dual-mode cavity filter is built on the ceramic 996 substrate of thickness 10 mils with dielectric constant ε_r 9.9. Fig.6.3 illustrates the top view of the SIW dual-mode filter and related dimensions are listed as follows

$a1$ = 119.2 mil, $l1$ = 9.8 mil, $w1$ = 6.2 mil, d = 62.5 mil, c = 101.5 mil,

a = 169.7 mil, l = 163.9 mil, w = 10 mil, s = 69 mil, $g1 = g2$ = 6 mil,

all other gaps = 10 mil, and the sizes of SIW-microstrip transition are the same as that designed in Section 4.5.2.

Fig.6.3 A Planar SIW Single Dual-Mode Cavity Filter

The SIW slots are fabricated by a laser micro-machine at the Poly-Grame Research Center in Montreal. An expected mechanical error of ±0.5 mil is pre-accounted into the dimensions of draw layout. Thus a final precision within ±0.3 mil can be achieved.

Network analyzer is used to perform measurement and obtained S parameter responses are shown in Fig.6.3. It can be observed that a TZ appears at 24.8 GHz above the passband with a rejection of 34 dB, the return loss yields a very good performance of better than 25dB over the entire passband and the maximum insertion loss within the passband is 1.9dB. To give a comparison, a HFSS simulation result is plotted into Fig.6.4 and we can see that the measured responses have a very good agreement with the simulated ones.

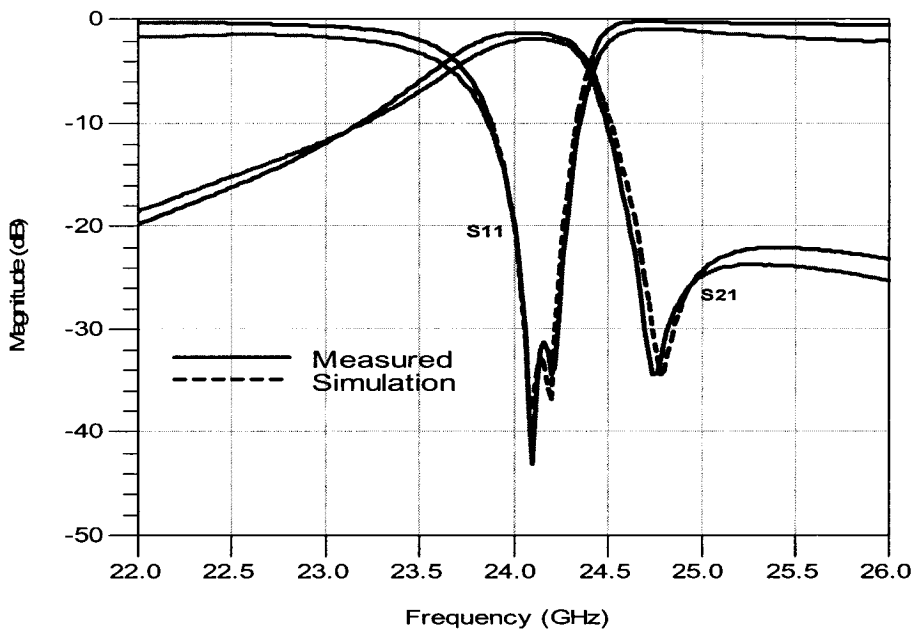

Fig.6.4 Measured and Simulated Frequency Responses

with A TZ above the Passband

6.3 Single SIW Dual-Mode Cavity Filter with a TZ below the Passband

The single dual-mode cavity filter without intracavity coupling has an interesting property that allows a change of the TZ from either side of the passband to the other by only detuning the cavity size and without changing the coupling coefficients. This can be proved by Equation (6.1) which is from Equation (3.21) when $S_{21} = 0$

$$\omega' = \frac{M_{11}M_{S2}M_{L2} + M_{22}M_{S1}M_{L1}}{M_{S2}M_{L2} + M_{S1}M_{L1}} \tag{6.1}$$

It can be clearly seen from Equation (6.1) that altering the signs of M_{11} and M_{22} and keeping other coupling coefficients unchanged will change ω' into $-\omega'$, as stated above.

Based on the design of the single TE_{102}/TE_{201} dual-mode cavity filter with a TZ above the passband, we modify the sizes a and l of the cavity only and leave other dimensions unchanged to move the TZ from the upper stopband to the lower stopband. By using HFSS to carry out the simulation, we have determined the filter dimensions as follows

a = 175.7 mil, l = 159.5 mil, w = 10 mil,

$a1$ = 119.2 mil, $l1$ = 9.8 mil, $w1$ = 6.2 mil, d = 63.4 mil, c = 101.1 mil, $g1 = g2$ = 6 mil, all other gaps = 10 mil.

We found that when increasing size a and decreasing l of the cavity at the same time, the TZ position will move from the high frequency to low frequency without changing cavity resonant frequency. Fig.6.4 shows that both measured and simulated frequency responses and they are in a good agreement with each other. The measured bandwidth

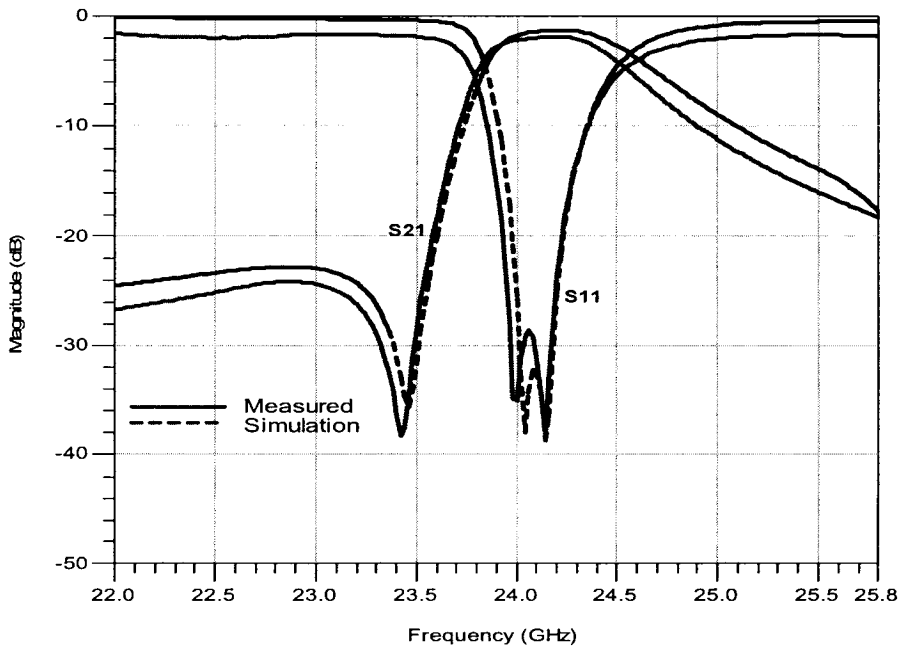

Fig.6.5 Measured and simulated Frequency Responses

with a TZ below the Passband

is a little wider than designed one since it is a very narrow-bandwidth filter, even imperceptible mechanical imperfections will easily deteriorate the bandwidth by a few percent. A TZ appears at 23.4 GHz below the passband with a rejection of 38 dB, the passband return loss yields a very good performance of less than –27dB and the maximum insertion loss within the passband is 1.9dB.

Fig.6.6 shows a photo of the two practical SIW single dual-mode cavity filters on the ceramic 996 substrate, and a very compact size of the filters has been reached.

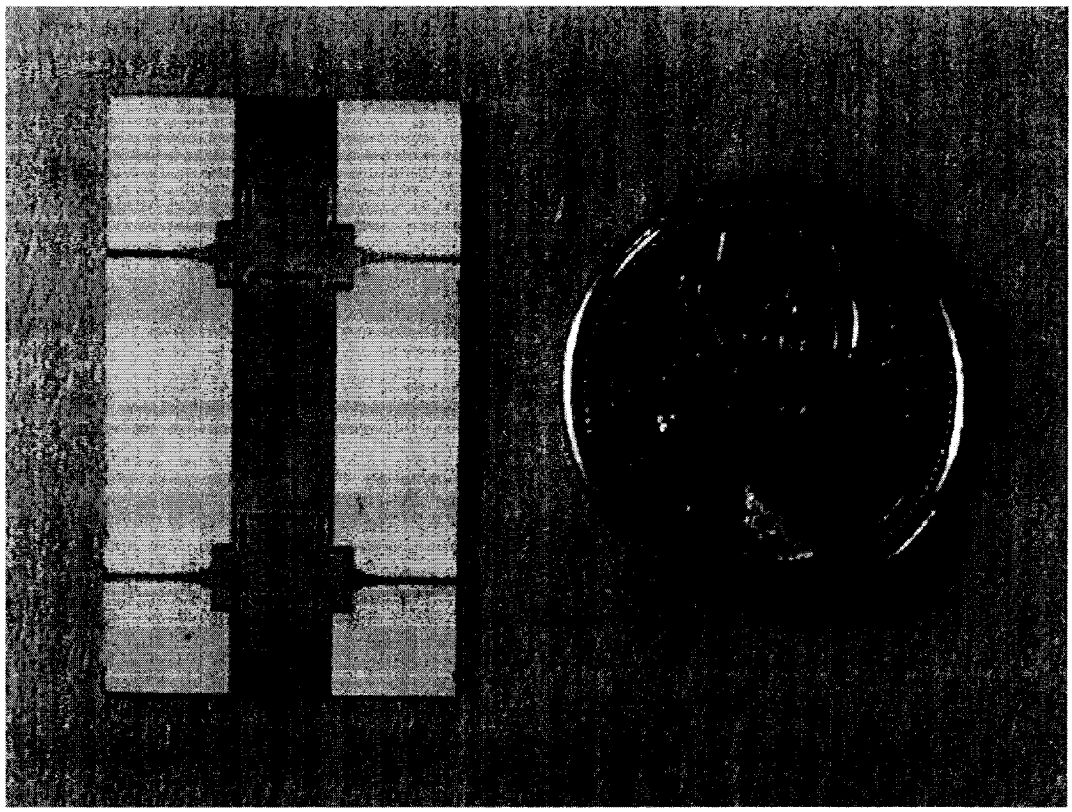

Fig.6.6 Two Fabricated SIW Single Dual-Mode Cavity Filters, a TZ above the Passband (upper) and a TZ below the Passband (bottom)

6.4 Cascaded SIW TE_{102}/TE_{201} Dual-Mode Cavity Filter with two TZs

A relatively simple implementation of this filter is to use two TE_{102}/TE_{201} dual-mode cavities of the same structure as in the previous single cavity filter. The two cavities are then cascaded with a small coupling between them as suggested by the coupling matrix (6.2) calculated by GWT simulator, Waveguide EM Filter Analysis and Design [40].

$$M = \begin{bmatrix} 0 & 1.057 & 0.837 & 0 & 0 & 0 \\ 1.057 & -0.037 & 0 & 1.192 & -1.278 & 0 \\ 0.837 & 0 & 0.037 & 0.496 & 1.008 & 0 \\ 0 & 1.192 & 0.496 & 0.04 & 0 & 0.572 \\ 0 & -1.278 & 1.008 & 0 & -0.019 & 1.221 \\ 0 & 0 & 0 & 0.572 & 1.221 & 0 \end{bmatrix} \tag{6.2}$$

The required specifications are as follows

center frequency: 23.8 GHz,

bandwidth: 1,000 MHz,

passband return loss: ≤ -20 dB,

passband insertion loss: ≤ 2 dB,

stopband rejections: > 45 dB at f = 22.6 GHz and at f = 25.1 GHz.

The coupling routing scheme is the same as shown in Fig.1.5 b and E-plane metal insert illustrated in Fig.5.4 b is adopted for coupling structures. The SIW filter is integrated in a single ceramic 996 substrate with SIW-microstrip transitions as shown in Fig.6.7.

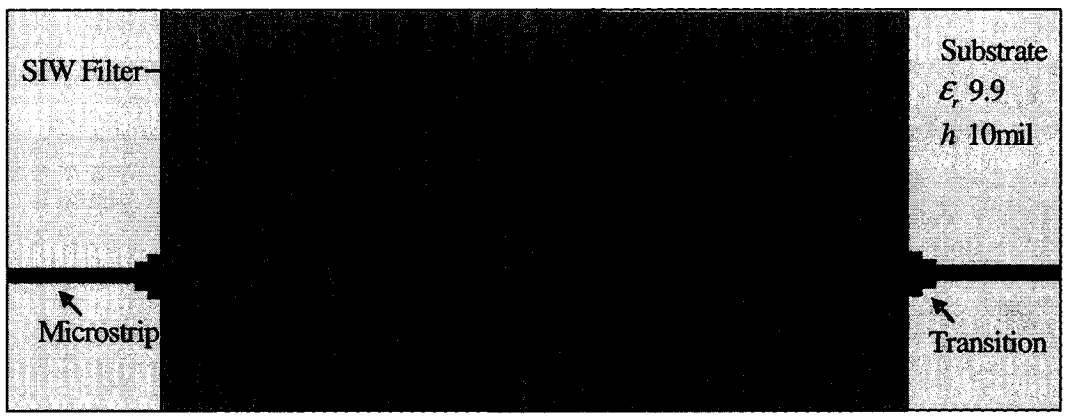

Fig.6.7 A Planar SIW Two Cascaded Dual-Mode Cavity Filter

By using HFSS simulator, a final fine optimization of the structure, actually focusing on adjusting the sizes of coupling structure between two cavities, yields a satisfactory performance with the whole dimensions of the filter below.

a1 = 119.2 mil, *l1* = 37.5 mil, *w1* = *w2* = *w3* = 7 mil, *d1* = 74.5 mil, *c1* = 92.4 mil, *a2* = 182.3 mil, *l2* = 150.9 mil, *l4* = 38 mil, *d2*= 70.1 mil, *c2* = 103.7 mil, *w* = 10 mil, *a3* = 167.9 mil, *l3* = 163.9 mil, *l5* = 9 mil, *d3*= 74.2 mil, *c3* = 81.3 mil, *g1* = *g2* = *g3* = *g4* = 6 mil, other gaps = 10 mil, and the sizes of SIW-microstrip transition are the same as that designed in Section 4.5.2.

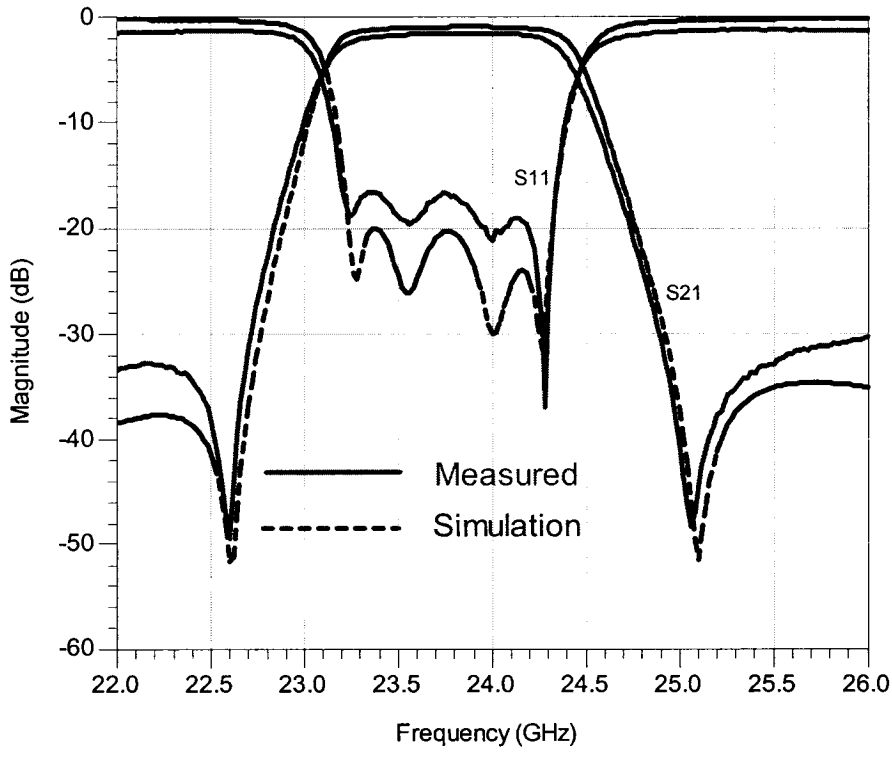

Fig.6.8 Fig.6.5 Measured and simulated Frequency Responses with Two TZs at upper and lower Stopband

Fig.6.8 shows that both measured and simulated passband responses with two TZs at upper stopband and lower stopband. One TZ appears at 22.6 GHz and the other at 25.05 GHz together with rejections better than 45 dB. The maximum insertion loss within the passband is 1.9 dB, but passband return loss reaches only 17 dB that is worse than 20 dB of design goal. Fig.6.9 shows a photo of the SIW two cascaded dual-mode cavity filters on the ceramic 996 substrate.

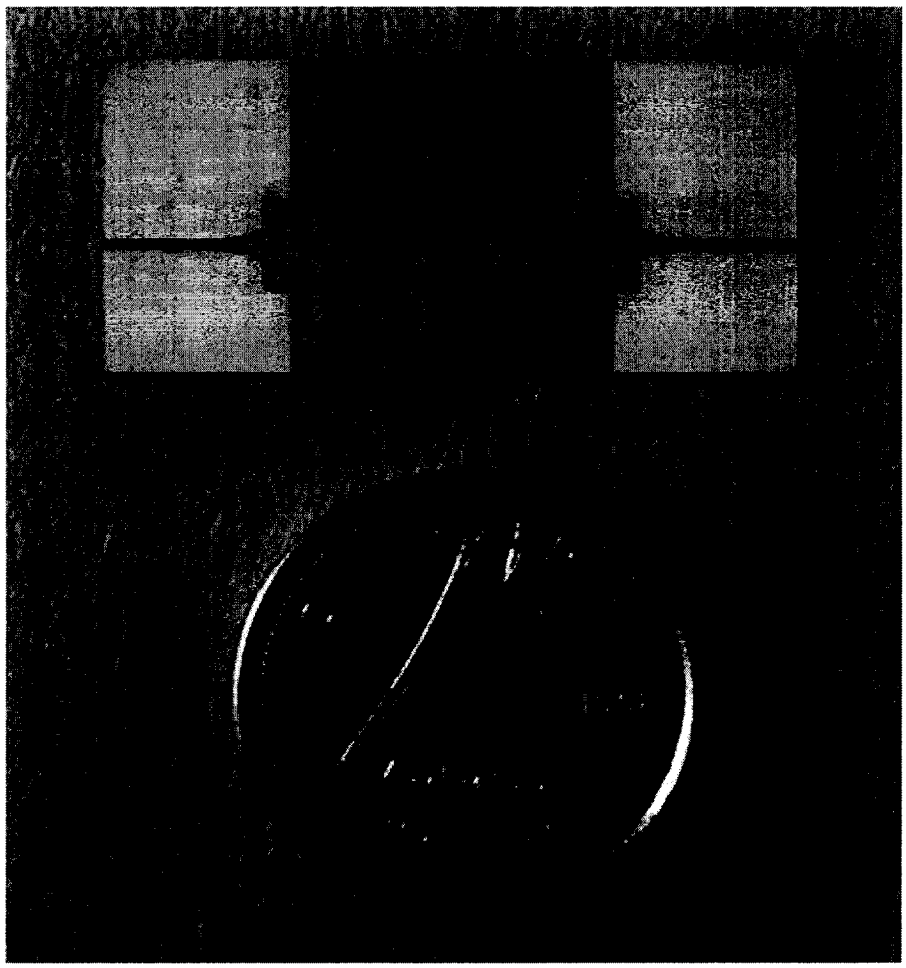

Fig. 6.9 Fabricated SIW Two Dual-Mode Cavity Filters with Four Poles and Two TZs

CONCLUSIONS

Thesis Summary

Substrate Integrated Waveguide (SIW) is playing an important role in the millimeter wave circuits and Substrate Integrated Circuits (SICs) due to its high Q factor, high power capability and low transmission loss in electrical properties and its compact size, low cost and free tuning in mass production. In this dissertation, a new version of the SIW using metallic via slots is developed. The unique feature of this new technique is that the designs of rectangular waveguide components can be directly mapped into designs of SIW using metallic slots without degrading performances. There is no need of adjusting the dimensions. This will extremely simplify the design and manufacture of SIW circuits. As its demonstrations, three SIW TE102/TE201 dual-mode cavity filters with pseudo-elliptic responses are designed and fabricated and excellent performances are achieved.

Chapter 2 gives a short review of developing waveguide dual-mode cavity filters and various techniques of resonant mode transformation are presented. Circular and rectangular waveguide dual-mode filters incorporate with coupling structures cascaded cavities that support dual orthogonal degenerate modes, mainly TE_{11n} modes for circular structures and TE_{n01}/TE_{01n} for rectangular ones. The modes in each cavity are coupled together via coupling screws that are oriented at 45° to the normal electric field polarization. As an improvement, square corner cuts on the rectangular waveguide cavities are used to substitute the tuning screws and a wide range of coupling values can

be reached. Recently, a novel structure of rectangular waveguide dual-mode filters without intracavity coupling has been introduced. One important feature of the filter is that the cavity supports only TE_{m0n}-like degenerate modes but TE_{01n} mode cannot exist since physical height of the cavity is same as the height of feed-in standard rectangular waveguides. A new concept of coupling of source and load to more than one resonant is then investigated and applied to design this kind of dual-mode filters. It is concluded that all existing procedures and theoretical frameworks developed for the rectangular waveguide dual-mode cavity employing TE_{m0n}-like family degenerate modes are directly applicable to their synthesized SIW counterparts, but TM_{mn} and TE_{mn} ($n \neq 0$) modes cannot be guided due to the nature of the SIW structure.

Chapter 3 established a general approach for accurate modeling and synthesis of the equivalent circuit of the multimode cavity filter. The attractive feature of the filter is that both source and load are coupled to more than one resonator and possibly to one another by frequency-independent coupling coefficients M_{si}, M_{Li} and M_{SL} respectively. The coupling matrix are conducted in a matrix equation of the form as

$$\left[-j[R]+\omega'[U]+[M]\right][I]=[Z][I]=-j[E] \qquad j^2=-1$$

Using this equation, the scattering parameters for input and output of the prototype network are given by

$$S_{21}=2\sqrt{R_S R_L}I_{n+2}=-2j\sqrt{R_S R_L}\left[Z^{-1}\right]_{n+2,1}$$

$$S_{11}=1-2R_S I_1=1+2jR_S\left[Z^{-1}\right]_{11}$$

Thus the coupling matrix becomes more important for determining and generating the required finite transmission zeros in design of pseudo-elliptic filters. The coupling of a dual-mode cavity filter comprises of not only interface coupling, intercavity coupling but also intracavity coupling which is exchanging wave energy between different modes in a cavity. The choice of an appropriate coupling structure depends on several variables, the mode excited; the transmission line used and the amount of the coupling desired.

Chapter 4 developed the technique of SIW synthesized using metallic via slots instead of via holes. It takes advantage of allowing the ratio of gap size to slot length g/s varied to fit in physical dimensions of waveguide circuit components. Two design rules are conducted from both theory and simulation results as

$$g/s < 1/10 \text{ , } g/a < 1/20$$

These rules ensure SIW radiation loss, or leakageless, at a negligible level, but, more importantly, make structure mapping from the RW to the SIW with scale factor 1:1, that is no physical size changed. To account for how a gap between two slots affecting SIW resonant frequency, we inspirit a study on a resonant cavity by using FDFD method and HFSS simulation to figure out the relationship of the gap size and position to the resonant frequency shift. In this chapter, transition between SIW and microstrip has been explored in detail. The design procedure for transition with two section stepped quarter-wave transformer is given and two examples designed at center frequency 24 GHz on different substrates are demonstrated with perfect results.

Chapter 5 depicts that design of SIW dual-mode cavity filters involves three major portions, first synthesizing a prototype of the RW dual-mode cavity filter relying on the specifications of pursued filter, then mapping the structure of RW design to the SIW form on the substrate and finally integrating the mapped SIW filter with stepped microstrip transitions on the same substrate. A conventional design procedure based on K inverters and coupling equivalent circuits is introduced first, and then an alternate way to determine physical dimensions of the inductive coupling structures involves coupling matrix, M, which can be derived from filter synthesis. Since coupling matrix presents both direct coupling and cross coupling, the procedure based on K inverters and coupling matrix is more applicable to the elliptic filters. An analysis of unloaded Q_u of a SIW resonant cavity is carried out in this Chapter and it is concluded that dissipated power on conducting wall has the primary effect on the unloaded Q_u. The low Q_u is resulted mainly from the small height b of the cavity. Increasing the substrate thickness will achieve higher Q and lower the insertion loss of passband, but it leads to an increase of radiation loss in the microstrip lines in SICs. The solution to overcome this problem is to use coplanar waveguide (CPW).

Chapter 6 demonstrated that very good agreement among measured, simulated and designed results is achieved. The TZ-shifting characteristic of TE_{102}/TE_{201} dual-mode cavity structure is investigated. Employing this property, the single SIW dual-mode cavity structure can be utilized as a building block in design of higher order cascaded filters. Three SIW dual-mode cavity filter are manufactured, first one with two poles and a TZ above the passband, second one with two poles and a TZ below passband and the

last with four poles and two TZs at upper and lower stopband. The SIW slots are fabricated with a laser micro-machine at the Poly-Grame Research Center. An expected mechanical error of ±0.5 mil is pre-accounted into the dimensions of draw layout. Thus a final precision within ±0.3 mil can be achieved.

Future Work

A novel technology of SIW synthesized with metallic via slots specialized for designing dual-mode cavity filters has already been developed in the thesis. This opens up a number of possibilities for future studies including further development of the SIW technology to enhance its applications on commercial mass production. In this direction, a broad-band of well-developed waveguide components, such as folded elliptic multiplexers, narrow-wall or broad-wall coupling directional couplers, much higher order filters and power splitters, can be redesigned by SIW concept and integrated with solid-state devices to realize wide band SICs.

Another attracting extension of the SIW technology is to apply real 3D hybrid multiport waveguide components, such as magic-T, to a purely planar structure of the SIW. The matching problem in three-port network is likely improved by utilizing matching circuits combined with different transitions, like microtrip, CWP and fin line.

APPENDIX

```
% %%%%%%%%%%%%%%%%%%%%%%%%%%%%%%%%%%%%
%          Matlab code for coupling matrix synthesis          %
%%%%%%%%%%%%%%%%%%%%%%%%%%%%%%%%%%%%%%


n=2;               % order of the filter
rf0=24.06e9;       % center frequency in Hz
rdf=0.32e9;        % BW in Hz
Lf=22e9;           % start frequency in Hz;
Uf=26e9;           % stop frequency in Hz;
df=20e6;           % step in Hz
N=(Uf-Lf)/df;      % point number

R=zeros(4,4);      % zeros: zero Marrix
R(1,1)=1;          % set non-zero entry
R(4,4)=1;

W=eye(4,4);        % eye: identity Matrix
W(1,1)=0;          % % set some entries
W(4,4)=0;

%M=[0,     1.221,  0.74,   0;...
%  1.221,  -1.88,  0,      -1.221;...
%  0.74,   0,      1.999,  0.74;...
%  0,      -1.221, 0.74,   0];        % Coupling Matrix [n+2, n+2]

%M=[0,     0.74,   1.221,  0;...
% 0.74,    1.999,  0,      0.74;...
%  1.221,  0,      -1.88,  -1.221;...
%  0,      0.74,   -1.221, 0];        % same performence as the above,Pole1<-->pole2


%M=[0,     -0.74,  -1.221, 0;...
% -0.74,   1.999,  0,      0.74;...
% -1.221,  0,      -1.88,  -1.221;...
%  0,      0.74,   -1.221, 0];        % same performence as the above, both
%  signs of M12/M21 & Ms1/M1s changed at same time.

M=[0,      0.74,   1.221,  0;...
  0.74,    1.999,  0,      0.74;...
```

```
1.221,    0,    -1.88,   -1.221;...
  0,       0.74,  -1.221,    0];            % same performence as the above,both
%   signs of M12/M21 & ML1/M1L changed at same time.

for m=1:(N+1)                               % frequency array
   rf(m)=Lf+(m-1)*df;                       % frequency in radius.

   omg(m)=(rf(m)/rf0-rf0/rf(m))*rf0/rdf; % Normalized frequncies.
   A=-j*R+omg(m)*W+M;                       % A matrix expression
   IA=A^(-1);                               % inverse of A
   S21(m)=-2*j*IA(n+2,1);
   S11(m)=1+2*j*IA(1,1);

end;

figure,plot(rf/1e9, 20*log10(abs(S21)),'b',rf/1e9,20*log10(abs(S11)),'b'), grid on;
```

REFERENCES

[1] Ralph Levy and Seymour B. Cohn, "A History of Microwave Filter Research Design, and Development," *IEEE Trans. on MTT.,* Vol. MTT-32, pp.1055-1067, Sep. 1984.

[2] Albert E. Williams and Ali E. Atia, "Dual-Mode Canonical Waveguide Filters," *IEEE Trans. on MTT.,* Vol. MTT-25, pp.1021-1026, Dec. 1977.

[3] G. Matthei, L. Young, E. Jones "Microwave Filters, Impedance-matching Networks, and Coupling Structures," *McGRAW-HILL BOOK COMPANY.,* N. Y. 1980.

[4] G. Pfitzenmaier, "Synthesis and Realization of Narrow-band Canonical Microwave Bandpass Filters Exhibiting Linear Phase and Transmission Zeros," *IEEE Trans. on MTT.,* Vol. MTT-30, pp.1300-1311, Sep. 1982.

[5] Ralph Levy, "Filter with Single Transmission Zeros at Real or Imaginary Frequencies," *IEEE Trans. on MTT.,* Vol. MTT-24, pp.172-181, April 1976.

[6] R.M. Kurzrok, "General Three-reasonator Filters in Waveguide," *IEEE Trans. on MTT.,* Vol. MTT-14, pp.46-47, Jan 1966.

[7] R.J. Cameronand J.D. Rhodes, "Asymmetric Realizations of Dual-mode Bandpass Filters," *IEEE Trans. on MTT.,* Vol. MTT-29, pp.51-58, Jan. 1981.

[8] S.B. Cohn, "Direct-coupled-resonator filters," *Proc. IRE, Vol. 45, pp. 187-196,* Feb. 1957.

[9] A.E. Atia and A.E. Williams, "Narrow Bandpass Waveguide Filters," *IEEE Trans. on MTT.,* Vol. MTT-20, pp.258-265, April 1972.

[10] Uwe Rosenberg and Smain Amari, "Novel Design Possibilities for dual-mode Filters without Intracavity Couplings," *IEEE Microwave and Wireless Components letters,* Vol 12, No. 8, pp. 296-298, Aug. 2002.

[11] Lei Zhu and Ke Wu, "A Joint Field/Circuit Design Model of microstrip Ring Dual-Mode Filter: Theory and Experiments ," *1997 Asia Pacific Microwave Conference,* pp.865-868.

[12] V.M.Vladimirov, S.N. Kulinich, A.k. Savin and Yu.G. Shihov, "Microstrip Elliptic Filters with Adjustable Attenuation Poles," *2003 IEEE MTT-S Digest,*, pp. 356-359.

[13] A.E. Williams, "A Four-cavity Elliptic waveguide filter," *IEEE Trans. on MTT.,* Vol. MTT-18, pp.1109-1114, Dec. 1970.

[14] A.E. Atia, A.E. Williams, "Non-minimum Phase Optimum Amplitude Bandpass Waveguide Filters," *IEEE Trans. on MTT.,* Vol. MTT-22, pp.425-432, April 1974.

[15] A.E. Atia, A.E. Williams and R.w. Newcomb, "Narrow-band multiple-coupled cavity synthesis," *IEEE Trans. Circuit Syst.,* Vol. CAS-21, pp.649-655, Sept. 1974.

[16] Marco Guglielmi, Olivier Roquebrun, Pierre Jarry, Eric Kerherve, etc. "Low-cost Dual-mode Asymmetric Filters in Rectangular Waveguide," 2001 *IEEE MTT-S Digest*, pp.1878-1790.

[17] Ji-fuh Liang, Xiao-Peng Liang, Kawthar A. Zaki and Ali E. Atia, "Dual-Mode Dielectric or Air-Filled Rectangular Waveguide Filters," *IEEE Trans. on MTT.*, Vol. MTT-42, pp.1330-1336, July. 1994.

[18] Patrizia Savi, Daniele Trinchero, Riccardo Tascone and Renato Orta, "A new Approach to the Design of Dual-Mode Rectangular Waveguide Filters with Distributed Coupling," *IEEE Trans. on MTT.*, Vol. MTT-45, pp.2294-2302, Feb. 1997.

[19] Mareo Guglielmi, Pierre Jarry, Eric Kerherve, Olivier Roquebrun and Dietmar Schmitt, "A New Family of All-Inductive Dual-Mode Filters," *IEEE Trans. on MTT.*, Vol. MTT-49, pp.1764-1769, Oct. 2001.

[20] Smain Amari, Uwe Rosenberg and Jens Bornemann, "Inline TM_{110}-Mode Filters with High-design Flexibility by Utilizing Bypass Couplings of Nonresonating $TE_{10/01}$ Modes," *IEEE Trans. on MTT.*, Vol. MTT-51, pp.1735-1742, June 2003.

[21] Xiao-Peng Liang, Kawthar A. Zaki and Ali E. Atia, "Dual Mode Coupling by Square Corner Cut in Resonators and Filters," *IEEE Trans. on MTT.*, Vol. MTT-40, pp.2294-2302, Dec. 1992.

[22] Uwe Rosenberg and Smain Amari, "Novel coupling Schemes for Microwave Resonator Filters," *IEEE Trans. on MTT.*, Vol. MTT-50, pp.22896-2902, Dec. 2002.

[23] A.E. Atia, A.E. Williams, "New Types of Waveguide Bandpass Filters for Satellite Transponders," *COMSAT Tech. Rev.*, vol. 1, pp. 21-43,1971.

[24] Smain Amari, Uwe Rosenberg and Jens Bornemann, "Apaptive Synthesis and Design of Resonator Filters with Source/Load-Multiresonator Coupling," *IEEE Trans. on MTT.,* Vol. MTT-50, pp.1764-1769, Aug. 2002.

[25] David M. Pozar, "Microwave Engineering" pp. 120

[26] K. Wu, D. Deslandes, and Y. Cassivi, "The Substrate Integrated Circuits-A New Concept for High-Frequency Electronics and Optoelectronics," *In Proc. 6th* Int. *Conf. Telecommunications Modern Satellite, Cable, Broadcasting Service (TELSIKS'03),* vol. 1, Oct.1-3, 2003, pp P-III-P-X.

[27] D. Deslandes, and K. Wu, " Integrated Microstrip and Rectangular Waveguide in Planar Form," *IEEE Microwave and Wireless Components letters,* Vol 11, No. 2, pp. 68-70, Feb. 2001.

[28] Feng. Xu, and Ke Wu, "Guided-Wave and Leakage Characteristics of Substrate Integrated Waveguide," *IEEE Trans. on MTT.,* Vol. MTT-53, No.1, pp.66-73, Jan. 2005.

[29] Y. Cassivi, L. Perregrini, P. Arcioni, M. Bressan, K. Wu and G. Conciauro, "Dispersion Characteristics of Substrate Integrated Rectangular Waveguide, " *IEEE Microwave and Wireless Components letters,* Vol 12, No. 9, pp. 333-335, Sep. 2002.

[30] D. Deslandes, and K. Wu, "Single-Substrate Integration Technique of Planar Circuits and Waveguide Filters," *IEEE Trans. on MTT.,* Vol. MTT-51, No.2, pp.593-596, Feb. 2003.

[31] S. Germain, D. Deslandes, and K. Wu, "Development of Substrate Integrated Waveguide Power Dividers," *CCECE 2003 Proceedings*, pp. 1921-1924, May 2003.

[32] D'Orazio, K. Wu, and J. Helszajn, "A Substrate Integrated Waveguide Degree-2 Circulator," *IEEE Microwave and Wireless Components Letters,* vol. 14, pp 207-209, May 2004.

[33] F. Xu, Y. Zhang, W. Hong, Ke Wu, and T. J. Cui, "Finite-difference Frequency-domain Algorithm for Modeling Guided-wave Properties of Substrate Integrated Waveguide," *IEEE Trans. on MTT.,* Vol. MTT-51, No.11, pp.2221-2227, Nov. 2003.

[34] D. Deslandes, and K. Wu, "Integrated Transition of Coplanar to Rectangular Waveguide," *IEEE int. Microwave Symp.* Dig., 2001, pp. 619-622.

[35] David M. Pozar, "Microwave Engineering" *Wiley,* 1998. pp. 83

[36] G. Matthaei L. Young and E.M.T. Jones, "Microwave Filters, Impedance-Matching Networks, and Coupling Structures" 1980

[37] Ian Hunter, "Theory and Design of Microwave Filters" *The Institution of Electrical Engineers,* 2001. pp. 55

[38] Yoshihiro Konishi, Katsuaki Uenakada, "The Design of a Bandpass Filter with Inductive Strip-Planar Circuit Mounted in Waveguide," *IEEE Trans. on MTT.,* Vol. MTT-22, No.10, pp.809-873, Oct. 1974.

[39] N. Marcuvitz, "Waveguide Handbook," *Boston Technical Publishers, Inc,*1964

[40] GWT, "Waveguide EM Filter Analysis and Design" *www.guiddwavetech.com*